FUNCTIONAL ANALYSIS OF A 5′ UNTRANSLATED VARIANT IN RHODOPSIN: IMPLICATIONS FOR THE RETINITIS PIGMENTOSA PHENOTYPE?

By

Maureen Veronica Akinyi BSc (Hons)

AKNMAU001

SUBMITTED TO THE UNIVERSITY OF CAPE TOWN

In fulfilment of the requirements for the degree of MSc (Med) in Human Genetics

14 February 2011

Supervisor: Prof. R. Ramesar

Co-Supervisors: A/Prof. D. Lang, Ms L. Roberts & Mrs A. Pandor

Division of Human Genetics, University of Cape Town

Plagiarism Declaration

I, Maureen Akinyi, hereby declare that the work on which this dissertation/thesis is based is my original work (except where acknowledgements indicate otherwise) and that neither the whole work nor any part of it has been, or is to be submitted for another degree in this or any other university.

I empower the university to reproduce for the purpose of research the whole or any portion of the contents in any manner whatsoever.

Signature: ……

Date:……

To

my mother Priscah Achieng Dondo

and

brother Lionel R. Omondi

Acknowledgements:

With the utmost sincerity, I would like to thank:

- My supervisor Prof. Ramesar, for mentorship, for challenging me to think 'outside the box' and for providing a stimulating work environment.

- My co-supervisors: A/Prof. Dirk Lang for welcoming me into his lab and for teaching me the marvels of microscopy, Ms Lisa Roberts for unwavering support both academically and personally-thank you for always having time to listen to my ideas and rants, Mrs Aisha Pandor for patiently teaching me new techniques, brainstorming sessions and for the never-ending encouragement. The quote '*If I have seen further it is by standing on the shoulders of giants'* has a new meaning for me. Thank you for pushing me to be the best that I can be and helping me achieve my goals.

- The Retina SA foundation and all its members, for funding and their patience and enthusiasm for our research.

- My Human Genetics Family; I could not have wished for a better working environment. Thank you all for the laughter, stories and making it a joyful experience to come to the lab every day. Oh, and of course for the random reasons to gather and eat! Special thanks to Kusha Kalideen for assistance with bioinformatics.

- My friends in Cape Town who have now become my adaptive family, for always being there and understanding when I was too busy or exhausted to 'hang' and still being there. Thank you for all the wonderful experiences so far.

- My new friends in Dirk and Lester's lab for welcoming me with open arms, for always being so enthusiastic about my experiments and for all the fun moments and stories. Thank you to Susan Cooper her patience and tireless assistance with microscopy, and of course the entertaining stories.

- My dearest love and best friend David. Thank you for your patience and understanding, even with the long hours and nights. Thank you for trying your best to make my life easier and for taking this journey with me.

- My family; especially my parents, for their unwavering support and tireless generosity in helping me achieve my dreams. There are not enough words to express my gratitude. Thank you for always doing the best that you can, to support me. My siblings; Victor, Charles and Michelle, for just being themselves and providing me with encouragement and laughter.

Table of Contents

List of figures 3
List of Tables 4
Abbreviations 5
Abstract 8
Chapter 1: Introduction 10
1.1. Vision 10
1.1.1. Photoreceptors and the phototransduction cascade. 12
1.2. Inherited retinal degenerative disorders 15
1.2.1. Mechanisms of photoreceptor death 16
1.3. Retinitis Pigmentosa 17
1.3.1. Autosomal dominant retinitis pigmentosa 19
1.4. RHO and disease 20
1.4.1. RHO mutations in South Africa 22
1.5. Phenotypic variation 23
1.5.1. Genetic disease modifiers 24
1.5.2. Functional significance of SNPs 25
1.5.3. Variation in non-coding regions of DNA 25
1.6. Aims and objectives 26
Chapter 2: Materials and Methods 28
2.1. Bioinformatic analyses of the *RHO* 5′UTR c.-26A>G variant and screening in an AdRP Cohort 28
2.1.1. Bioinformatic analyses of the *RHO* c.-26A>G variant 28
2.1.2. Cohort selection for c.-26A>G screening 29
2.1.3. DNA quality control 29
2.1.4. PCR amplification 30
2.1.5. Restriction fragment length polymorphism analysis 31
2.1.6. DNA sequencing 32
2.2. Functional *in vitro* analyses of the c.-26A>G variant in mammalian cell lines 33
2.2.1. Cloning 33
2.2.1.1. Preparation of competent cells 33
2.2.1.2. E.coli bacteria transformation 34
2.2.1.3. Small-scale and large-scale plasmid preparations 34
2.2.2. Site-directed mutagenesis 35
2.2.2.1. Mutagenic primer design and PCR 35
2.2.2.2. Restriction endonuclease screening 39
2.2.3. Mammalian cell culture 40
2.2.3.1. Cell culture maintenance and transient transfections 41
2.2.4. Immunocytochemistry 41
2.2.4.1. DAPI nuclear staining 42
2.2.4.2. Fluorescence microscopy 42
2.2.5. Western blotting 42
2.2.5.1. Immunodetection of RHO 44

2.2.6. Quantitative real time-PCR (qPCR) 44
2.2.6.1. RNA extraction 44
2.2.6.2. cDNA synthesis 46
2.2.6.3. Quantitative PCR (qPCR) 46
2.2.6.4. Analysis-Standard curve method 48
Chapter 3: Results 49
3.1. Bioinformatic analyses of the *RHO* 5′UTR c.-26A>G variant and screening in an AdRP Cohort 49
3.1.1. Bioinformatic analyses of the *RHO* c.-26A>G variant 49
3.1.1.1. Protein interaction profile of RHO 49
3.1.1.2. RHO vertebrate species alignment 50
3.1.1.3. RNA folding prediction using mFOLD software 51
3.1.1.4. Transcription factor binding site analysis 52
3.1.2. *RHO* 5′UTR c.-26A>G variant screening in an AdRP cohort 57
3.2. Functional *in vitro* analyses of the c.-26A>G variant in mammalian cell lines 60
3.2.1. Site-directed mutagenesis of *RHO* gene variants 60
3.2.2. The effect of the *RHO* 5′UTR variant on protein localisation 63
3.2.2.1. Threonine 4 Lysine (T4K) 63
3.2.2.2. Threonine 17 Methionine (T17M) 65
3.2.2.3. Proline 347 Leucine (P347L) 67
3.2.3. Protein expression differences between WT and mutation variants of RHO 69
3.2.3.1. HT-1080 69
3.2.3.2. SKNSH 70
3.2.4. Altered transcript expression in *RHO* mutants carrying the 5′UTR variant 72
Chapter 4: Discussion 79
4.1. The Predicted effects of the c.-26A>G variant and frequencies in AdRP families 80
4.2. The differential effect of the 5′UTR variant on glycosylation mutants: T4K and T17M 82
4.2.1. T4K and UTR-T4K 82
4.2.2. T17M and UTR-T17M 85
4.3. The effect of the 5′UTR variant may be determined by the distance between the c.-26A>G variant and the mutation; the case of P347L 88
4.4. Does the 5′UTR variant elicit transcriptional regulation or translational repression? 90
Chapter 5: Conclusions 93
5.1. Future prospects 95
References: 97
Appendix A: Consent Forms and Cohort Pedigrees 106
Appendix B: Reagents and protocols 114
Appendix C: Supplementary Figures 126

List of figures

Figure 1. 1: Diagrammatic cross section of a human eye showing the anatomical location of the retina and components of the eye that facilitate vision. 11
Figure 1. 2: Schematic diagram of the retina showing the arrangement of the four nuclear layers. 12
Figure 1. 3: Schematic diagram of a rod photoreceptor cell showing the outer (containing the disc membranes) and inner segments. 13
Figure 1.4: Schematic diagram of the phototransduction cascade……..15
Figure 1. 5: A pie chart depicting the functional contribution of various genes to photoreceptor degeneration. 16
Figure 1. 6: Comparison of fundus photographs of a normal retina (left) and an RP affected retina (right)..... 18
Figure 1.7: Schematic diagram of the secondary structure of RHO.. 21
Figure 2. 1: Digital image of an SDM PCR gel.. 38
Figure 2. 2: Schematic diagram representing four main cDNA constructs created using SDM. 39
Figure 2. 3: Digital image of 5′UTR digest gel..... 40
Figure 2. 4: Digital image of a gel used to determine the integrity of total extracted RNA after transfection with the constructs. 45
Figure 3. 1: Interaction profile of RHO as depicted by STRING.. 50
Figure 3. 2: A screen print image of the *RHO* sequence alignment across various vertebrates.. 51
Figure 3. 3: Images of the predicted *RHO* mRNA secondary structure obtained from mFOLD using the 5′UTR sequence containing the ‘A’ allele (5′UTR *RHO*). .. 53
Figure 3. 4: Images of the predicted *RHO* mRNA 5′UTR secondary structures obtained from mFOLD using the 5′UTR sequencing containing the ‘G’ allele.54
Figure 3. 5: The table of results obtained from TESS using the *RHO* ‘A’ allele. 55
Figure 3. 6: The table of results obtained from TESS using the *RHO* ‘G’ allele. 56
Figure 3. 7: Image of information on the ARP-1 transcription factor retrieved from TESS.. 57
Figure 3. 8: Example of a typical agarose gel image, showing PCR products digested with Ksp I to determine genotype status. 57
Figure 3. 9: Sequencing electropherogram of a sample with an AA genotype obtained using the reverse primer. 58
Figure 3. 10: Distribution frequencies of the c.-26A>G genotype in 35 AdRP family members.. 59
Figure 3. 11: Distribution frequencies of the three c.-26A>G genotypes in AdRP patients only. 59
Figure 3. 12: Sequencing electropherogram of *RHO* single mutants. 61
Figure 3. 13: Sequencing electropherograms of *RHO* T4K and T17M with the 5′UTR (c.-26A>G) variant *in cis*. 62
Figure 3. 14: Fluorescent images of cells expressing WT RHO and the T4K mutant constructs. 64
Figure 3. 15: Fluorescent images of cell lines expressing WT RHO and T17M mutant constructs.. 66

Figure 3. 16: Fluorescent images of cells expressing WT RHO and P347L mutant constructs. 68
Figure 3. 17: Western blot analysis of WT and mutant opsins in cell lysates from HT-1080 cells. 69
Figure 3. 18: Western blot analysis of WT and mutant opsins in cell lysates from SKNSH cells.. 71
Figure 3. 19: Graph showing expression differences between WT RHO and mutant constructs.. 73

List of Tables

Table 1. 1: Classification of RHO mutations.. 22
Table 2. 1: SDM primers used to introduce mutations in hRHO cDNA……...36
Table 2. 2: Summary of cycling conditions used in mutagenic PCRs. 37
Table 3. 1: Summary of results from functional analyses of each of the different mutations and RHO 5′UTR variant……75

Abbreviations

°C	degree Celcius
µg	micrograms
µl	microlitre
µm	micrometre
AdRP	Autosomal dominant retinitis pigmentosa
ADAM10	a disintegrin and metalloprotease
ArRP	Autosomal recessive retinitis pigmentosa
ARP-1	Apoliprotein A1 regulatory protein
Arg	Arginine
Asp	Aspartate
Asn	Asparagine
bp	base pair
$CaCl_2$	Calcium Chloride
cDNA	complementary DNA
cGMP	cyclic guanosine monophosphate
dbSNP	SNP database
DNA	Deoxyribonucleic acid
dNTPs	deoxynucleotide triphosphates
EtBr	Ethidium bromide
ER	Endoplasmic reticulum
ERG	Electroretinograms
fwd	Forward
g	gram
GAPDH	Glyceraldehyde-3-phosphate dehydrogenase
Gly	Glycine
GPCR	G-protein coupled receptor
H_2O	water
HCl	Hydrochloric Acid
ICC	Immunocytochemistry
IS	Inner segment
kDa	kilo Dalton
Leu	Leucine
Lys	Lysine
LCA	Leber's Congenital Amaurosis
Met	Methionine
$MgCl_2$	Magnesium Chloride
mM	millimolar
mRNA	messenger RNA
NCBI	National Center for Biotechnology Information
ng	nanogram
Oligo(dT)	Oligo (deoxythymidine
OS	Outer segment
PCR	Polymerase chain reaction
PDE	Phosphodiesterase

Abbreviations continued

Pro	Proline
qPCR	quantitative real-time PCR
RDD	retinal degenerative disorders
rev	reverse
RHO	Rhodopsin protein
RHO	Rhodopsin gene
RNA	Ribonucleic acid
RP	Retinitis pigmentosa
RPE	Retinal Pigment Epithelium
RT-PCR	Reverse-transcriptase PCR
SA	South Africa
SDM	site-directed mutagenesis
sec	second
SNP	Single nucleotide polymorphism
Ta	Annealing temperature
TBE	Tris Borate EDTA buffer
TEMED	NNN'N"-tetramethylethylenediamine
TESS	Transcription Element Search System
Thr	Threonine
Tris	tris[hydroxymethyl]aminomethane
U	Units
UCT	University of Cape Town
UK	United Kingdom
USA	United States of America
UTR	Untranslated region
UV	Ultraviolet
V	volts
XlRP	X-linked RP

"And above all, watch with glittering eyes the whole world around you, because the greatest secrets are always hidden in the most unlikely places."

-Roald Dahl

Abstract

Retinitis Pigmentosa (RP) is a group of heterogeneous retinal degenerative diseases that predominantly affect rod photoreceptor cells. Symptoms include night blindness and gradual peripheral vision loss, which progresses to a complete loss of vision. Clinical, phenotypic and genetic heterogeneity are frequently observed in RP. Mutations in Rhodopsin (RHO) have been identified as a major cause of RP. A sequence variant identified in the 5′untranslated region of *RHO*, g.269A>G, also known as c.-26A>G, was proposed to increase the risk of developing RP. In this study, the functional effect of this variant, individually and *in cis* with known pathogenic variants, was investigated using mammalian cell lines in order to determine whether the variant is a modifier of disease phenotype.

Restriction fragment length polymorphism analysis was performed to determine the location (*cis* or *trans*) and frequencies of the c.-26A>G variant in a cohort of families with autosomal dominant RP due to RHO mutations. Expression constructs containing three pathogenic mutations; T4K, T17M & P347L and the c.-26A>G variant were created using site-directed mutagenesis and expressed in HT-1080, HEK-293 and SKNSH cell lines. Analyses to determine protein localisation and expression differences were performed using immunocytochemistry, western blot analysis and qPCR.

Immunocytochemistry on cells transfected with wild-type RHO and the c.-26A>G variant constructs, showed that the protein was typically localised to the plasma membrane. The misfolding mutant constructs (T4K and T17M), exhibited protein aggregate formation, which decreased significantly in the presence of the c.-26A>G RHO variant. The P347L mutant protein, an instability mutant, exhibited slightly increased fluorescence when the P347L mutation construct was expressed *in cis* with the c.-26A>G variant. Quantification of transcript levels (determined by qPCR) revealed a significant reduction in expression of mRNA for the c.-26A>G variant transcript compared to cells expressing the wild-type transcript. Transcript levels of

the T4K and T17M mutation constructs differed significantly when each of the mutations were expressed *in cis* with the c.26A>G variant; T4K transcript expression increased in the presence of the c.-26A>G variant, whereas expression of the T17M transcript decreased significantly. RNA quantification of the P347L constructs, revealed a temporal effect of expression, as transcript levels differed in each cell line, when this construct was expressed *in cis* with the c.-26A>G variant. Western blot analyses correlated with qPCR results for both the T4K and T17M mutants. There was however, no discernable difference in protein levels when the P347L mutant was expressed on its own and when it was expressed *in cis* with the c.-26A>G variant.

Taken together, these results suggest that the c.-26A>G variant appears to affect the expression of RHO, through transcriptional or translational regulation. Furthermore, the extent of the effect of the c.-26A>G variant appears to be a function of physical distance from the disease-causing mutation. This may indicate a modifying effect of the variant on the RHO protein, in a mutation-dependent manner and could potentially impact on the severity of RP.

Chapter 1: Introduction

One third of human inherited diseases involve the eye (Hims et al. 2003). Retinal degenerative disorders (RDDs) are characterised by photoreceptor cell death in the retina, resulting in a loss of vision. The type of cell primarily affected typically distinguishes the various RDDs from one another. A number of techniques, including positional cloning and candidate gene approaches have been utilised to identify gene defects in photoreceptors that are causative of RDDs (Molday, 1998). These gene defects associated with retinal dystrophies exhibit a vast amount of clinical, allelic, genetic, and phenotypic heterogeneity (Daiger, 2004; Baehr & Frederick 2009). Currently, Lebers Congenital Amaurosis (LCA) is reported to be the most severe form of RDD, with visual impairment from birth, progressing to total loss of vision in the first two decades of life (Smith et al. 2009). Although LCA is more severe, retinitis pigmentosa appears to be the most commonly inherited form of RDD (Hims et al. 2003). A comprehensive review of the visual process is essential to understanding the effects of underlying mutations and mechanisms of photoreceptor degeneration, which apart from contributing to the disease phenotype, may also be influencing disease heterogeneity.

1.1. Vision

Vision is described as the ability to interpret information from visible light. The visual process is mediated by photoreceptors, which form part of the retina that lines the posterior section of the eye. Light from the environment passes through the cornea and is directed to the retina, which contains layers of neuronal cells, which in turn, transmit the signal via the optic nerve to the brain (Figure 1.1).

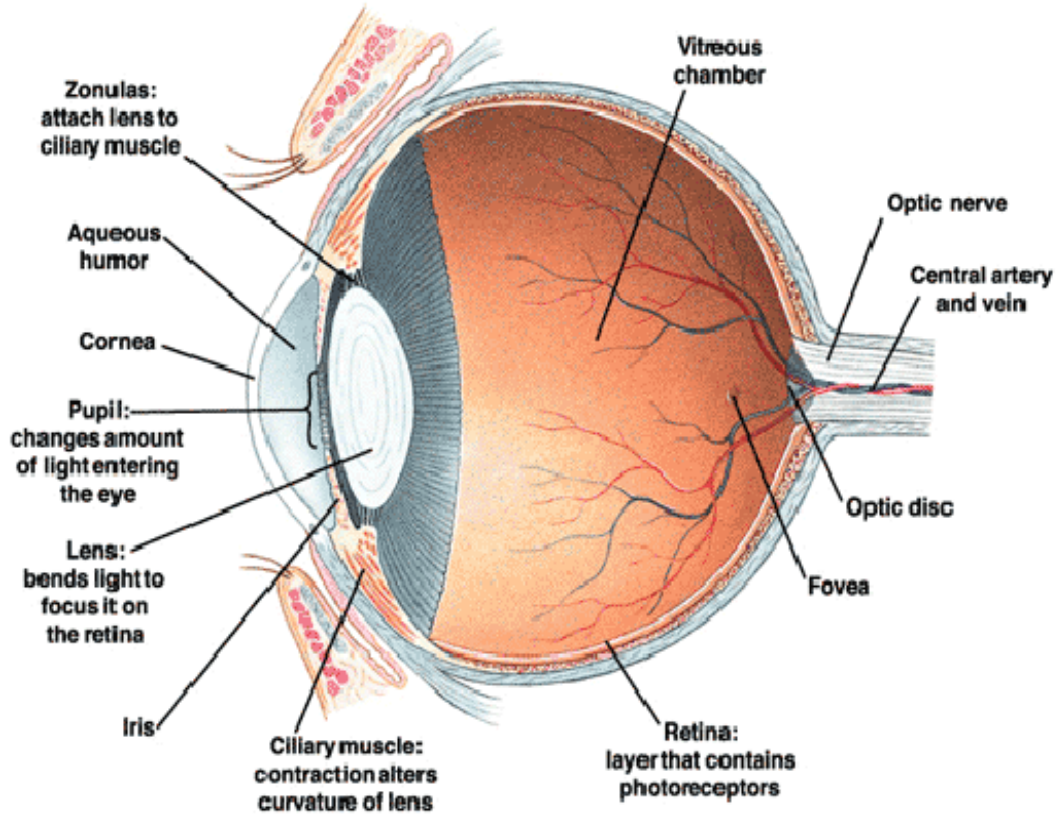

Figure 1. : Diagrammatic cross section of a human eye showing the anatomical location of the retina and components of the eye that facilitate vision. Reproduced from (http://www.big-images.com/).

The retina, which originates from the embryonic neuroectoderm (Dowling 1987; Clarke et al. 2000), is organised into four nuclear layers (Figure 1.2), namely: the retinal pigment epithelium (RPE), outer nuclear (OL), inner nuclear (IL), and the ganglion cell. Each layer contains distinct cells that perform specific functions in the phototransduction cascade. Photoreceptors, which are found in the OL of the retina adjacent to the RPE, perceive and convert light into a neuronal signal that is transmitted to the brain via the optic nerve. This process, in which light signals are converted into electrical signals that can be transmitted to the brain, is known as phototransduction.

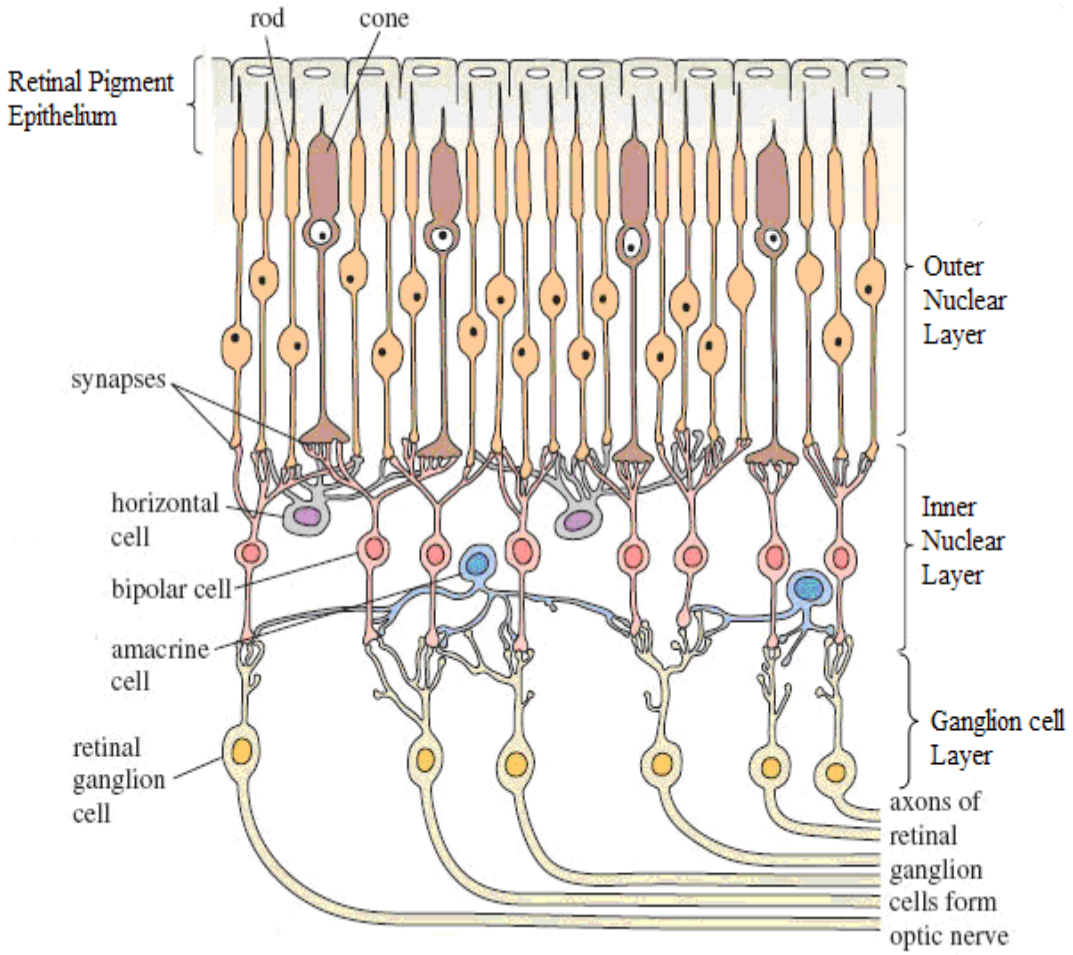

Figure 1. : Schematic diagram of the retina showing the arrangement of the four nuclear layers. The Retinal Pigment Epithelium (RPE) (top most layer) supplies nutrients and metabolites for the photoreceptors that are below it. The outer nuclear layer consists of rod and cone photoreceptor cells whereas the inner nuclear layer contains neurons such as bipolar, amacrine and horizontal cells that transmit neurotransmitters to the ganglion cell layer. Adapted from (http:\\www.openlearn.open.ac.uk).

The RPE and photoreceptors form a functional unit in that the RPE provides nutrients and metabolites to the photoreceptors, and performs phagocytosis of the membrane discs, which are found in the outer segment of the photoreceptors.

1.1.1. Photoreceptors and the phototransduction cascade.

The outer nuclear layer in the retina contains an uneven distribution of rod and cone cells (van Soest et al. 1999; Clarke et al. 2000). Rod cells, which represent the majority of photoreceptors in the retina, mediate vision in dim light conditions. In contrast, cone cells, concentrated at the centre of the retina, (also known as the

macula), mediate vision in bright light, and allow for the perception of details and colours (van Soest et al. 1999). Rods and cones effectively employ the same phototransduction cascade, but with different homologs for most of the components of the signalling pathway (Hims et al. 2003). A substantial body of research on RDDs to date has focused on rod photoreceptor cells and RHO (Kennan et al. 2005) and for the purposes of this study, cone cells shall not be discussed further.

Rod photoreceptors consist of an outer segment (OS) and an inner segment (IS) (Figure 1.3). The rod IS contains the metabolic machinery of the cell and is connected to the OS by the connecting cilium (van Soest et al. 1999; Clarke et al. 2000). The OS is a highly specialised compartment, containing numerous membrane discs stacked in an ordered array along the axoneme (Liu et al. 2004). The axoneme, which forms a backbone for the arrangement of the discs, is a micro-tubule cytoskeleton that runs from the IS to the OS through the connecting cilium (A. Kennan et al. 2005).

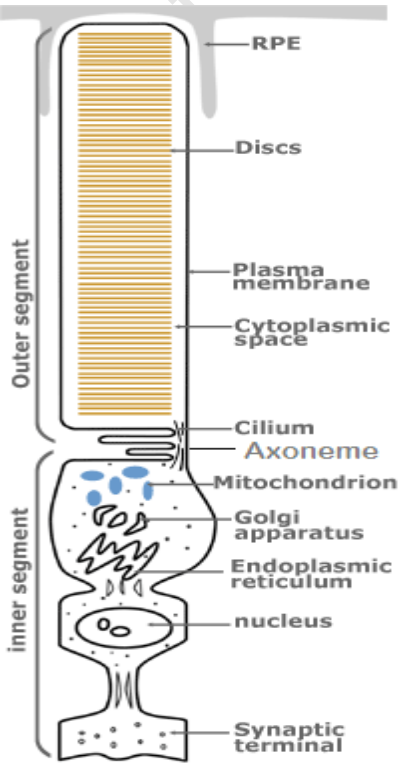

Figure 1. : Schematic diagram of a rod photoreceptor cell showing the outer (containing the disc membranes) and inner segments. RHO is transported from the inner segment (metabolic machinery) to the outer segment where it is targeted to the plasma membrane of the discs. Adapted from (www.chm.bris.ac.uk/webprojects2002/upton/rods.htm).

The membrane discs in the OS are constantly shed and removed through phagocytosis, by the RPE (van Soest et al. 1999). RHO, a transmembrane protein covalently linked to the 11-*cis* retinal chromophore, initiates the phototransduction cascade in rod cells. Mature RHO is found exclusively in the disc membranes of the OS of rod cells. Upon photon absorption by the retina, 11-*cis* retinal is converted to its isomeric form, all-*trans* retinal, which results in a conformational change of RHO to Meta II RHO (Figure 1.4). This action triggers transducin to activate phosphodiesterase (PDE) which hydrolyses cyclic-guanosine 5′-monophosphate (cGMP) to guanosine 5′-monophosphate (5′-GMP). The decrease in cGMP results in the closing of cGMP-gated channels. Once the channels are closed, the influx of Na^{+} and Ca^{2+} ceases, resulting in the hyperpolarisation of the OS membrane. The hyperpolarisation of rod photoreceptors triggers closure of the voltage-gated Ca^{2+} channels at the synapses, which results in a decrease in the release of excitatory neurotransmitter molecules (Clarke et al. 2000). These molecules then transmit the signal to the visual cortex of the brain (van Soest et al. 1999; Hims et al. 2003; Rattner et al. 1999). Subsequently, rhodopsin kinase phosphorylates all-*trans* retinal rhodopsin, returning it to its original state (Smith et al. 2009).

A deluge of research in the 1980s capitalised on the aetiology of many RDDs and the availability of genetic tools aimed at identifying underlying genes. As a result, many RDDs were linked to components of the phototransduction cascade. Most importantly, this led to the identification of novel processes and physiological components, including structures within the retina, underlying RDDs.

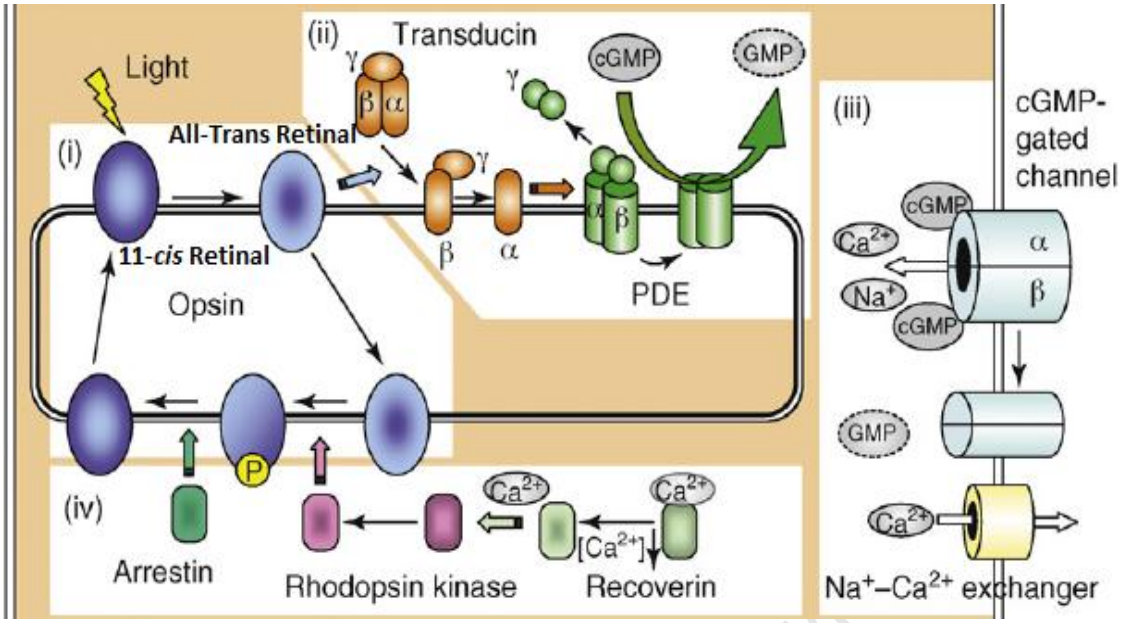

Figure 1. : Schematic diagram of the phototransduction cascade. (i) All–*trans* retinal activates (ii) transducin by detaching the α-subunit from the βγ-complex. The α-subunit of transducin in turn activates phosphodiesterase (PDE) by detaching the γ-subunit from the αβ-complex. The αβ-PDE complex hydrolyses cyclic GMP to 5′GMP. (iii) Hyperpolarisation of cGMP channels creates a signal that is transmitted to the neurons in the retina. The Na+-Ca^{2+} exchanger, however, continues its activity and the decreased levels of Ca^{+} result in the release of Ca^{2+} from the recoverin protein, thereby activating it. (iv) Activated recoverin activates rhodopsin kinase which phosphorylates (P) all-*trans* retinal RHO, after which, arrestin returns RHO to its original conformation, 11-*cis* retinal. Reproduced from Smith et al. (2009).

1.2. Inherited retinal degenerative disorders

Numerous proteins are involved in the formation and maintenance of the rod photoreceptor cell (Kennan et al. 2005). The diagram below (Figure 1.5) depicts a functional categorisation of genes in which mutations may be involved in photoreceptor degeneration.

Understandably, defective genes involved in ciliary transport, plasma membrane (lipid metabolism) and ion channel formation, make the largest contribution to photoreceptor degeneration (Figure 1.5). Proteins involved in these processes significantly determine the survival and integrity of photoreceptor cells.

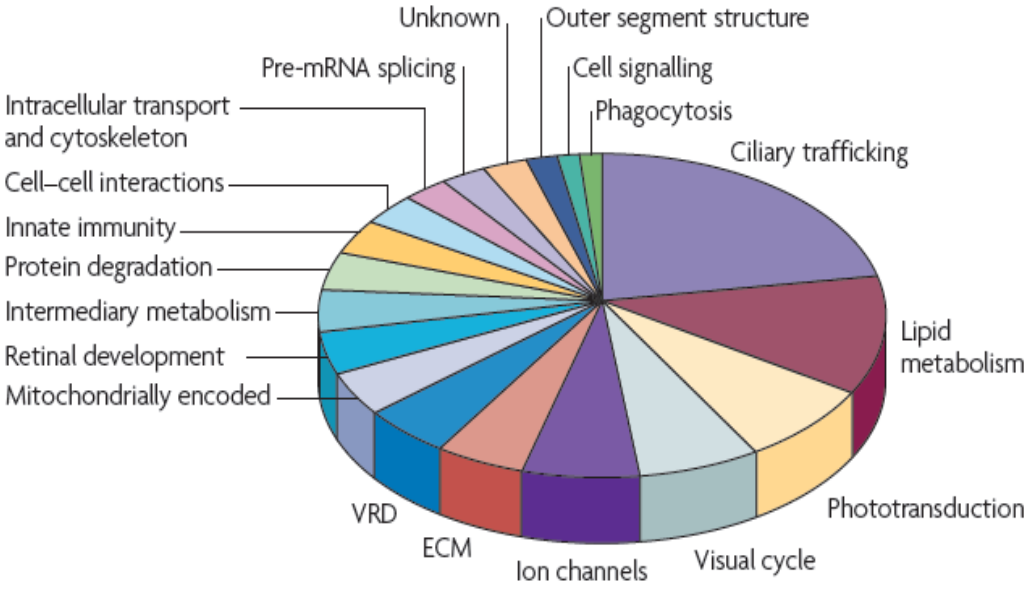

Figure 1. : A pie chart depicting the functional contribution of various genes to photoreceptor degeneration. Defective genes coding for proteins involved in ciliary trafficking, which occurs in the inner segment of photoreceptor cells make the largest contribution, followed by lipid metabolism which plays an integral part in plasma membrane formation. ECM represents the extra-cellular matrix and VRD represents vitreoretinal degeneration. Reproduced from Wright et al. (2010).

1.2.1. Mechanisms of photoreceptor death

Mechanisms by which mutations in genes and associated proteins expressed in photoreceptors result in cell death are still widely unknown. Nonetheless, there seems to be consensus on the process of apoptosis being the main mode of cell death (Wright et al. 2010). Cellular defects proposed to activate pro-apoptotic pathways include ciliary transport defects, endoplasmic reticulum stress, and metabolic stress. Ciliary transport defects in rod cells involve the axoneme, through which newly synthesized proteins, such as RHO, are transported to the outer segment of the cell. A defect in this transportation system as a result of ciliary-associated protein defects may thus lead to photoreceptor degeneration.

Similarly, mutations that confer a misfolding phenotype on proteins lead to inhibited trafficking through the endoplasmic reticulum. The misfolded proteins form aggregates which prompt the unfolded protein response (UPR) that ultimately activates pro-apoptotic pathways (Mendes & Cheetham, 2008; Tam & Moritz, 2006; Kosmaoglou et al. 2008; Hartong et al. 2009; Griciuc et al. 2010; Wright et al. 2010).

Finally, mutations in genes coding for proteins involved in the metabolism process of photoreceptor cells, are thought to induce metabolic stress, which consequently activates the apoptotic pathway (Wright et al. 2010).

Clinical analyses of retinal dystrophies have shown that cell death can be regional (Rattner et al. 1999; Pacione et al. 2003). This phenomenon has been attributed to specific mutations which affect certain areas of the retina more severely than other regions, possibly due to differences in cellular gradients such as those of growth factors found in the surrounding photoreceptor cell environment (Pacione et al. 2003).

1.3. Retinitis Pigmentosa

Retinitis Pigmentosa (RP) is the most common form of inherited RDD and affects approximately one in 3,500-4,000 individuals, worldwide (Bowne et al. 1999; Hartong et al. 2006; Tan et al. 2009). RP is a collective term used to describe a highly heterogeneous group of retinal diseases that are characterised by a degeneration of rod cells, followed by cone death (Hims et al. 2003; Hartong et al. 2009; Mendes et al. 2005; Kennan et al. 2005). Typical symptoms of RP include night blindness and gradual loss of peripheral vision, both of which occur as a direct result of the death of rod photoreceptor cells (Hartong et al. 2006; Kennan et al. 2005; Rattner et al. 1999). Subsequent death of cone cells leads to central vision loss which progresses to complete blindness in approximately 30% of cases (Hims et al. 2003; Ziviello et al. 2005).

In addition to vision loss, the death of rod and cone cells leads to the migration of RPE cells into the degenerating retina, which results in an accumulation of intra-retinal pigment deposits (Figure 1.6) (Phelan & Bok 2000) . These deposits resemble ‘bony spicules’ and it is this phenomenon that gave rise to the name ‘retinitis pigmentosa’ (Phelan & Bok 2000; Kennan et al. 2005). Other features of RP include a waxy pale pallor of the optic discs and a reduced electroretinogram (ERG). In some cases, cataracts, astigmatism, and myopia may occur (Phelan & Bok 2000).

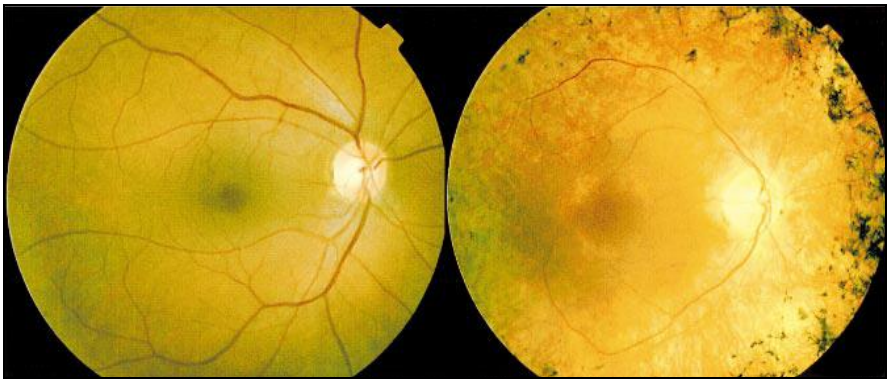

Figure 1. : Comparison of fundus photographs of a normal retina (left) and an RP affected retina (right). The pigmentary 'bony spicule' deposits are visible as dark spots on the fundus and blood vessels appear attenuated in comparison to those on the left. Reproduced from www.snof.org

RP can be classified according to inheritance patterns, which include autosomal dominant (AdRP), accounting for 15-20% of cases, autosomal recessive (ArRP) which accounts for 20-25% and X-linked RP (XlRP) accounting for 10-15% of cases (Daiger et al. 2007). In addition, there have been reports of mitochondrial (Mansergh et al. 1999) and digenic forms of RP, however these are rare (Hartong et al. 2006; Daiger et al. 2007; Wright et al. 2010). In addition to these multiple modes of inheritance, RP may also be a component of complex syndromes that exhibit retinopathy as part of a clinical feature such as Usher's and Bardet-Biedl syndromes (Hartong et al. 2006; Daiger et al. 2007; Farrar et al. 2002). Collectively, cases of RP that have a retinal phenotype only, can be described as non-syndromic RP. To date, approximately 46 genes have been associated with these non-syndromic forms of the disease (http://www.sph.uth.tmc.edu/Retnet/sum-dis.htm). The remaining 50% of RP cases do not have a known genetic component and can be sporadic i.e. spontaneous mutations that show no family history (Hims et al. 2003; Wright et al. 2010; Daiger et al. 2007; Wang et al. 2005). The age of onset of RP, a significant feature in clinical diagnosis, has been suggested to correlate with the relevant mode of inheritance, where dominant forms of RP generally have a later age of onset compared to recessive and X-linked forms (Phelan & Bok 2000).

An accurate diagnosis of RP in patients is further confounded by the clinical heterogeneity observed, with symptoms which range from mild to severe (Rattner et al. 1999; Phelan & Bok 2000). At present, clinical tests used to diagnose RP (apart

from clinical presentation), include measurements of visual acuity, imaging fundus (retina) reflectometry, electroretinograms (ERGs) which measure rod and cone function and Goldman visual fields (Niemeyer et al. 1992; Jacobson et al. 1994; Iannaccone et al. 2006). Family history is a similarly useful tool in diagnosis and tracking of disease penetrance.

1.3.1. Autosomal dominant retinitis pigmentosa

Autosomal dominance describes a mode of inheritance in which a single copy of the defective gene results in disease. AdRP exhibits clinical heterogeneity within family members who carry the same mutation, showing differences in severity and progression of the disease. According to Fishman et al., (1985), up to four AdRP subtypes have been distinguished on the basis of clinical phenotype, with most cases being classified as either type 1 or type 2. For the purposes of this review, only types 1 and 2 will be discussed. Type 1 AdRP is characterised by diffuse pigmentary changes with non-detectable rod function whereas cone function is preserved. In type 2 there is regional photoreceptor dystrophy resulting in regional or 'sectoral' pigmentary changes. Type 1 AdRP has been associated with early onset of RP symptoms whereas in Type 2, symptoms present later (in the third decade) of life (Fishman et al. 1985).

Currently, 17 genes have been linked to AdRP, including *CA4*, *CRX*, *FSCN2*, *GUCA1B*, *1MPDH1*, *NR2E3*, *NRL*, *PRPF3*, *PRPF8*, *PRPF31*, *PRPH2 (RDS)*, *RHO*, *ROM*, *RP9*, *SEMA4A*, *TOPORS* and *RP1* (http://www.sph.uth.tmc.edu/Retnet/sum-dis.htm#B-diseases). A few genes, including *RHO*, have been implicated in both AdRP and ArRP. In general, recessive forms of RP have been associated with genes that play a role in the visual cycle and phototransduction cascade, whereas genes encoding for proteins involved in photoreceptor structural maintenance, such as *RHO*, transcription factors and splicing factors have been shown to cause dominant RP (Hims et al. 2003; Wright et al. 2010). The RHO protein, as mentioned previously is involved in the initial process of the phototransduction cascade and is found in the plasma membrane of outer segment membrane discs. To date, more than 150 mutations have been identified in the *RHO* gene alone (Farrar et al. 2002). A comprehensive database of identified genes and mutations can be found in

(http://www.sph.uth.tmc.edu/Retnet/disease.htm#03.202d). This review will focus on *RHO* and mutations thereof.

1.4. RHO and disease

The RHO protein is encoded by the *RHO* gene, found on the long arm of chromosome three at position 3q21-24. The *RHO* gene consists of five exons, with the 5'UTR and initiation codon being found in exon 1. These five exons code for RHO, a seven transmembrane protein and a prototypic guanine nucleotide-binding protein coupled receptor (GPCR) that transduces photosignals from the environment into the rod photoreceptor cell (Mendes et al. 2005; Morris et al. 2009; Murray et al. 2009). RHO consists of the rod opsin protein, which is a 348 amino acid protein (containing the cytoplasmic transmembrane, and intradiscal domains), bound to the chromophore 11-*cis* retinal by a Schiff base (Figure 1.7) (Garriga & Manyosa 2002; Kaushal & Khorana 1994). RHO is exclusively found in the outer segment of rod photoreceptor cells where it facilitates phototransduction (Breikers et al. 2002; Morris et al. 2009). In addition to its involvement in the initial step of the phototransduction cascade in rod cells, RHO is suggested to play an important structural role in maintaining the shape of outer segments (Hims et al. 2003).

A pathogenic mutation in *RHO* was originally identified in 1990 (Dryja et al. 1990). Mutations in *RHO* have since been found to be the most common cause of RP, accounting for approximately 16%-30% of AdRP cases internationally (Macke et al. 1993; Gal et al. 1997; Phelan & Bok 2000; Weleber 2003; Iannaccone et al. 2006). Of the more than 150 *RHO* mutations identified, two mutations, namely Pro-347-Leu (P347L) and Thr-58-Arg (T58R) have been reported to commonly occur in Europe and the USA (Farrar et al. 1990; Daiger et al. 1995; Weleber 2003). Incidences of the P347L mutation have been reported in Germany, UK and the USA (Tartellin et al. 1996). The Thr-58-Arg mutation has also been reported to be a common mutation in the USA and UK (Daiger et al. 1995; Weleber 2003).

Following the discovery of mutations in *RHO*, two major classes of mutations were proposed (Sung et al. 1993; Sung et al. 1991). Class I (Type I) mutations were found to occur in the C-terminus of the RHO protein and were similar to the wild type protein in terms of folding, translocation to the plasma membrane and formation of a

functional chromophore (Sung et al. 1991; Sung et al. 1993; Rajan & Kopito 2005). Class II (Type II) mutations on the other hand, implicate misfolding of the protein, accumulation in the Endoplasmic Reticulum (ER) and an inability to form a functional chromophore with 11-*cis* retinal (Sung et al. 1991; Sung et al. 1993). Since then, other groups proposed a third class of mutations based on structure-function studies as well as biochemical and cellular pathologies (Chuang et al. 2004; Kaushal & Khorana 1994).

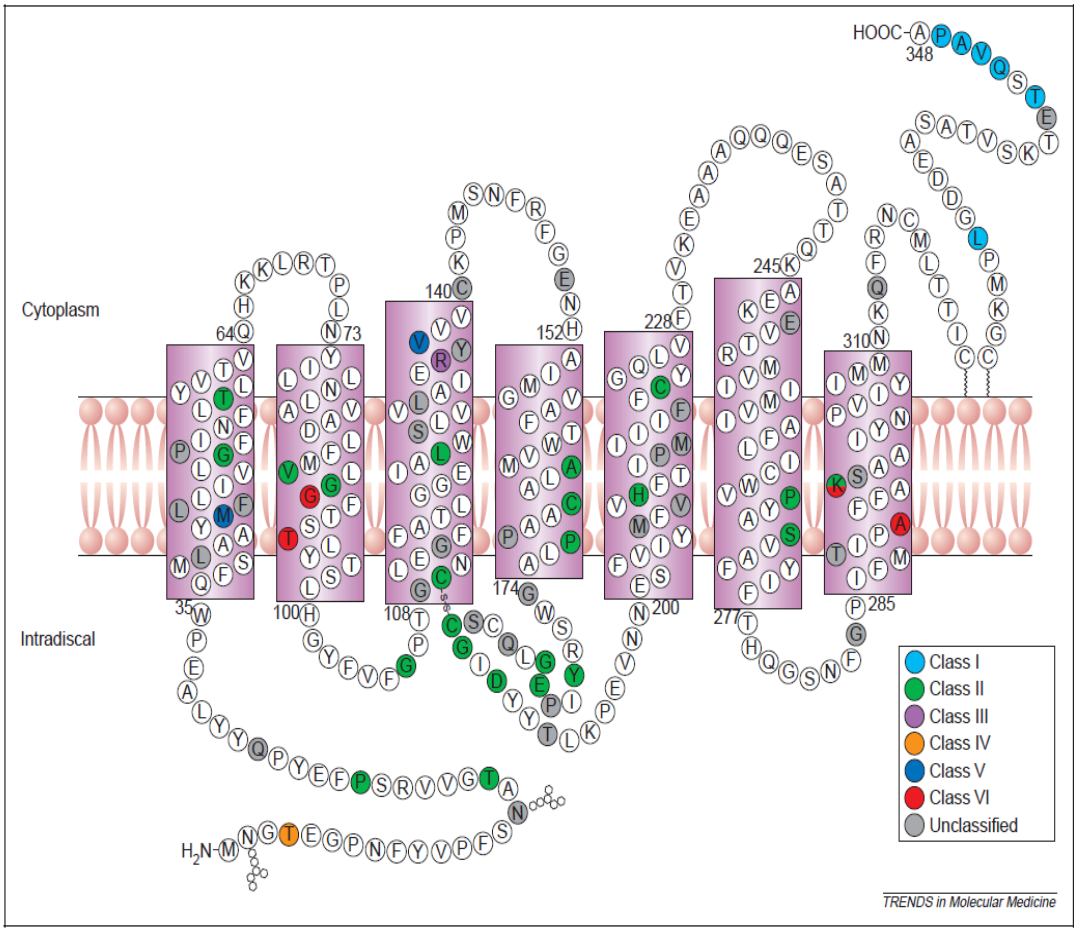

Figure 1.: Schematic diagram of the secondary structure of RHO. The seven transmembrane segments (shaded and boxed in purple) are shown spanning the plasma membrane. The different classes of mutations are highlighted in various colours. The two asparagine amino acids with moieties attached (positions 2 and 15), are representative of N-glycosylation sites in the protein. Reproduced from Mendes et al. (2005).

Subsequently, the Cheetham group (University College London) devised an updated system of classification of *RHO* mutants that includes the previous information and new data (Mendes et al. 2005). This method of classification is outlined in Table 1.1.

Molecular mechanisms by which mutations in *RHO* result in AdRP have also been proposed by Mendes et al. (2005), including misfolding, gain of function and dominant negative effects. Of these, misfolding of the RHO protein, which refers to the incorrect folding of the tertiary structure of the protein in a manner that limits functionality and processing, appears to be the major molecular pathology causing RP (Garriga & Manyosa 2002).

Table 1. : Classification of RHO mutations. (Reproduced from Mendes et al. (2005)**.**

CLASS	DESCRIPTION
Class I	Mutants resemble wild type protein but are not transported to the outer segment
Class II	Mutants are misfolded, do not form a functional chromophore and are retained in the endoplasmic reticulum
Class III	Mutants affect endocytosis
Class IV	Mutants do not affect folding only but also affect rod opsin stability and post-translational modifications
Class V	Mutants exhibit increased activation rate for transducin
Class VI	Mutants result in the constitutive activation of rod opsin in the absence of chromophore and in dark states

1.4.1. RHO mutations in South Africa

In South Africa, the 'Genetics of RDD' project was initiated in 1990 in the Division of Human Genetics at the University of Cape Town (UCT) (Greenberg et al. 1994; Rebello et al. 2002) . Biological samples from over 1,200 (Unpublished data) South African families with corresponding clinical and demographic data have been collected and recorded in the registry. The main objective of the RDD project is to identify the causative mutation in each family registered in the database, with the aim of improving disease management (Greenberg et al. 1994).

Similar classes of mutations documented in European and Western countries, have also been reported in South Africa, although at different frequencies. The frequency of AdRP cases observed in South Africa was originally documented by Oswald et al. (1985) as 22% of all recorded RP cases, and was subsequently reported to be 28% (Greenberg et al. 1994). To date five distinct *RHO* mutations have been identified in five South African families, with AdRP. The T58R mutation was found to be present in two members of a Caucasian family and the P347L mutation was found in one

member of an indigenous African family (Greenberg et al. 1999). The other three mutations, Thr-17-Met (T17M), Gly-109-Arg (G109R) (Goliath et al. 1998) and Asp-190-Asn (D190N), were found in each of three Caucasian families respectively.

A case-control study on sequence variants in *RHO* suggested that a particular single nucleotide polymorphism (SNP) in the 5′UTR promoter region of the *RHO* gene, g.269A>G (c.-26A>G), was associated with an increased risk of RP (Wang et al. 2005a) . Subsequently, a study performed in the Division of Human Genetics at UCT (Roberts L, MSc Thesis, UCT, 2006) on samples from the South African population identified the c.-26A>G SNP in 43% of RP-affected individuals screened; a much higher frequency than the 14% reported in a USA cohort. In addition, the frequency of the c.-26A>G SNP in control cohorts in South Africa consisting of Caucasian and indigenous African individuals, was 34% and 95% respectively. An investigation into the functional effect of this *RHO* c.-26A>G variant, could contribute to improved understanding of the molecular mechanisms underlying RP.

1.5. Phenotypic variation

The widely accepted premise of monogenic 'Mendelian' disorders is that mutations in the relevant genes consistently result in disease. This impression is however gradually changing, with differences being observed in the penetrance and expressivity of some diseases that suggest the influence of other factors (Knight 2004b). These factors may contribute to the heterogeneity observed in these diseases, of which RP is a typical example.

The environment and genetic modifiers, as well as allelic and molecular heterogeneity may play a significant role in the manifestation of the disease (Daiger et al. 2006). Numerous theories have been proposed to account for the variable phenotypes observed in patients suffering with RP. One such theory is that molecular heterogeneity within photoreceptors plays a role in progression of disease (Pacione et al. 2003). The gradient distribution of growth and neurotrophic factors across the retina (which determines the distribution and function of photoreceptors in the retina), has been suggested to play a role in the rate and region of retinal degeneration (Lavail et al. 1998; Ozawa et al. 2010). Experiments with transgenic mice containing known retinal degenerative mutations, have shown that the addition

of the growth and neurotrophic factors, also known as survival factors, reduce the rate of degeneration of photoreceptors (Lavail et al. 1998; Ozawa et al. 2010). Gradients in these factors, although not proven, may account for the prolonged survival of rod photoreceptor cells in some individuals with RP (Pacione et al. 2003).

Furthermore, epigenetics, which involves differences in the expression patterns of genes as a result of chromatin modification, may also contribute to phenotypic variation. Methylation patterns and histone modifications, which determine the specific expression of genes, have been shown to be altered considerably in diseased tissues (Cvekl & Mitton 2010). Factors such as environment and ageing may also influence chromatin modifications, thereby altering the disease course (Cvekl & Mitton 2010). Non-coding RNAs, such as microRNAs that are normally expressed in tissues have also been shown to play a role in chromatin regulation and transcription. For instance, in a recent study, altered microRNA expression profiles were observed in a mouse model of RP associated with the P347L mutation (Loscher et al. 2007).

Similarly, sequence variations existing in the disease-causing gene itself and/or other interacting genes (also known as genetic modifiers) may significantly affect the phenotypic manifestation of the disease (Nadeau 2003).

1.5.1. Genetic disease modifiers

The Human Genome Project (HGP) has allowed the identification of many genes underlying disease. Furthermore, due to the wide range of phenotypic variation exhibited by organisms as a result of primary mutations, genetic modifiers have recently garnered interest (Nadeau 2003; Knight 2004b; Lammich et al. 2010). Modifier genes and alleles provide clues to the functional aspects and molecular interaction of gene products, which may provide insight for novel treatments and prevention of disease (Haider et al. 2002; Nadeau 2003). In most diseases where modifiers are thought to play a role, methods employed to identify the modifying effect have included haplotype and linkage disequilibrium analysis (Pacione et al. 2003).

Generally, modifier genes have been shown to cause a more severe phenotype with an earlier onset of disease. Modifiers can, however, suppress the mutant phenotype such that the disease is milder or has a slower rate of progression (Haider et al.

2002). This class of modifiers are termed 'protective alleles' (Nadeau 2003). Protective alleles are proposed to occur in higher frequencies in healthy individuals, preventing the manifestation of the disease despite the presence of a disease-causing allele (Nadeau 2003). Genetic modifiers may be in the form of single nucleotide changes, also known as single nucleotide polymorphisms (SNPs) that may or may not result in an amino acid change.

1.5.2. Functional significance of SNPs

SNPs are reported to occur on average once in every 1000 base pairs, and account for some of the genetic variation observed in organisms (Knight 2003). Two different categories of SNPs exist: synonymous SNPs that do not alter the amino acid component of the protein, and non-synonymous SNPs (missense or nonsense mutations) which change the amino acid component of the protein, and may ultimately alter its properties. Non-synonymous SNPs occurring in coding DNA sequences may result in changes such as truncation of the protein or alteration of the binding affinity of regulatory factors to the protein. The functional effect caused by a missense mutation depends on the location of that mutation as well the resulting change in amino acid.

1.5.3. Variation in non-coding regions of DNA

Most genetic variants known to have functional consequence are located in exonic or coding sequences. However, more recently, genetic variations in non-coding regions have garnered interest (Knight 2004b). These non-coding regions range from the un-translated regions in mRNA to the intronic sequences, which are found between exons. Variation in each of these regions, depending on the significance of the motif or DNA sequence and location, may elicit some kind of functional significance on the gene. The effects of these genetic variants range from changing protein composition through altered splicing to regulation of gene expression. For instance, in a recent study on Alzheimer's disease, it was found that the expression of the ADAM10 protein was significantly regulated by the 5′UTR of the corresponding gene (Lammich et al. 2010). Polymorphisms in areas such as the 5′UTR and intronic regions are proving to be more significant than previously thought in terms of regulatory mechanisms, which could potentially determine disease progression

and severity (Wilkie et al. 2003; Chung et al. 2006; Halder et al. 2009; Cenik et al. 2010; Lammich et al. 2010).

Numerous techniques have been employed to identify the functional effect of non-synonymous SNPs, including western blotting and immunocytochemistry. The effects of variants found in non-coding regions, such as promoters and intronic sequences, may be more difficult to measure, although these may significantly alter the expression profile of the gene or protein altering binding affinities (Knight 2003; Knight 2004b). Several techniques have been employed in an attempt to elucidate the effects of SNPs in non-coding regions, including *in-vitro* assays of protein-DNA interaction, Allelic Expression Imbalance (AEI) and luciferase assays (Knight 2004a). These assays, together with the above mentioned techniques, have increased the potential of determining the functional significance of DNA variants and assessing their impact on the clinical variability of disease (Rebbeck et al. 2004). More specifically, the identification of modifiers in this study could increase the prognostic utility of RDD investigations by enabling health care professionals to better predict the effect of the SNP on the RP disease course.

1.6. Aims and objectives

The aim of this study was to determine whether the c.-26A>G SNP in the *RHO* gene potentially modifies the phenotype of RP in South African patients, using various mammalian cell lines as a model.

The objectives included;

a) Determining *in silico* the effects of the c.-26A>G variant using bioinformatic tools to:

    i. Establish the protein-protein interactions of RHO

    ii. Establish the conservation status of the area surrounding the SNP, and

    iii. Predict the effect of the variant on expression of RHO

b) Screening a cohort of five families with known *RHO* mutations, using restriction fragment length polymorphism (RFLP) analysis and sequencing, to determine whether patients who are affected with RP, carry the c.-26A>G 5′UTR variant *in cis* or *in trans* with their specific disease-causing mutation.

c) Establishing the *in vitro* effects of the c.-26A>G variant on the RHO protein by:-

    i. Investigating the effect of the c.-26A>G variant when *in cis* with three pathogenic mutant constructs, using western blot analyses to determine any differences in RHO protein expression, and immunocytochemistry to localise the transfected protein. The c.-26A>G variant, together with three known pathogenic mutations namely; T4K, T17M and P347L, will be created using site-directed mutagenesis and transfected into HT1080, HEK-293 and SKNSH cell lines.

    ii. Quantifying mRNA transcript expression differences for each of the above mentioned variants using RT-qPCR.

Chapter 2: Materials and Methods

2.1. Bioinformatic analyses of the *RHO* 5'UTR c.-26A>G variant and screening in an AdRP Cohort

The first approach of this study employed bioinformatic tools to predict the potential effects of the c.-26A>G variant in RHO. In addition, the incidence and location (*cis* or *trans*) of the c.-26A>G SNP variant was determined in five families with known *RHO* mutations.

2.1.1. Bioinformatic analyses of the *RHO* c.-26A>G variant

The objectives of the bioinformatic analyses were to a) determine the protein interaction profile of RHO; b) determine the sequence conservation status of the region surrounding the 5′UTR c.-26A>G (dbSNP: rs7984) variant, and c) predict the potential effects of the c.-26A>G variant. The protein interaction profile of RHO was determined using STRING (http://string-db.org/), which is a "database of known and predicted protein interactions, including direct (physical) and indirect (functional) associations" (Jensen et al. 2009). As an additional tool, BioGrid version 3.1 (http://www.thebiogrid.org), an online interaction database with comprehensive data on major organisms, was used. In both cases, the protein name 'Rhodopsin' was entered as a search term.

In order to determine sequence conservation status of the *RHO* 5′UTR region, an alignment of vertebrate species sequences was retrieved using the UCSC (University of California Santa Cruz) Genome Browser (http://genome.ucsc.edu/index.html?org=Human&db=hg19&hgsid=183146199). Similarly here, the protein name was used as a search term and the sequence region of the 5′UTR was expanded to reveal alignment and conservation.

Further analysis using the mFOLD web software (Zuker, 2003), was performed to determine differences in RNA secondary structure that may determine the effect of the c.-26A>G SNP in *RHO*. The mFOLD webserver (http://mfold.rna.albany.edu/?q=mfold/RNA) predicts RNA secondary structure, providing structural folding efficiencies and free energies. *RHO* 5'UTR mRNA

sequences containing either the 'A' allele or the 'G' allele were submitted for analysis.

Lastly, the Transcriptional Element Search System (TESS) (http://www.cbil.upenn.edu/cgi-bin/tess/tess) was used to determine whether the c.-26A>G variant altered any transcription factor binding sites. TESS is a web-based tool for predicting binding sites in DNA sequences (Schug & Overton 1998). *RHO* sequences containing the 'A' or 'G' alleles were submitted and analysed. The tabular option of results was analysed in order to identify altered binding sites at the position of the SNP.

2.1.2. Cohort selection for c.-26A>G screening

The RDD registry in the Division of Human Genetics at the University of Cape Town was interrogated for families with *RHO* mutations known to cause AdRP. DNA samples were retrieved from the RDD DNA archive, which contains DNA that has been collected and stored for the broader RDD project. As a standard, when acquiring biological material, informed consent is obtained. Consent forms (Appendix A) used for the RDD project had been designed according to the conditions of the Declaration of Helsinki (2008). These consent forms had previously been approved by the University's Research Ethics Committee (REC REF 168/99 amended 2002 and 2005). For this particular study, ethics approval was also obtained (REC REF 185/2009, renewed 2010).

A total of 35 DNA samples, from five families with known *RHO* mutations, were retrieved. In addition, patient information including, ethnic origin, age of onset of RP, clinical description of disease and mutation location was obtained. Family pedigrees depicting ethnic origin and mutation can be found in Appendix A.

2.1.3. DNA quality control

Due to the fact that samples had been stored for long periods of time, it was necessary to perform integrity testing in order to establish the quality of DNA before proceeding with experiments. The concentration and purity of DNA samples was determined using the Nanodop® ND 1000 spectrophotometer (Nanodrop Technologies, USA). Working stock solutions of a total volume of 10 µl were then

prepared by diluting an aliquot of the stock DNA sample to a final concentration of 200 ng/µl using sterile distilled water (dH_2O) (SABAX-Adcock Ingram, SA). Approximately 2 µl of diluted DNA sample from each family member together with 5 µl loading dye (Fermentas, USA) was electrophoresed on a 1% agarose gel (Appendix B) (SeaKem, USA) containing Ethidium Bromide (EtBr) (0.6 µg/ml), at 160 V in Tris-Borate EDTA (TBE) electrophoresis buffer for 40 minutes (min). Visualisation was performed under Ultra Violet (UV) light on the UVIpro Gel Documentation system transilluminator (Uvitec, UK). The presence of smearing in a lane indicated degraded DNA whereas intact DNA was observed as bands of distinct high molecular weight.

2.1.4. PCR amplification

Polymerase chain reaction (PCR) amplification was employed to isolate and amplify the 5′UTR region containing the c.-26A>G variant, using previously designed *RHO* primers (Roberts L, MSc UCT, 2006). The sequences of both reverse and forward primers were as follows: forward 5′-TTCGCAGCATTCTTGGGTGG-3’ and reverse 5′-AGCAGGATGTAGTTGAGAGG-3’.

The above primers were diluted to a working concentration of 20 µM and used in a standard PCR, in a total volume of 25 µl which was prepared as follows: 5 µl 1X GoTaq™ reaction buffer (1.5 mM $MgCl_2$, pH 8.5) (Promega. Madison, WI, USA), 1 µl (200 µM) deoxynucleotide triphosphates (dNTPs) (Bioline, Michigan, USA), 0.5 µl (0.4 µM) each of forward and reverse *RHO* primers, 0.1 µl (0.5 U/µl) GoTaq™ DNA Polymerase (Promega), 1 µl (200 ng/µl) DNA and dH_2O to a total volume of 25 µl.

A temperature gradient PCR was performed to determine the optimum annealing temperature (Ta°C) of the primers, using the following cycling conditions: a denaturing step of 95°C for 5 min, followed by 30 cycles of 94°C for 30 seconds (sec), Ta°C ranging from 50°C-60°C for 30 sec, 72°C for 40 sec, and a final extension step of 72°C for 7 min. A volume of 5 µl loading dye (Appendix B) was added to 8 µl PCR products before electrophoresis on a 2% agarose gel (Appendix B) containing EtBr for approximately 40 min, prior to visualisation on the Uvidoc transilluminator. A size standard, Gene Ruler™ 100 bp DNA Ladder Molecular Weight Marker (Fermentas Life Sciences, Hanover, USA) (Appendix B), was used

to estimate the sizes of the PCR products. The expected product of 285 bp was amplified at an optimum Ta of 58.4°C. This annealing temperature and the previously listed amplification conditions were used for all subsequent PCR amplifications. A negative control (water blank) containing the PCR reagents and water instead of DNA was used in each PCR experiment.

2.1.5. Restriction fragment length polymorphism analysis

Restriction endonuclease digests were performed to determine the genotype of the c.-26A>G variant in amplified DNA samples. The full amplicon sequence was analysed using Web Cutter 2.0 (http://rna.lundberg.gu.se/cutter2/) to establish whether the variant introduced or deleted a restriction site. Restriction enzymes were prioritised based on their ability to cleave the amplicon only once or twice, resulting in easily distinguishable digest products. The restriction enzyme selected was *Ksp* I (Roche Applied Science, Mannheim, Germany). No *Ksp* I is present with the 'A' allele of the SNP, however a *Ksp* I restriction site is created by the 'G' allele, yielding digest products of either 255 bp and 30 bp for homozygous (GG) or 285 bp 255 bp and 30 bp for heterozygous (AG) genotypes. The duration of incubation, reaction buffer (supplied with the enzyme), and incubation temperature were guided by the manufacturer's instructions. As a standard, 8 µl of PCR product, 5 U of enzyme, 2.5 µl (1X) buffer L (Roche, Germany) and 14 µl of dH_2O (a total volume of 25 µl), was used in each reaction, with a further 1 U of *Ksp* I added after three hours and left to incubate overnight. The optimal incubation temperature of the digest was 37°C.

Analysis of restriction products was performed by electrophoresis of whole digest volumes, together with 5 µl of loading dye on a 2% agarose gel containing 0.6 µg/ml EtBr, at 160 V for approximately 40 min. The GeneRuler™ 100 bp DNA Ladder Plus (Fermentas Life Sciences, USA) was included in each gel for product size estimation. Electrophoresis gels were visualised under UV transillumination. For each digest reaction, four controls were included, namely an uncut amplicon and three DNA samples with the known c.-26A>G genotypes of 'GG', 'AA', and 'AG'. Each of the DNA samples with known genotypes had distinct banding patterns, which were used as a reference with which to compare the test samples.

A total of six DNA samples were chosen at random from the cohort for direct sequencing in order to verify the genotypes determined by restriction fragment length polymorphism analysis.

2.1.6. DNA sequencing

Direct cycle sequencing was performed for six DNA samples in order to validate genotypes obtained from the digest reaction. PCR products were purified using the QIAquick® gel extraction kit (Qiagen, UK) according to the manufacturer's instructions (Appendix B). Purified PCR products were sequenced using the same reverse primer used in PCR amplification (Table 2.1). The reverse primer was chosen for sequencing as opposed to the forward primer, due to the primer location and distance from the position of interest (c.-26A>G). Sequencing was performed using the BigDye® terminator cycle sequencing kit version 3.1 (Applied Biosystems, USA). Each sequencing reaction was prepared by combining the following in a 0.2 ml microfuge tube: 3 µl of PCR product, 0.5 µl primer (10 pmol), 2 µl (1X) BigDye® reaction mix and 4 µl of Big Dye Termination buffer, in a total volume of 20 µl made up with dH_20. The following cycling conditions were used: 96°C for 5 min and 30 cycles of (96°C for 30 sec; 50°C for 15 sec; 60°C for 4 min).

Subsequently, sequencing products were purified using the ethanol precipitation method outlined in Appendix B. Following ethanol precipitation, samples were air-dried for 30-60 min before being resolved on the ABI Prism™ 3100 capillary-based automated sequencer (Applied Biosystems, USA). A volume of 5 µl of purified sequencing product together with 8 µl Hi-Di™ Formamide was heat-denatured at 95°C for 5 min , cooled on ice for 10 min and loaded onto a 96-well plate, before being run on the ABI Prism™ 3100 automated sequencer. Analysis was performed using ABI Prism™ DNA Sequencing Analysis Software version 3.7.

The resulting sequences were analysed by Clustal W alignment to a reference (NM_000539.3) sequence, using BioEdit software version 7.0.9.0 (Hall, 1999).

2.2. Functional *in vitro* analyses of the c.-26A>G variant in mammalian cell lines

In this phase of the study, functional studies using mammalian cell lines were performed to determine the effect of the 5′UTR c.-26A>G variant. The wild-type *RHO* cDNA construct was used as a template for the creation of mutant variants, which were then cloned and isolated to facilitate transfection into cells.

2.2.1. Cloning

Human wild-type (WT) *RHO* (h*RHO*) cDNA in pCDNA 3.1+ vector was a kind gift from Professor Peter Humphries' Lab (Trinity College Dublin, Ireland) courtesy of Dr Sophia Millington-Ward. The structure of the pCDNA3.1+ vector is illustrated in Appendix B. RHO cDNA was cloned into Hind *III* and Eco*RI* multiple cloning sites of pcDNA 3.1 and consisted of the full length 5'UTR (96 bp), all five exons and part of the 3'UTR extending to 1, 000 bp after the last codon.

2.2.1.1. Preparation of competent cells

DH5α *Escherischia coli* (*E.coli*) cells were obtained from Dr Sharon Prince's Lab (University of Cape Town, South Africa). Competent cells were prepared according to the Calcium Chloride ($CaCl_2$) method as described in Sambrook et al. (1989) with minor alterations.

Specifically, a single colony of bacteria was inoculated in 5 ml Luria Broth (LB) (Appendix B) and incubated in a 37°C shaker overnight. A 1/100 dilution, i.e. 1 ml of the overnight culture was inoculated in 100 ml LB using aseptic technique and left to grow for 2-3 hr in a 37°C shaker until mid-log phase i.e. optical density of LB at 600 nm was between 0.5 and 0.8. Optical density was determined using a spectrophotometer. The 100 ml LB containing bacteria was then poured into two separate 50 ml tubes (BD-Falcon, USA) and pelleted by centrifugation at 3,000 revolutions per minute (rpm) for 10 min at room temperature. The pellet was resuspended using 1 ml ice cold 100 mM $CaCl_2$; an extra 30 ml was added before a second spin at 3,000 rpm for 10 min at 4°C. The pellet produced was resuspended again in 1 ml $CaCl_2$ and stored at -80°C in 200 µl aliquots with added glycerol. The

resulting competent cells were used for the initial transformation of h*RHO* in pCDNA 3.1+ vector and subsequent variants.

2.2.1.2. E.coli bacteria transformation

Previously frozen competent cells (in 1.5 ml microfuge tubes) were thawed on ice and 1 µl (315 ng/µl) of WT h*RHO* plasmid DNA was added, and subsequently incubated on ice for 10 min. The cells were subsequently heat shocked at 42°C for 2 min and snap cooled on ice for a further 2 min. Antibiotic-free LB medium (300 µl) was added to the cells, which were then incubated in a 37°C shaker for 30 min-1 hr. Following the incubation, 200 µl of *E.coli* cells (in LB) were plated onto pre-warmed selective agar plates containing Ampicillin (50 µg/ml) (Appendix B) using aseptic technique in order to select for transformed colonies. The agar plates were then incubated at 37°C overnight. As a negative control, cells 'transformed' with sterile dH_2O instead of DNA were also plated onto Ampicillin-containing agar.

Cells transformed with *RHO* constructs formed colonies (Ampicillin-resistant) on the plates and these were inoculated into 5 ml LB containing 50 µg/ml Ampicillin and incubated at 37°C overnight in a shaker prior to small-scale plasmid preparations (mini-prep). When a large-scale (midi-prep) preparation was required, 1 ml of the overnight culture was inoculated into 100 ml LB selective medium containing Ampicillin (50 µg/ml).

2.2.1.3. Small-scale and large-scale plasmid preparations

Small-scale preparations, were performed using the QIAprep® miniprep kit according to the manufacturer's guidelines (Qiagen, USA) whereas large-scale (midi-preps) preparations were performed using the HiSpeed® Plasmid Midi and Maxi Kit (Qiagen, USA). Purified WT h*RHO* plasmid obtained from the above preparations was used in a restriction endonuclease digest, followed by cycle sequencing to confirm the presence of the h*RHO* insert. Once confirmed, the purified WT h*RHO* plasmid was used as template DNA for site-directed mutagenesis PCR.

2.2.2. Site-directed mutagenesis

Site-directed mutagenesis (SDM) was performed to introduce mutations into the WT h*RHO* cDNA sequence, for the purposes of expression work in mammalian cells. A modification of the *Dpn* I method (Quikchange® Site-directed mutagenesis, Stratagene, USA) was used together with KAPA Hifi™ DNA polymerase. This site-directed mutagenesis method is a PCR-based assay, which employs mismatched primers to introduce mutations in a specified region of DNA. A flow diagram depicting the SDM process is provided in Appendix B.

2.2.2.1. Mutagenic primer design and PCR

SDM primers are designed to introduce point mutations at specific residues/nucleotides. In addition, the primers can also be used to introduce or remove a restriction endonuclease site through a 'silent' (synonymous) mutation to enable screening for the introduced change. In contrast to standard PCR primers, SDM primers range between 25-45 bp in length, are 100% complementary to one another and mismatched to the sequence of interest in order to introduce the desired mutation and are located 10-15 bp on either side of the mismatch (mutation site); preferably with an even number of base pairs on each side. The melting temperature of the primer is recommended to not be lower than 78°C, with a GC content of at least 40% and a G/C clamp at each end. The selection of primers was facilitated by DNAMAN software version 5.2.9. Selection of restriction endonuclease sites was facilitated by WATCUT software (http://watcut.uwaterloo.ca/watcut/watcut/template.php).

Putative primer sequences were analysed as follows: regions flanking mutation sites were analysed for the presence of restriction sites, following which, potential sites near the mutation point were selected (selecting for 6 bp cutters and common restriction endonucleases wherever possible). For some primers, a 'silent' mutation as described above had to be introduced to create a restriction endonuclease site adjacent to the desired point mutation.

Subsequently, vector and insert DNA was analysed using WATCUT software for the presence of the selected restriction sites and the number of cuts expected for these restriction sites (sequences with more than five sites in both vector and insert DNA were excluded). Finally, a restriction endonuclease was chosen based on the digest

products being readily distinguishable from the wild type sequence upon electrophoresis.

SDM was employed to create cDNA constructs containing the c.-26A>G variant, and three pathogenic mutations: T4K, T17M and P347L. The pathogenic mutations included in this study were selected based on their occurrence in the South African AdRP cohort except for the T4K mutation, which was chosen based on its *RHO* mutation class (IV) (Mendes et al., 2005). Primer sequences are outlined in Table 2.1 below.

Table 2. : SDM primers used to introduce mutations in hRHO cDNA. The nucleotide change in each primer is highlighted in red and the codon is indicated in the box. The silent restriction sites are underlined in blue. Lower case letters represent nucleotides in non-coding regions i.e. the 5′UTR and upper case letters represent nucleotides found in exons/coding regions of DNA. Each of the primers introduced a restriction site, except for c.-26A>G, in which the 'G' allele resulted in a restriction site.

Mutation	Sequence: 5'-3' Orientation	GC content (%) & primer length	Melting Temperature (Tm)	Silent Restriction Site	Total number of mismatches in primer sequence
c.-26A>G	**Fwd:** [ttcttgggtgggagcagccgcgggtcagccacaagg] **Rev:** [ccttgtggctgacccgcggctgctcccacccaagaa]	66.7; 36 bp	**87.3°C**	***Sac* II**	1 (introduces a SacII RE site)
T4K	**Fwd:** [GCCATGAATGGCAAAGAGGGCCCTAACTTCTACG] **Rev:** [CGTAGAAGTTAGGGCCCTCTTTGCCATTCATGGC]	52.9; 34 bp	**77.5°C**	***Apa* I**	2
T17M	**Fwd:** [CCTTCTCCAATGCGATGGGTGTCGTACGCAGC] **Rev:** [GCTGCGTACGACACCCATCGCATTGGAGAAGG]	78.5; 32 bp	**78.5°C**	***BsiW* I**	2
P347L	**Fwd:** [CGAGCCAGGTGGCCCTGGCCTAAGATCTGCCTAGG] **Rev:** [CCTAGGCAGATCTTAGGCCAGGGCCACCTGGCTCG	65.7; 35 bp	**83.4°C**	***Bgl* II**	2

The above primers were synthesised by Integrated DNA Technologies (IDT) (WhiteSci, SA). Mutagenesis PCR was set up as follows; in a single reaction, 10 µl of HiFi Buffer (5X), 1.5 µl of dNTPs (10 mM), 1.5 µl of 10 mM primers (forward

and reverse), 2 µl of cDNA (10 ng/µl) and 1 ul of Hifi™ Polymerase (1 U/µl) were added to 16.5 µl of nuclease free dH_2O.

For each of the mutations, the PCR was performed in duplicate with different concentrations of added $MgCl_2$ (no $MgCl_2$, 2 mM or 4 mM) in order to determine optimal PCR conditions. For each primer, the Ta°C was obtained from the accompanying information sheet received from the oligo manufacturer (IDT), as this value often differed with the theoretical value. The total reaction volume after addition of 4 mM $MgCl_2$ was 50 µl, and when 2 mM or no $MgCl_2$ was added, dH_2O was used to make up the volume. These reaction volumes and reagent concentrations were used for all mutagenic PCRs. The cycling conditions used are outlined in Table 2.2 below.

Table 2. : Summary of cycling conditions used in mutagenic PCRs.

Amplicon	**Cycling Conditions**				**$MgCl_2$ Concentrations used for optimal amplification**
	PCR Stage	**Temperature (°C)**	**Duration**	**Number of Cycles**	0 mM
5′UTR A>G	Denaturation	94 °C	2 min	1	
		98 °C	20 sec	20	
	Annealing	73.9 °C	15 sec		
	Primer Extension	68 °C	30 sec/kb (4.5 min)		
	Elongation	68 °C	30 sec/kb (4.5 min)	1	
T4K	Denaturation	94 °C	2 min	1	4 mM
		98 °C	20 sec	20	
	Annealing	65.7 °C	15 sec		
	Primer Extension	68 °C	30 sec/kb (4.5 min)		
	Elongation	68 °C	30 sec/kb (4.5 min)	1	
T17M	Denaturation	94 °C	2 min	1	2 mM
		98 °C	20 sec	20	
	Annealing	67.7 °C	15 sec		
	Primer Extension	68 °C	30 sec/kb (4.5 min)		
	Elongation	68 °C	30 sec/kb (4.5 min)	1	
P347L	Denaturation	94 °C	2 min	1	2 mM
		98 °C	20 sec	20	
	Annealing	71. 1°C	15 sec		
	Primer Extension	68 °C	30 sec/kb (4.5 min)		
	Elongation	68 °C	30 sec/kb (4.5 min)	1	

PCR products exhibiting the most significant amplification (greatest band intensity) following electrophoresis on a 2% agarose gel, were selected and digested with *Dpn I* overnight at 37°C, to eliminate remaining template DNA. *Dpn* I cleaves methylation sites on DNA sequences. Figure 2.1 below shows a typical gel image of SDM PCR for the T4K mutation constructs.

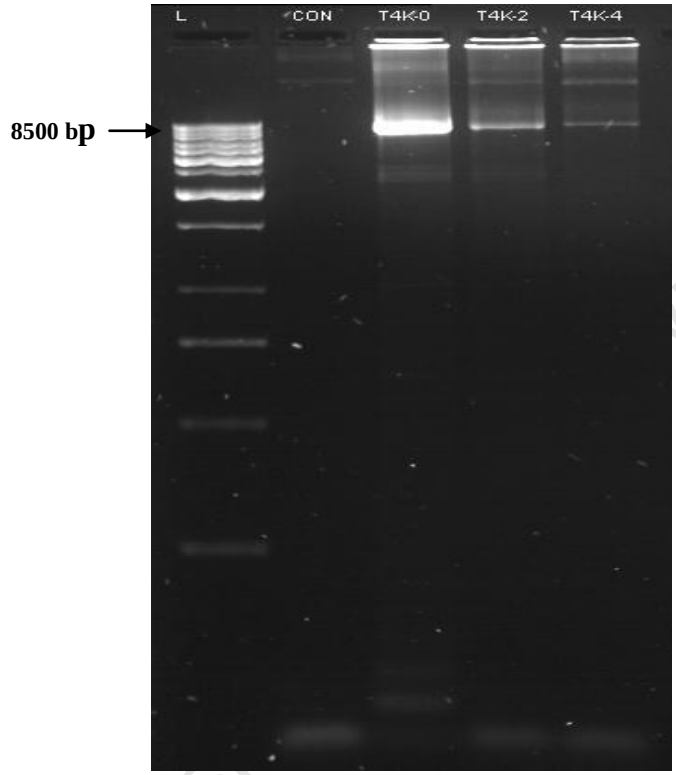

Figure 2. : Digital image of an SDM PCR gel. The lane marked L represents the ladder. All PCR runs included controls (CON) in which no cDNA construct was added to the reaction mix. The T4K SDM PCR was performed in three reactions containing 0 mM, 2 mM and 4 mM $MgCl_2$ as indicated by the numbers above the lanes. The arrow indicates the approximated size of the amplicon, which was 8500 bp.

The expected PCR product sizes for all PCRs was the same as that of the original cDNA construct and vector, which was approximately 8500 bp. In essence, a total of seven cDNA constructs were created using site-directed mutagenesis. Figure 2.2 depicts the constructs carrying the mutations, together with the c.-26A>G variant. Constructs carrying each of the mutations without the variant were also created.

2.2.2.2. Restriction endonuclease screening

The *Dpn I*-digested PCR products were transformed into competent DH5α cells as previously described (section 2.2.1.2). Transformed cells were plated onto agar plates containing Ampicillin (50 mg/ml). Ampicillin-resistant colonies were selected and grown further i.e. inoculated on selective growth medium (LB containing 50 mg/ml Ampicillin) (section 2.2.1.2). Plasmid DNA was isolated using STET (mini-lysate boiling preparation) (Appendix B) or small-scale plasmid preparations as described previously (section 2.2.1.3), and digested using the appropriate restriction enzyme (Table 2.2). As described previously, restriction sites were incorporated into the primers to facilitate identification of correctly incorporated mutants. Figure 2.3 shows a typical diagnostic digest gel of the 5′UTR variant.

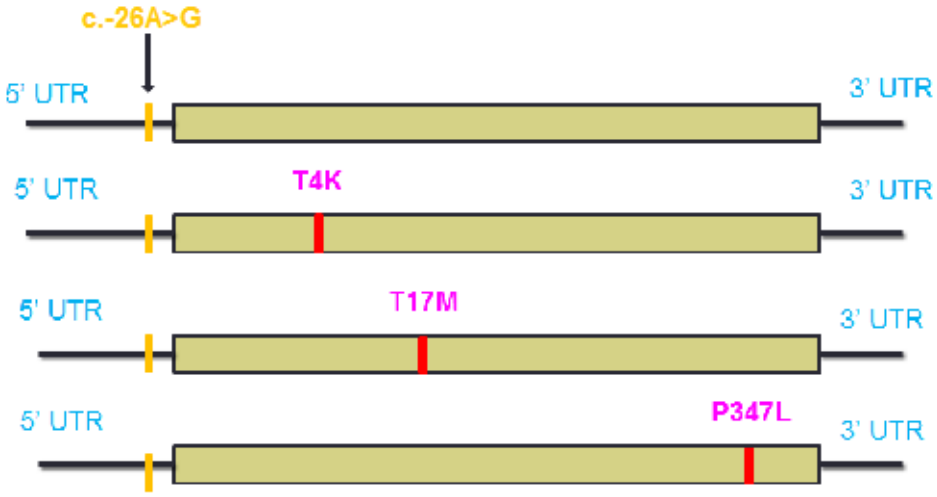

Figure 2. : Schematic diagram representing four main cDNA constructs created using SDM. Constructs carrying each of the mutations only (without the c.-26A>G variant), were also created resulting in a total of seven cDNA constructs.

Following restriction screening, all positive clones were sequenced using the pcDNA3.1+ forward sequencing primer (Appendix B) to confirm the presence of the various mutations. The P347L mutation construct however, could not be sequenced with the above primer or the pcDNA3.1+ reverse primer as the mutation was located too far from the primer binding region to give an accurate result. A new primer was thus designed (Appendix B). The sequencing protocol used was the same as that described in section 2.1.6. Large-scale preparations as described in section 2.2.1.3

were used to isolate larger quantities and concentrations of plasmids in preparation for transfection into mammalian cells.

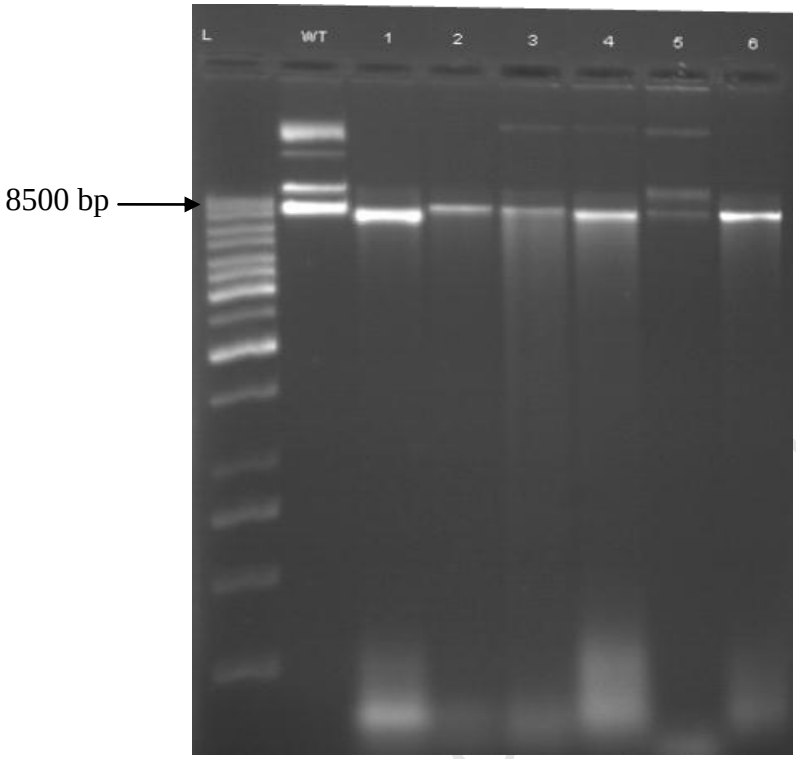

Figure 2. : Digital image of 5′UTR digest gel. Restriction endonuclease digest using the *Sac* II enzyme was employed as a diagnostic tool to determine the mutation status of purified plasmid following *E.coli* transformation. The lane marked 'L' represents the molecular weight marker. A wild-type (WT) 'uncut' control was included in each digest. The numbers 1-6 are representative of picked anti-bacterial resistant colonies. The *Sac* II enzyme only cut once thus linearizing the plasmid as shown by the single bands in lanes 1-4 and lane 6. In this image, all colonies except for number 5 had the 5′UTR 'G' nucleotide incorporated.

2.2.3. Mammalian cell culture

Mammalian cells provide a synthetic framework in which investigators are able (to a limited extent) to simulate events in the human body and more specifically in cells. For the purposes of this study, obtaining photoreceptor cells or established cell lines proved to be particularly challenging, and as such three substitute cell lines were used, namely HT-1080 (Human fibro-sarcoma) (Rasheed et al. 1974), SKNSH (Human neuroblastoma) (Biedler et al. 1973) and HEK-293-(Human embryonic kidney) (Graham et al. 1977) cell lines. All the cell lines were readily available from the Department of Human Biology at the University of Cape Town, South Africa.

2.2.3.1. Cell culture maintenance and transient transfections

All cell lines were plated in 10 cm cell culture dishes at concentrations of 6.0 x 10^5 and maintained in Dulbecco's Modified Eagle Medium (DMEM) (Highveld Biological Pty, RSA) (Appendix B) supplemented with 10% heat inactivated Fetal Calf Serum (FCS) (Highveld Biological, RSA), 1% Penicillin/Streptomycin (Appendix B) and 2 mM glutamine in a 37°C with 5% CO_2 atmosphere. Cells were passaged every 2-3 days at 80-100% confluence. Experimental culture plates (Greiner Bio-one, Germany) were seeded at concentrations of 1.5 x 10^5 in 35 mm culture plates. For immunocytochemistry, cells were seeded onto 22x22 mm, glass cover slips (Marienfeld, Germany) in 35 mm dishes.

Each of the three cell lines were transiently transfected 24 hr after seeding, using 0.5 µg or 1 µg cDNA encoding either WT h*RHO* or mutated variants cloned into the pcDNA3.1 vector. JetPEI^{TM} (Polyplus, USA) was used as a transfection reagent and transfections were carried out according to the manufacturer's instructions with slight modifications (Appendix B). Cells were harvested 24 hr following transfection.

For immunodetection, anti-Rhodopsin, ID4 (C-terminal) and 4D2 (N-terminal) antibodies were a kind gift from Professor Bob Molday (University of British Columbia, Canada).

2.2.4. Immunocytochemistry

Immnunocytochemical (ICC) analyses were used to determine localisation of RHO protein in the cell. For this analysis, cells were washed once in 1X PBS 24 hr after transfection, and then fixed in ice cold (-20°C) methanol and incubated at -20°C for 5 min, following which they were washed three times in 1X PBS. After fixation, cells were permeabilized using 0.2% (w/v) Triton-X 100 in PBS (Appendix B) for 10 min at room temperature and then washed three times in 1X PBS. Cells were then incubated in 5% non-fat milk (Appendix B) in 1X PBS for 1 hr at room temperature, in order to prevent non-specific binding of primary antibody. Following blocking, cells were washed three times in PBS and incubated in primary ID4/4D2 antibody (enough to cover cells) diluted to a 1:80 concentration in 5% non-fat milk in 1X PBS. Culture dishes containing the coverslips were incubated in a humidified

chamber overnight at 4°C. The next day, unbound primary antibody was washed off using 1X PBS (three times) and Anti-mouse Cy3 conjugated secondary antibody (Jackson Immunoresearch Laboratories, USA) (red fluorescence), diluted to 1:1500 in 5% non-fat milk in 1X PBS, was then added. Cells were incubated in secondary antibody for 1.5-2 hr at room temperature in the dark and again washed three times in 1X PBS.

2.2.4.1. DAPI nuclear staining

4',6-Diamidino-2-phenylindole (DAPI) was used to stain the nuclei of cells for orientation, i.e. to determine where the protein was situated, relative to the nucleus and cytoplasm. DAPI staining also served as a tool for indicating transfection efficiency (number of antibody-stained cells relative to the number of total cells). DAPI (50 mg/ml) was diluted to a 1:50 concentration in 1X PBS and 100 µl was added to cover slips. Cells were incubated in DAPI for 10-30 min in the dark at room temperature. Where DAPI was not available, Hoechst (Appendix B) was used to stain the nuclei. Following staining, cover slips were washed briefly in 1X PBS and then again for 5 min. The coverslips were then mounted onto slides using autoclaved 50% Glycerol.

2.2.4.2. Fluorescence microscopy

Mounted slides were viewed on the Carl Zeiss LSM 510 Meta NLO confocal fluorescence microscope using Axiovision© software (Carl Zeiss MicroImaging GmbH, Germany) in order to obtain high resolution fluorescence images. The settings used for all images were as follows; Lasers-Mai Tai (2-Photon) (DAPI) at 750 nm and DPSS-561-10 (red fluorescence) at 561 nm, scan mode-plane original data multitrack at 12bit pixel depth, Objective-LDC Apochromat 40X/1.1 WM27 (water immersion lens). The images were acquired using the single scan setting. The same settings and exposure used to view the WT RHO protein were applied for all the other variants in each of the different cell lines.

2.2.5. Western blotting

Western blotting was performed to determine differences in protein expression between the WT RHO (rod opsin) protein, mutant proteins and mutant proteins

carrying the 5′UTR c.-26A>G variant. For the purposes of this study, rod opsin (the RHO apoprotein) will be referred to as RHO indicating protein expressed from the *RHO* cDNA constructs. Transfected cells were prepared for harvesting 24 hr after transfection by washing twice with 1X cold PBS. Protein was harvested using cell lysis buffer constituting 1% w/v n-Dodecyl-β-D-Maltoside (DM) (Merck, Germany) in 1X PBS supplemented with 2% v/v mammalian protease inhibitor cocktail (Appendix B) for at least 15 min. Cell lysates for each of the variants were collected in 1.5 ml microfuge tubes and centrifuged at 14,000 rpm on a bench centrifuge for 30 min at 4°C after which the pellet was discarded. The supernatant containing total protein was quantified using the Pearce BCA (bicinchoninic acid) protein assay kit (Thermo Scientific, USA) (Appendix B).

Quantified protein samples were prepared for sodium-dodecyl-sulfate polyacrylamide gel electrophoresis (SDS-PAGE) under non-reducing denaturing conditions. A 10% resolving gel (Appendix B) was overlaid with a 3% stacking gel (Appendix B) in a Bio-Rad Vertical Electrophoresis System (Bio-Rad Laboratories, USA). Running buffer (1X) (Appendix B) was added to the apparatus before protein samples were loaded. Total protein was diluted to a final concentration of 15-30 µg using incomplete DM lysis buffer (Appendix B) and 5 µl Laemmli buffer (to a final concentration of 1X) (Appendix B). A total volume of 30 µl protein samples were loaded onto individual wells and run on an initial voltage of 100 V, which was subsequently increased to 200 V when samples had reached the resolving gel. Five micro litres of protein size marker, (peqGOLD protein marker IV, PEQLAB Biotechnologie, Germany) was also included in the first lane of each gel. Electrophoresis was halted when the blue dye front (indicating protein migration) had reached the bottom of the resolving gel. Following the electrophoresis, protein transfer from the resolving gel onto a nitrocellulose membrane (Amersham, UK) was performed using the wet transfer method. Briefly, a cassette containing sponge filter paper and gel were placed in a transfer tank (cassette holder) and 1X transfer buffer added (Appendix B). The transfer was performed at 100 V for approximately 1 hr. Successful transfer of protein was confirmed using Ponceau S staining (Appendix B).

2.2.5.1. Immunodetection of RHO

Nitrocellulose membrane with bound protein was blocked for non-specific sites using 5% w/w non-fat milk in 1X PBS/0.1% Tween-20 (PBS/T) at room temperature for 1 hr. The blocking solution was discarded and anti-RHO ID4/4D2 antibody was added at a 1:100 dilution in 5% milk in PBS/T. The membrane was subsequently incubated overnight in a 4°C shaker. The following day, the membrane was subjected to three 5 min washes using PBS/T and then incubated with goat anti-mouse horse-radish peroxidase (HRP) conjugated secondary antibody (Bio-Rad Laboratories, USA) at a 1:1500 dilution in milk/PBS/T for 1 hr. Following secondary antibody incubation the membrane was again subjected to three 5 min washes with PBS/T. Detection was performed using SupaSignal® West Dura (ThermoScientific, USA) according to the manufacturer's instructions and visualised on X-ray film. The mitogen-activated protein kinase p38 control (a ubiquitously expressed protein in most cell lines), was used as a loading control to indicate uniform protein concentrations in all sample lanes.

2.2.6. Quantitative real time-PCR (qPCR)

Quantitative real-time PCR (qPCR) enables quantification of transcripts or messenger ribonucleic acid (mRNA) from cells. The values obtained can be used to determine differences in gene expression under specified conditions (Nolan et al. 2006; Pabinger et al. 2009). In this study qPCR was used to establish differences in transcript expression, between various mutant and WT constructs in each of the three different cell lines. To begin with, the cell lines i.e. HT-1080, SKNSH and HEK-293 were transfected with h*RHO* variants as described in section 2.2.3.1 and incubated at 37°C with 5% CO_2 for 24 hr.

2.2.6.1. RNA extraction

Total RNA was harvested 24 hr after transfection using the High Pure RNA Isolation Kit (Roche Diagnostics, USA) according to the manufacturer's instructions. Prior to the extraction, growth medium (DMEM+ FCS+1% Pen/Strep) was suctioned off and cells were washed with 1X PBS before trypsinization with Trypsin/EDTA (Appendix B). Once cells had lifted off the dishes, they were spun down three times; once in growth medium and twice in 1XPBS at 10, 000 rpm for 10 min in preparation for

RNA extraction. Briefly, cells resuspended in 1X PBS underwent a series of centrifugation steps, in which the cells were lysed and bound to the membrane in the High filter tube using lysis/binding buffer. *DNAse* I was then added to the tubes, and left to incubate for 15 min at room temperature in order to remove any contaminating DNA. Subsequently, the membrane was subjected to washes using wash buffer I and II to remove residual impurities. A final volume of 50 µl total RNA was eluted from all transfected cells and either stored at -80°C or immediately used in subsequent analyses. 10 µl of eluted total RNA was subjected to spectrophotometry and electrophoresis on a 2% gel containing EtBr for quality and quantification purposes. An example of a gel image used to determine RNA integrity is shown in Figure 2.4 below. This analysis was performed for all RNA extractions before proceeding to cDNA synthesis.

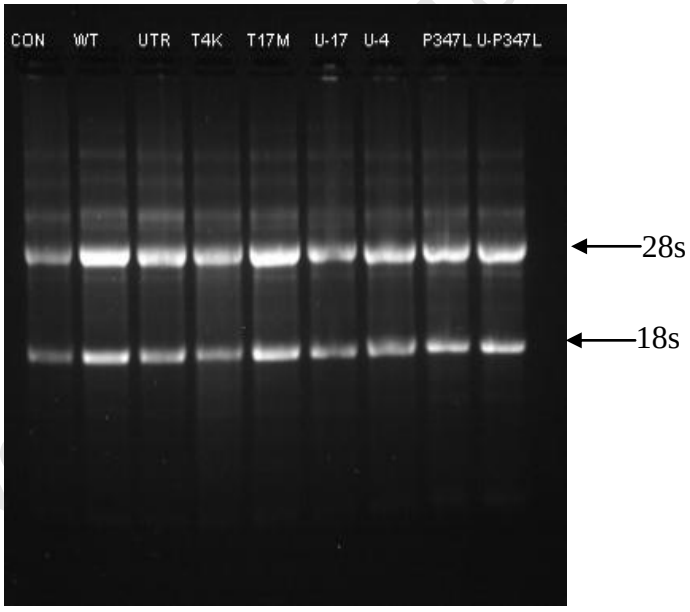

Figure 2. : Digital image of a gel used to determine the integrity of total extracted RNA after transfection with the constructs. The pattern observed here is typical of total RNA electrophoresis and the most prominent bands are representative of 28s and 18s ribosomal RNA (rRNA). In this image, total RNA extracted from cells expressing all the above constructs; wild-type (WT), c.-26A>G (UTR), T4K, T17M, UTR-T17M (U-17), UTR-T4K (U-4), P347L and UTR-P347L (U-P347L) had good integrity.

The remaining total RNA was aliquoted into 1 µg concentrations and either used for cDNA synthesis or stored at -80°C for use at a later time.

2.2.6.2. cDNA synthesis

Reverse-transcriptase PCR (RT-PCR), also known as cDNA synthesis, incorporates the use of Moloney Murine Leukemia Virus (*MMLV)* reverse transcriptase polymerase to convert mRNA to the more stable cDNA which can be used for numerous analyses including quantitative PCR. RT-PCR was performed using the First Strand cDNA synthesis Kit (Novagen-Merck, Germany) according to the manufacturer's protocol. Briefly, in a sterile RNAse-free 1.5 ml microfuge tube, 1 µg of total RNA was combined with 0.5 µg (0.5 µl) of oligo deoxythymidylic acid (dT) primer and nuclease-free water was added to a total volume of 12.5 µl. This mixture was prepared for each mutation construct in all three cell lines. The RNA and primer mixture was heated to 70°C to denature RNA secondary structures, which allows for more efficient priming and cDNA synthesis. This was immediately followed by chilling on ice for 5-10 min and a brief centrifugation to collect the contents at the bottom of the tube. A Reverse Transcriptase cocktail containing 4 µl of 5X First strand Buffer (250 mM Tris-HCl, 375 M KCl, 15 mM $MgCl_2$ pH 8.3), 2 µl 100 mM Dithiothreitol (DTT), 1 µl dNTP mix (10 mM each) and 0.5 µl (100 U) *MMLV* reverse transcriptase was added to the RNA-primer mix to a final volume of 20 µl. This mixture was gently mixed by pipette action and incubated at 37°C for 60 min in a thermal cycler. The newly converted cDNA was either used immediately for qPCR amplification or stored at -20°C.

2.2.6.3. Quantitative PCR (qPCR)

Fluorescence-based qPCR amplification (Nolan et al. 2006) was performed using 1 µl (approximately 50 ng) of cDNA from each variant as template. A single reaction mixture consisted of 1 µl (50 ng) cDNA, 5 µl Sensimix^{TM} *Plus* SYBR Kit (2 X mix containing reaction buffer, heat-activated DNA Polymerase, dNTPs, 6 mM $MgCl_2$, internal reference, stabilizers and SYBR® Green I) (Quantace, USA), 1 µl (20 pm) *RHO* (forward and reverse-exons 4 and 5) Quantitect® primers (Qiagen, USA) and 3 µl nuclease-free water in a total reaction volume of 10 µl. For each experiment a master mix was prepared and reactions were performed in duplicate to account for common pipetting errors.

To enable analysis of qPCR data, a standard curve was established for each cell line, using a series of dilutions (10 fold) of WT *RHO* cDNA. The values obtained for each dilution were used to determine the amplification efficiencies of both the target (*RHO*) and reference genes. The reference gene used in this study, the Glyceraldehyde-3-phosphate dehydrogenase (*GAPDH*), was selected based on i) its ability to exhibit ubiquitous expression in all three cells lines and ii) its expression profile not being altered by experimental conditions (Nolan et al. 2006; Pabinger et al. 2009). Amplification was carried out in a LightCycler 2.0 (Roche, USA) and cycling conditions were as listed in Table 2.3:

Table 2. : Cycling conditions used for qPCR amplification on the LightCyler 2.0. Fluorescent signal was acquired after each amplification cycle. As a final step, a melt curve analysis was performed to determine melting temperatures of all PCR products.

Programme/Stage	Cycles	Target	Hold	Ramp rate
Enzyme Activation	**1**	95°C	10 sec	20
Amplification	**25**	95°C	15 sec	20
		60°C	15 sec	20
		72°C	5 sec	20
Melting Curve	**1**	95°C	0 sec	20
		65°C	15 sec	20
		95°C	0 sec	0.1
Cooling	**1**	40°C	40 sec	-

The expected amplicon size was 77 bp long and had a melting temperature of 83°C as determined by the melt curve analysis. The melt curve analysis provided melting

temperatures of all amplicons present in the PCR and was thus useful in determining non-specific amplification.

2.2.6.4. Analysis-Standard curve method

Quantification data can be analysed using two methods; the delta delta Ct method or the standard curve method depending on the amplification frequency values. According to previously published literature on qPCR data analysis (Livak & Schimttgen 2001; Nolan et al. 2006; Pabinger et al. 2009) if the slope of the delta standard curve is less than -1, then the delta delta Ct method of analysis may be used, where delta represents the difference in cycle thresholds (Ct) of the target gene from the reference gene. If however, the slope is greater than -1, then individual slopes (standard curves) of both the target and reference genes, also known as the standard curve method, should be used to obtain actual concentration values for each of the variant transcripts (Larionov et al. 2005). In this study the standard curve method was used to analyse qPCR data. Calculations were performed manually in an excel spread sheet. Transcript concentration values were obtained by solving for ***x*** in the slope equation ($y=mx + c$) for each standard curve i.e. *RHO* standard curve and *GAPDH* standard curve. The values obtained from the slope equations were then ***log reverse*** transformed for actual concentrations. All *RHO* transcript values were normalised (the target value was divided by the reference value) against *GAPDH* values. The resulting values were then expressed as fold differences; relative to the WT transcript (the WT value was divided by itself to give a value of 1). The fold differences in transcript expression were expressed in units representative of fold increase or decrease in expression.

Standard deviation values were calculated according to guidelines described in ABI User guidelines (User Bulletin #2, October 2001). The standard deviation of the normalised value is calculated from standard deviations of *RHO* and *GAPDH* values using the formulae:

$$CV=\sqrt{CV_1^2 + CV_2^2}$$

where CV= standard deviation ÷ mean value.

All data was presented in bar graphs depicting the fold change in expression in each cell line and between cell lines.

Chapter 3: Results

3.1. Bioinformatic analyses of the *RHO* 5'UTR c.-26A>G variant and screening in an AdRP Cohort

3.1.1. Bioinformatic analyses of the *RHO* c.-26A>G variant

3.1.1.1. Protein interaction profile of RHO

Two bioinformatic tools were used to determine potential effects of the c.-26A>G change in RHO namely, BioGrid (http://www.thebiogrid.org) and STRING (http://string-db.org/newstring_cgi/show_network_section.pl?identifier=P08100). BioGrid revealed six proteins that were shown to interact with RHO: adrenergic beta receptor kinase 1 (ADRBK 1), Arrestin 3 (ARR3), s-antigen (SAG), G protein-coupled receptor kinase 1 (GRK 1), G potein-coupled receptor kinase 5 (GRK 5) and polyubiquitin-C (UBC). All the above proteins except for UBC, were identified as interacting with RHO in the STRING database, in addition to neural retina-specific leucine zipper protein (NRL), arrestin Beta-1(ARRB1), cone-rod homeobox (CRX) guanine nucleotide-binding protein, gamma-transducing activity polypeptide 1 (GNGT 1) and guanine nucleotide-binding protein 1/2 (GNAT 1/ 2) , which were not identified in BioGrid. In addition, some subtypes of the above proteins were included in STRING, resulting in a total of ten protein interactions. All of the proteins in both STRING and BioGrid play a role in the visual system. The interaction profile of RHO is best depicted by the STRING database results as is shown in Figure 3.1 below.

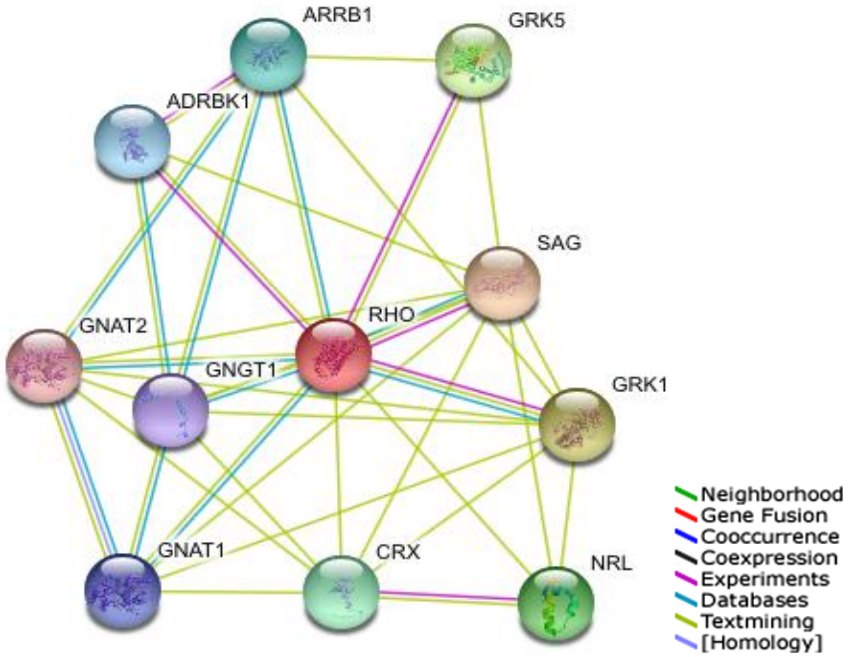

Figure 3. : Interaction profile of RHO as depicted by STRING. RHO was shown to interact with ten proteins. The interaction between RHO and other proteins is depicted ascoloured connecting lines, which also indicate the types of evidence for the association. The colour key is found in the legendon the right.

3.1.1.2. RHO vertebrate species alignment

A species alignment of the sequence surrounding c.-26A>G SNP (rs7984) was determined in order to establish whether the region was highly conserved. A highly conserved region would implicate the significance of the sequence in regulating expression of the protein. The aligned RHO sequence of twelve vertebrate species was retrieved from the University of California, Santa Cruz (UCSC) Genome Browser (http://genome.ucsc.edu) (Figure 3.2).

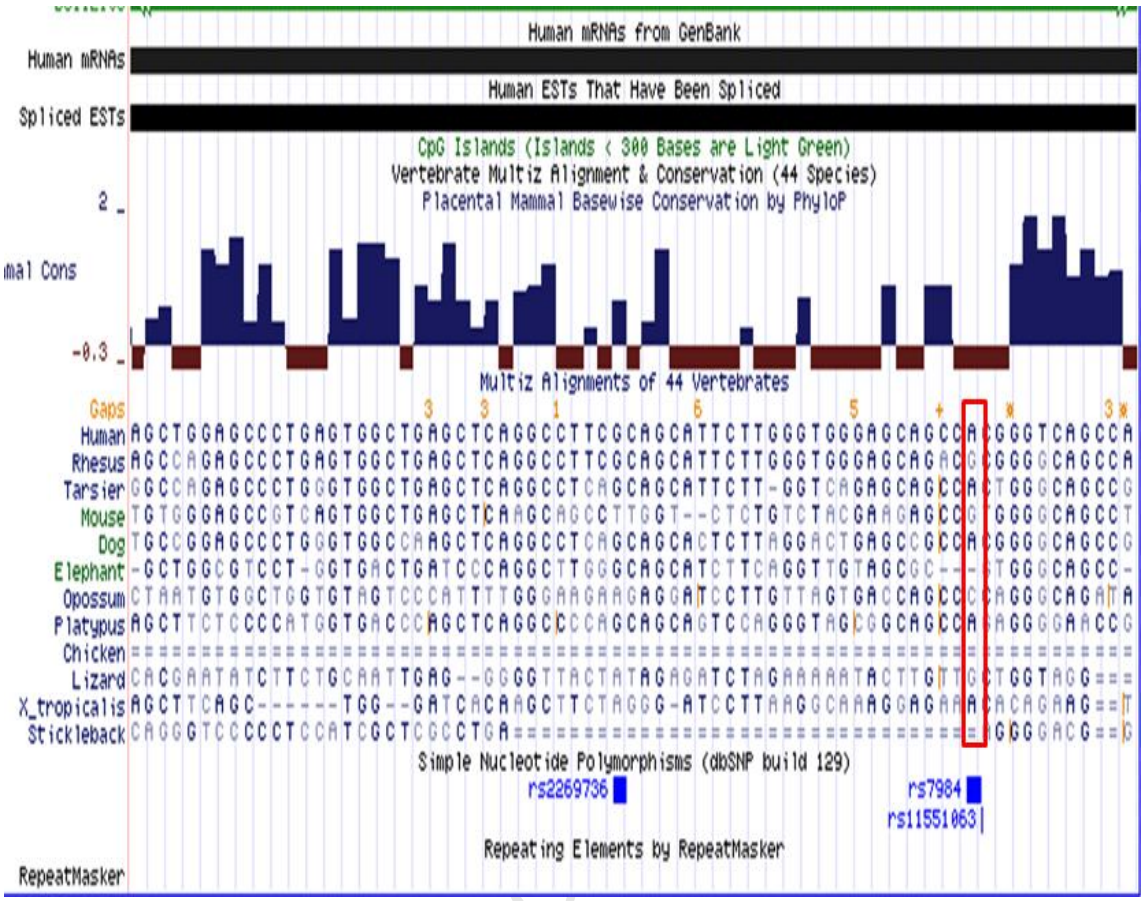

Figure 3. : A screen print image of the *RHO* sequence alignment across various vertebrates. The region highlighted by the red rectangle shows the variation in nucleotide at db SNP: rs7984 in twelve different species**.**

The nucleotide at dbSNP: rs7984 appears not be highly conserved in vertebrates as depicted in the above diagram with the most frequent allele being 'A'. Data from the National Centre for Biotechnology Information (NCBI) SNP cluster report, however, states that the ancestral allele is the 'G' allele. The other variant present in this SNP region is the 'C' allele which was observed in one vertebrate (Opposum) (Figure 3.2).

3.1.1.3. RNA folding prediction using mFOLD software

The RNA folding prediction software mFOLD was used to predict changes in the folding or secondary structure of *RHO* mRNA when the c.-26A>G SNP was present. For the purposes of this study, the whole 5′UTR region i.e. 95 bp upstream from the start codon, was submitted for analysis. The images below (Figure 3.3 and 3.4)

depict the predicted secondary structures retrieved from mFOLD and their free energies.

According to the results obtained from mFOLD prediction (Figure 3.3), there are three possible secondary structure formations for the 5'UTR *RHO* sequence carrying the 'A' allele. Each of the conformations has different free energies which determine the likelihood of the occurrence of that particular conformation (Jiang, 2010). Analysis of the 5'UTR *RHO* sequence containing the 'G' allele resulted in two different predicted secondary structure conformations (Figure 3.4), with variable free energies.

3.1.1.4. Transcription factor binding site analysis

The Transcriptional Element Search System (TESS) (http://www.cbil.upenn.edu/cgi-bin/tess/tess) was used to assess whether the 5′UTR variant changed the consensus binding site of any particular transcription factor. To this effect, *RHO* sequences containing either the 'A' or 'G' allele were analysed for potential changes in binding sites of transcription factors.

Tabulated results were viewed to determine which transcription factors bound the region within the c.-26A>G variant. The c.-26A>G change is at position 70 in the mRNA sequence and this position was examined for binding changes. Figures 3.5 and 3.6 depict results retrieved from TESS analysis for the 'A' and 'G' alleles, respectively.

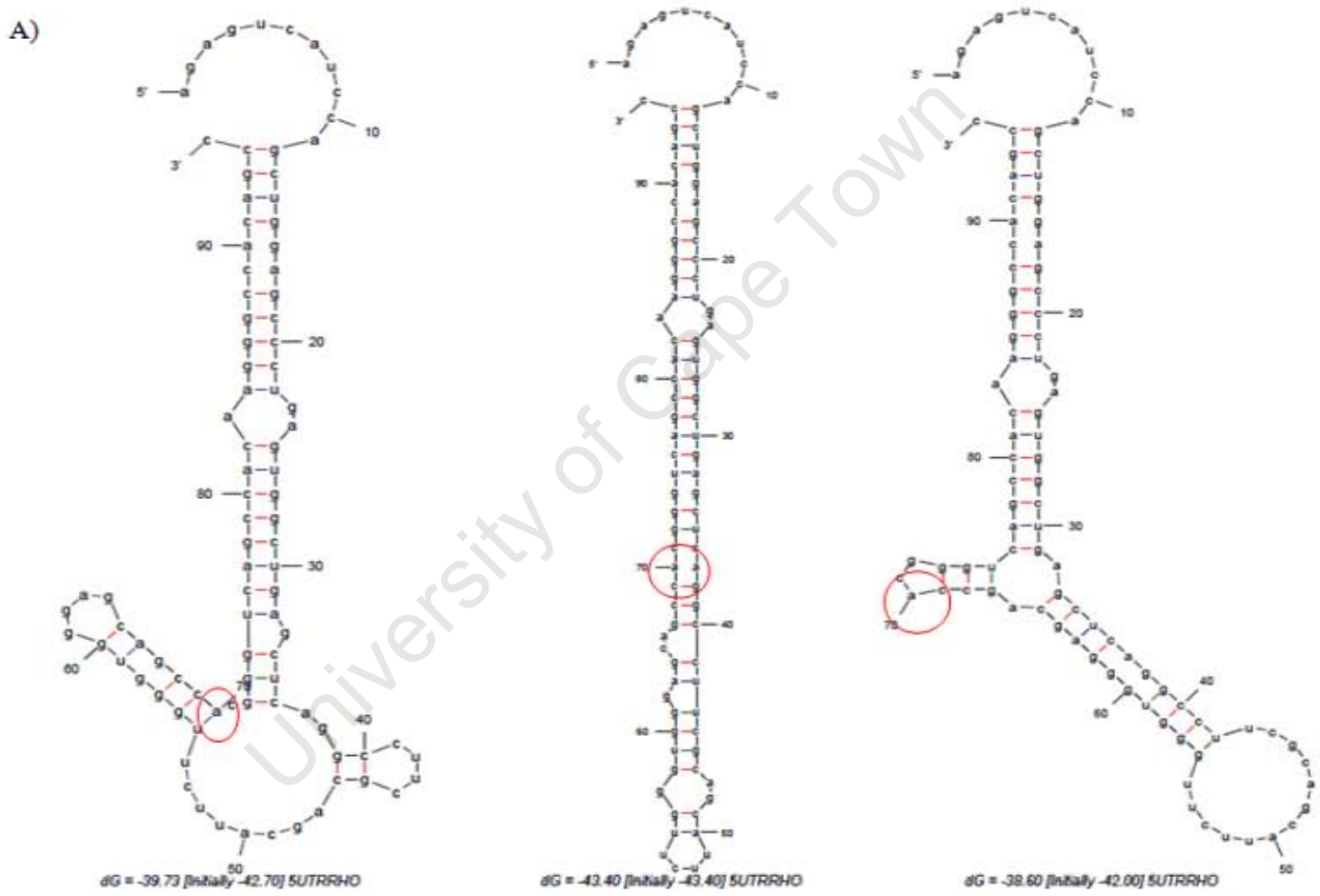

Figure 3. : Images of the predicted *RHO* mRNA secondary structure obtained from mFOLD using the 5′UTR sequence containing the 'A' allele (5′UTR *RHO*). The free energies (delta G) predicted here are -39.73, -43.40 and -38.60 respectively.

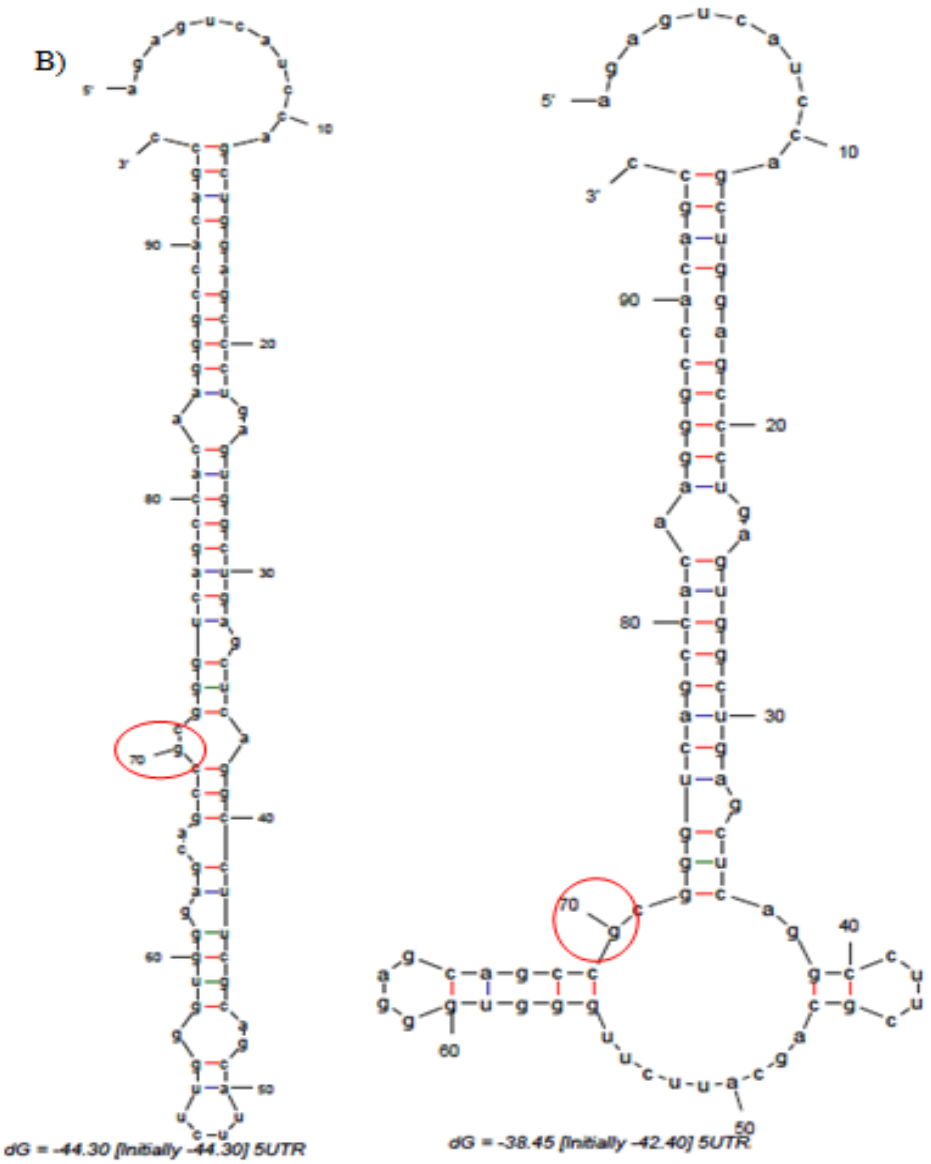

Figure 3. : Images of the predicted *RHO* mRNA 5′UTR secondary structures obtained from mFOLD using the 5′UTR sequencing containing the 'G' allele. The free energies (delta G) predicted here are -44.30 and -38.45 respectively. The more negative the free energy the less stable the conformation or structure. In this case the first conformation (-44.30) is less stable.

#	Factor	Model	Beg	Sns	Len	Sequence
108	T00149 COUP	Q00031 (-)	66	N	12	agccacgggtca
109	_00000 TAF-1	I00356 (TAF-1)	67	R	7	gccacgg
110	_00000 AP-2	I00151 (AP-2)	67	R	8	gccacggg
111	T00872 USF-1 T00874 T00875 T00876 USF1 T00877 T00870 USF	M00187 (V$USF_Q6)	67	N	10	gccacgggtc
112	T00872 USF-1 T00874 T00875 T00876 USF1 T00877 T00870 USF	M00217 (V$USF_C)	68	R	8	ccacgggt
113	T00264 ER	Q00059 (-)	68	N	10	ccacgggtca
114	_00000 RAR-alpha1	I00401 (RAR-alpha1)	69	R	9	cacgggtca
115	T00045 ARP-1	Q00011 (-)	69	N	9	cacgggtca
116	T00029 T00030 T00031 T00032 T01115 T01140 T01156 T00027 AP-1	M00174 (V$AP1_Q6)	69	R	11	cacgggtcagc
117	_00000 ARP-1	I00142 (ARP-1)	70	R	8	acgggtca
#	Factor	Model	Beg	Sns	Len	Sequence

Figure 3. : The table of results obtained from TESS using the *RHO* 'A' allele. The region highlighted in red indicates the position of the nucleotide change of interest and shows a binding site for the ARP-1 transcription factor.

The region highlighted in red (Figure 3.5) indicates the position of the 'A' allele of the c.-26A>G SNP, which according to the 'Sequence' column, is the beginning of the ARP-1 consensus sequence. The ARP-1 transcription factor consensus sequence is shown in different colours indicating the strength of match, i.e. black indicates a 'best or perfect match' and red is a 'mismatch'. Thus, the above results indicate that the 'A' allele is a significant part of the ARP-1 binding site, which may affect binding of the protein if altered. Indeed, when the *RHO* mRNA sequence containing the 'G' allele was analysed, it was found that there was no longer a binding site for the ARP-1 protein (Figure 3.6).

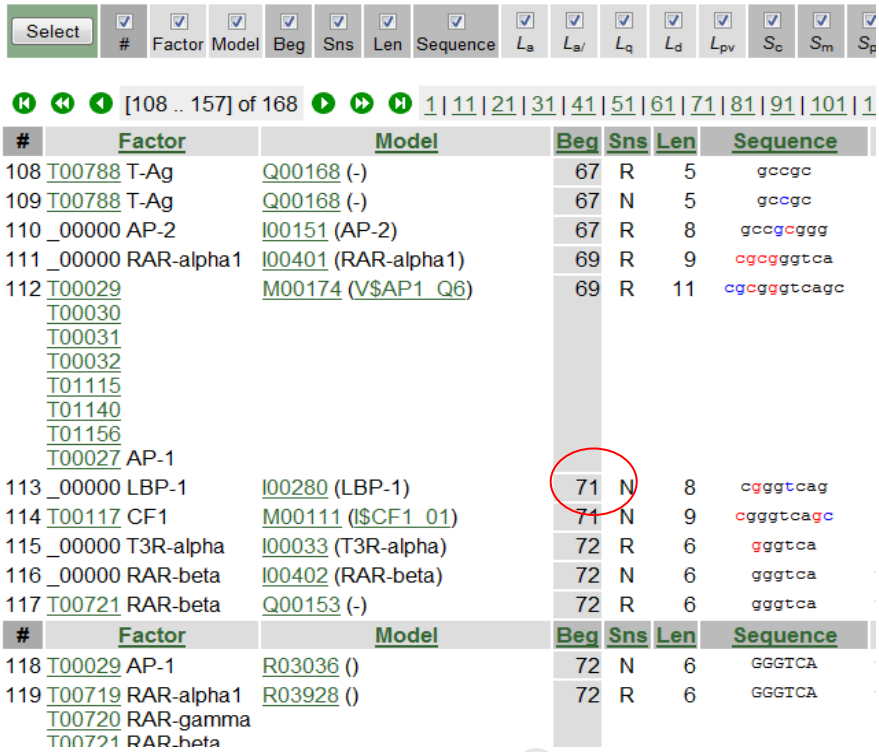

Select | # | Factor | Model | Beg | Sns | Len | Sequence | L_a | $L_{a/}$ | L_q | L_d | L_{pv} | S_c | S_m | S_p

[108 .. 157] of 168 | 1 | 11 | 21 | 31 | 41 | 51 | 61 | 71 | 81 | 91 | 101 | 1

#	Factor	Model	Beg	Sns	Len	Sequence
108	T00788 T-Ag	Q00168 (-)	67	R	5	gccgc
109	T00788 T-Ag	Q00168 (-)	67	N	5	gccgc
110	_00000 AP-2	I00151 (AP-2)	67	R	8	gccgcggg
111	_00000 RAR-alpha1	I00401 (RAR-alpha1)	69	R	9	cgcgggtca
112	T00029 T00030 T00031 T00032 T01115 T01140 T01156 T00027 AP-1	M00174 (V$AP1_Q6)	69	R	11	cgcgggtcagc
113	_00000 LBP-1	I00280 (LBP-1)	71	N	8	cgggtcag
114	T00117 CF1	M00111 (I$CF1_01)	71	N	9	cgggtcagc
115	_00000 T3R-alpha	I00033 (T3R-alpha)	72	R	6	gggtca
116	_00000 RAR-beta	I00402 (RAR-beta)	72	N	6	gggtca
117	T00721 RAR-beta	Q00153 (-)	72	R	6	gggtca
#	Factor	Model	Beg	Sns	Len	Sequence
118	T00029 AP-1	R03036 ()	72	N	6	GGGTCA
119	T00719 RAR-alpha1 T00720 RAR-gamma T00721 RAR-beta	R03928 ()	72	R	6	GGGTCA

Figure 3. : The table of results obtained from TESS using the *RHO* 'G' allele. The region highlighted by the red circle indicates the position of the nucleotide which abolishes the ARP-1 binding site.

According to the TESS results obtained using the 'G' allele (Figure 3.6), the nucleotide at position 70 is not present and the ARP-1 binding site appears to have been abolished. Furthermore, information on the ARP-1 transcription factor (also retrieved from TESS) reveals that it is a human transcription factor (Figure 3.7).

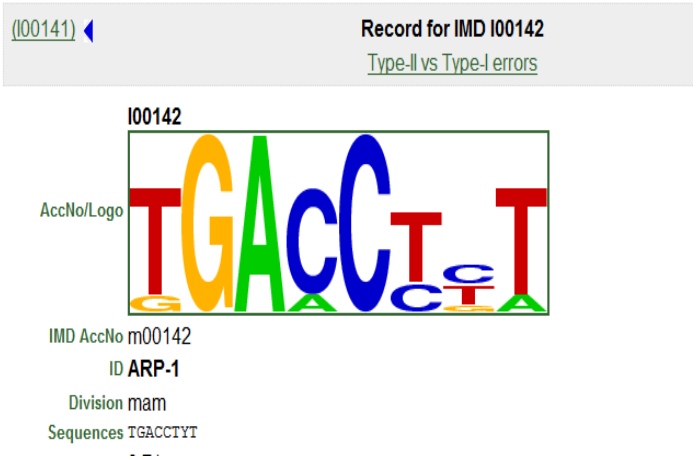

Figure 3. : Image of information on the ARP-1 transcription factor retrieved from TESS. The nucleotide logo represented above depicts nucleotides that are most likely to be found at the position of the consensus sequence. The size of the nucleotide (large or small) represents the likelihood of that nucleotide being present at the particular position. The first nucleotide of the ARP-1 consensus sequence shown here (T or G), is also the c.-26A>G variant nucleotide position.

3.1.2. *RHO* 5′UTR c.-26A>G variant screening in an AdRP cohort

RFLP analysis was used to screen for the c.-26A>G SNP variant in *RHO* and genotypes were confirmed by direct cycle sequencing. A typical post-restriction endonuclease digest agarose gel image and sequencing electropherogram are shown in Figure 3.8 and 3.9 respectively.

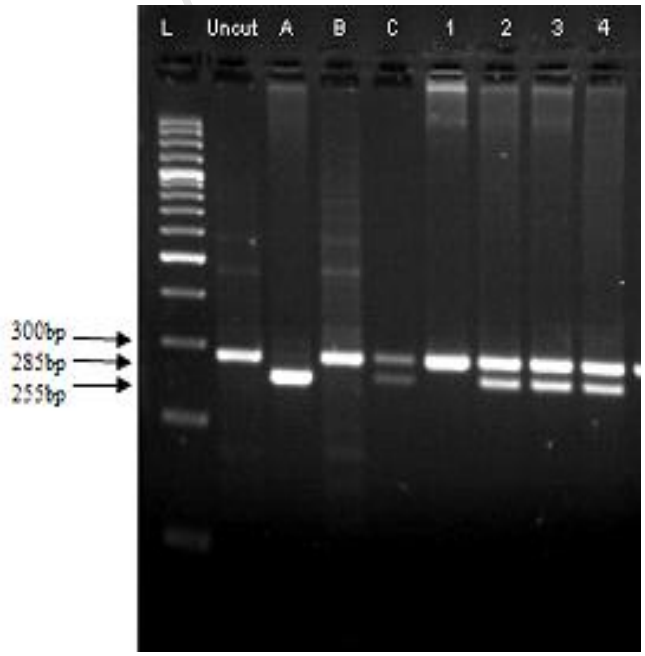

Figure 3. : Example of a typical agarose gel image, showing PCR products digested with Ksp I to determine genotype status. Patient samples were tested together with controls, for which the c.-26A>G genotypes were known: A (GG), B (AA), and C (AG). The numbers 1-4 represent samples from families with known *RHO* mutations. Gels were stained with EtBr and visualised on a UVIdoc transilluminator

In the absence of the c.-26A>G variant, in a particular amplicon, a single band of 285 bp would be observed, similar to that of an uncut amplicon, (visible in the lane marked 'uncut') or 'B' control. The banding patterns observed in lane 'A' indicate that the *Ksp I* enzyme cut both alleles once resulting in products of 255 bp and 30 bp (which was not observed on the gel). This banding pattern represents a homozygous individual ('GG' genotype). The other type of banding pattern is visible in lane 'C' and indicates that the enzyme only cut one allele yielding products of 285 bp and 255 bp and 30 bp. Individuals with this banding pattern are heterozygous for the variant ('AG' genotype).

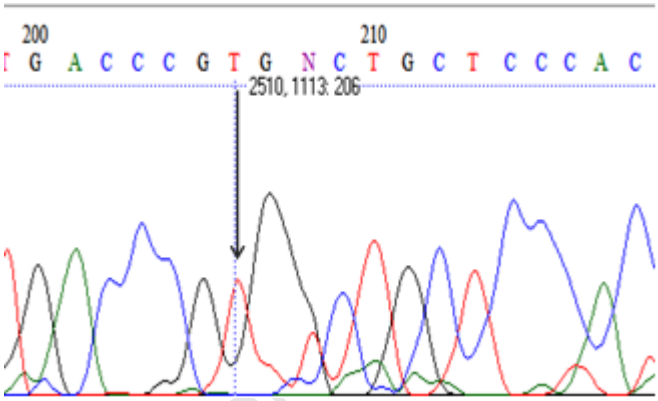

Figure 3. : Sequencing electropherogram of a sample with an AA genotype obtained using the reverse primer. The arrow represents the position of the nucleotide c.-26A, which is indicated by the 'T' nucleotide on the reverse strand.

Figure 3.10 below shows the distribution of genotypes in all family members including patients and unaffected relatives. The AdRP cohort was made up of mostly Caucasian individuals although there was one indigenous African family, with two members for whom information and DNA was available in the registry. According to the genotyping results represented below (Figure 3.10 and 3.11), the 'A' allele is over-represented in AdRP families. In affected individuals alone, the frequency of the c.-26A>G SNP was also much lower i.e. only four patients had the 'GG' genotype and they were both from the same indigenous African family (Figure 3.11).

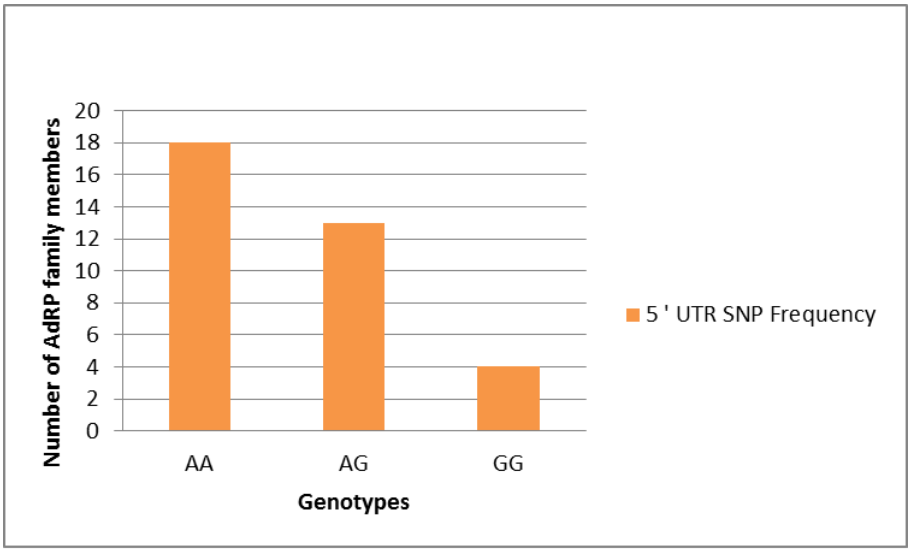

Figure 3. : Distribution frequencies of the c.-26A>G genotype in 35 AdRP family members. This data includes both affected and non-affected individuals and represent the distribution frequencies of the three genotypes in the whole cohort.

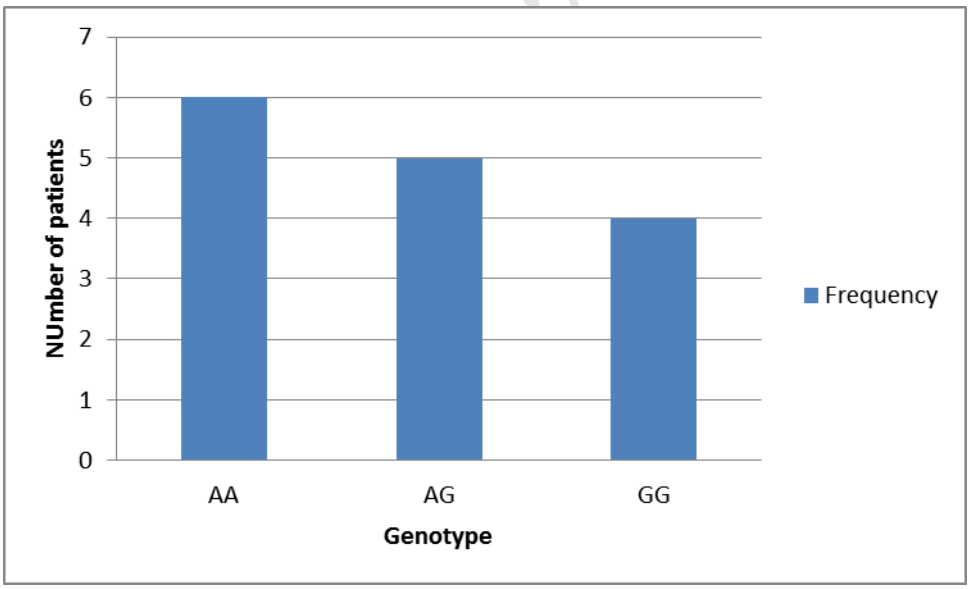

Figure 3. : Distribution frequencies of the three c.-26A>G genotypes in AdRP patients only.

Both graphs show similar trends in distribution frequencies of the SNP with the 'GG' genotype having the least occurrence in the whole AdRP family cohort and patients.

Pedigree analysis to determine the location of the c.-26A>G variant in relation (*cis* or *trans*) to the disease-causing mutations could not be obtained due to lack of

biological material from certain family members that would have enabled this genotype inference. Furthermore, a clinical effect of the c.-26A>G variant could not be established due to a lack of individuals with sufficient clinical data and different combinations of mutations and the variant.

3.2. Functional *in vitro* analyses of the c.-26A>G variant in mammalian cell lines

Mammalian cell models were used to investigate the functional effect of the c.-26A>G variant. As mentioned previously (section 2.2.3), three human cell lines namely, HT-1080, SKNSH and HEK-293, were used. The SKNSH neuroblastoma cell line was included in the study since it was more closely related to the neuronally derived photoreceptor cells. A recent study by Pandor et al. (2010), revealed that HEK-293 cells were able to correctly fold and traffic misfolded protein and as such, this cell line was included in the study since two of the chosen mutations i.e. T4K and T17M, exhibited a misfolding protein phenotype.

3.2.1. Site-directed mutagenesis of *RHO* gene variants

In order to create mutation constructs that could be transfected into the mammalian cell lines, site-directed mutagenesis was employed. For each of the constructs, successfully incorporated mutations were screened using restriction endonuclease digestion and confirmed by direct sequencing. Sequencing electropherogram images of each of the disease-causing mutations and the c.-26A>G variants are shown in Figures 3.12 and 3.13 below.

A total of seven constructs were thus created successfully; the c.-26A>G SNP (5′UTR) variant, T4K, UTR-T4K, T17M, UTR-T17M, P347L and UTR-P347L. Mention of the 5′UTR variant from hereon is used interchangeably with the c.-26A>G SNP variant. In all instances, expression of the *RHO* WT (c.-26A) construct was used as a reference point.

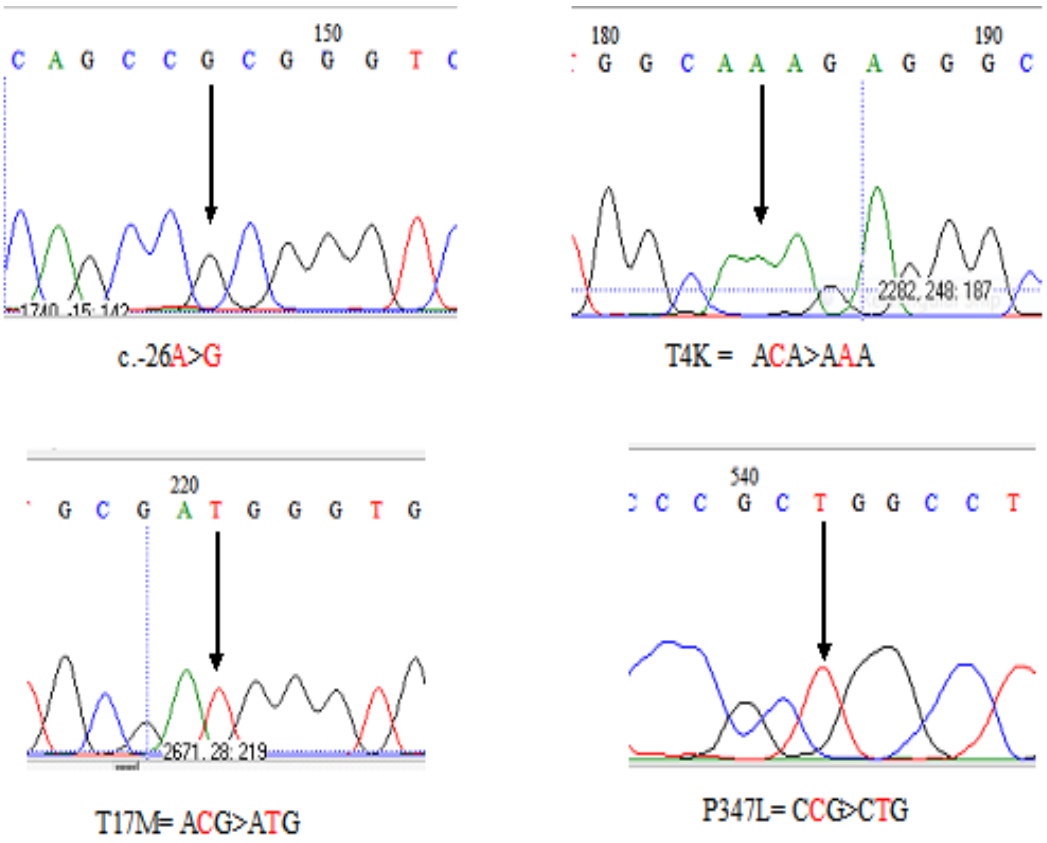

Figure 3. : Sequencing electropherogram of *RHO* single mutants. The arrows indicate positions of nucleotide changes for each of the mutants.

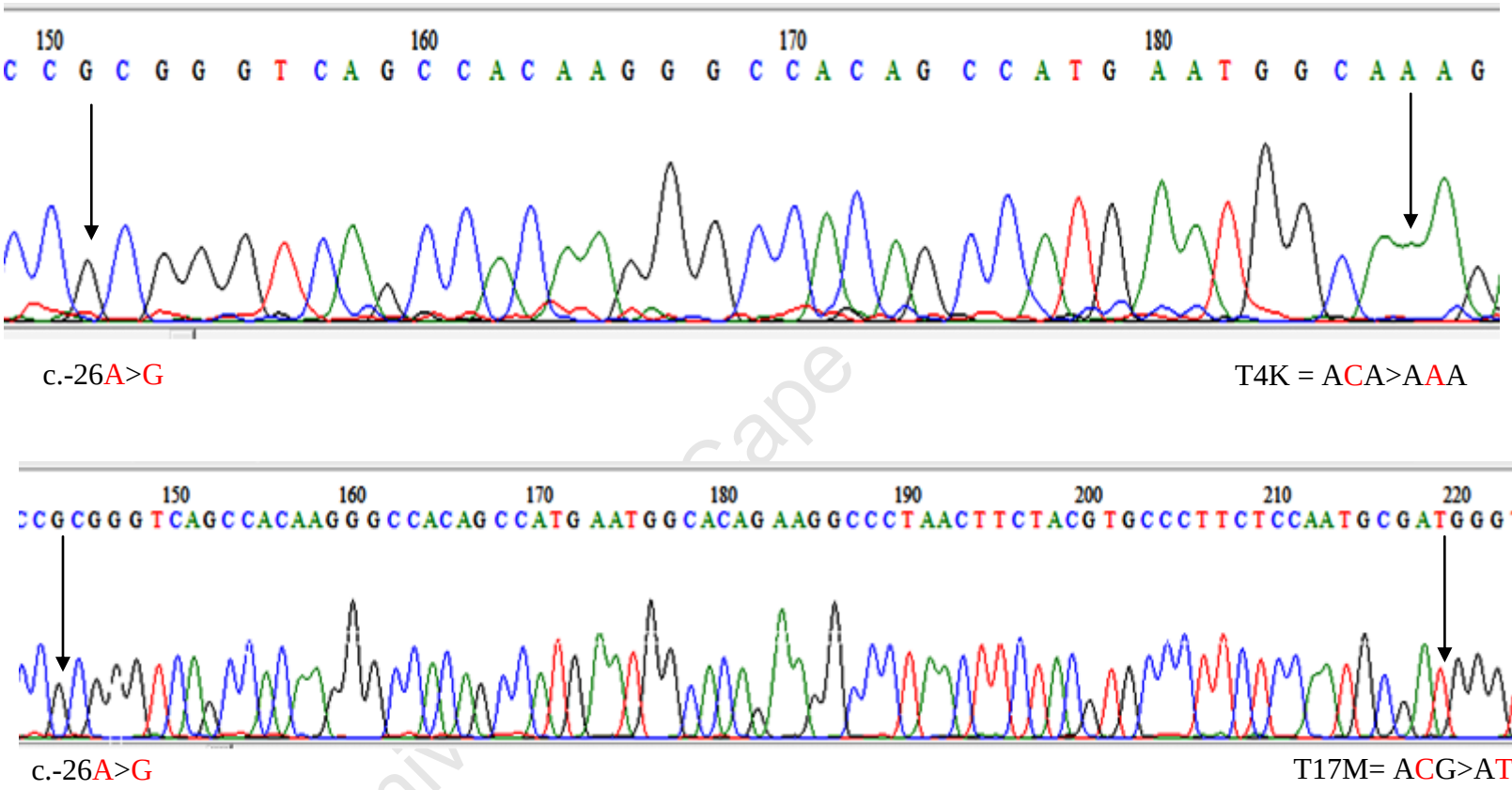

Figure 3. : Sequencing electropherograms of *RHO* T4K and T17M with the 5′UTR (c.-26A>G) variant *in cis*. The arrows indicate positions of nucleotide changes for each of the mutants. An electropherogram of the P347L mutation *in cis* with the c.-26A>G variant could not be screen captured as the relevant nucleotides were too far apart.

3.2.2. The effect of the *RHO* 5′UTR variant on protein localisation

Protein localisation was determined using ICC to observe differences between *RHO* variants and WT *RHO* constructs. All mutant constructs were expressed alone and *in cis* with the 5′UTR variant. Expression of the *RHO* 5′UTR variant construct in HT-1080 cells and SKNSH cells revealed protein localisation and fluorescent intensity similar to WT, with no visible aggregate formation (Figure 3.14 b, f; Figure 3.15 b f; Figure 3.16 b, f).

3.2.2.1. Threonine 4 Lysine (T4K)

The T4K mutation was selected for inclusion in this study since it is classified as belonging to a distinct class of *RHO* mutations (Class IV) (Mendes et al. 2005) and would thus allow analysis of a wider spectrum of mutations. In photoreceptor cells, RHO is trafficked to the outer segment in the membrane discs (Sung et al. 1991). In cultured cells, however, WT RHO is trafficked to the cellular plasma membrane, with some staining found in the cytoplasmic regions indicating normal biogenesis of the protein, as evident in Figure 3.14 below (Figure 3.14 a, e, i). When the *RHO* T4K mutant construct was expressed in HT-1080 and SKNSH cells, there appeared to be accumulation of protein (in protein aggregates) in juxtanuclear regions (Figure 3.14 c, g) which have been previously reported as the Golgi and intermediate compartments (Saliba et al. 2002). In contrast, when the *RHO* T4K construct was expressed *in cis* with the 5′ UTR variant in HT-1080 and SKNSH cells, there appeared to be normal trafficking with little to no accumulation of protein observed (Figure 3.14 d, h).

A similar trend in which no aggregates were formed when the T4K mutant was expressed *in cis* with the 5′UTR variant was observed in the SKNSH (Figure 3.14 g, h) cell line but not in the HEK-293 cell line (Figure 3.14 j, k). Expression of the 5′UTR variant in the SKNSH cell lines, revealed similar fluorescent intensity to cells expressing WT *RHO* (Figure 3.14 e, f).

There was no significant difference in trafficking between the WT and T4K proteins (either expressed alone or when expressed *in cis* with the 5′UTR variant) in the

HEK-293 cell line (Figure 3.14 k, l). The 5′UTR variant alone however, exhibited low fluorescence compared to WT, T4K and UTR-T4K constructs (Figure 3.14 j).

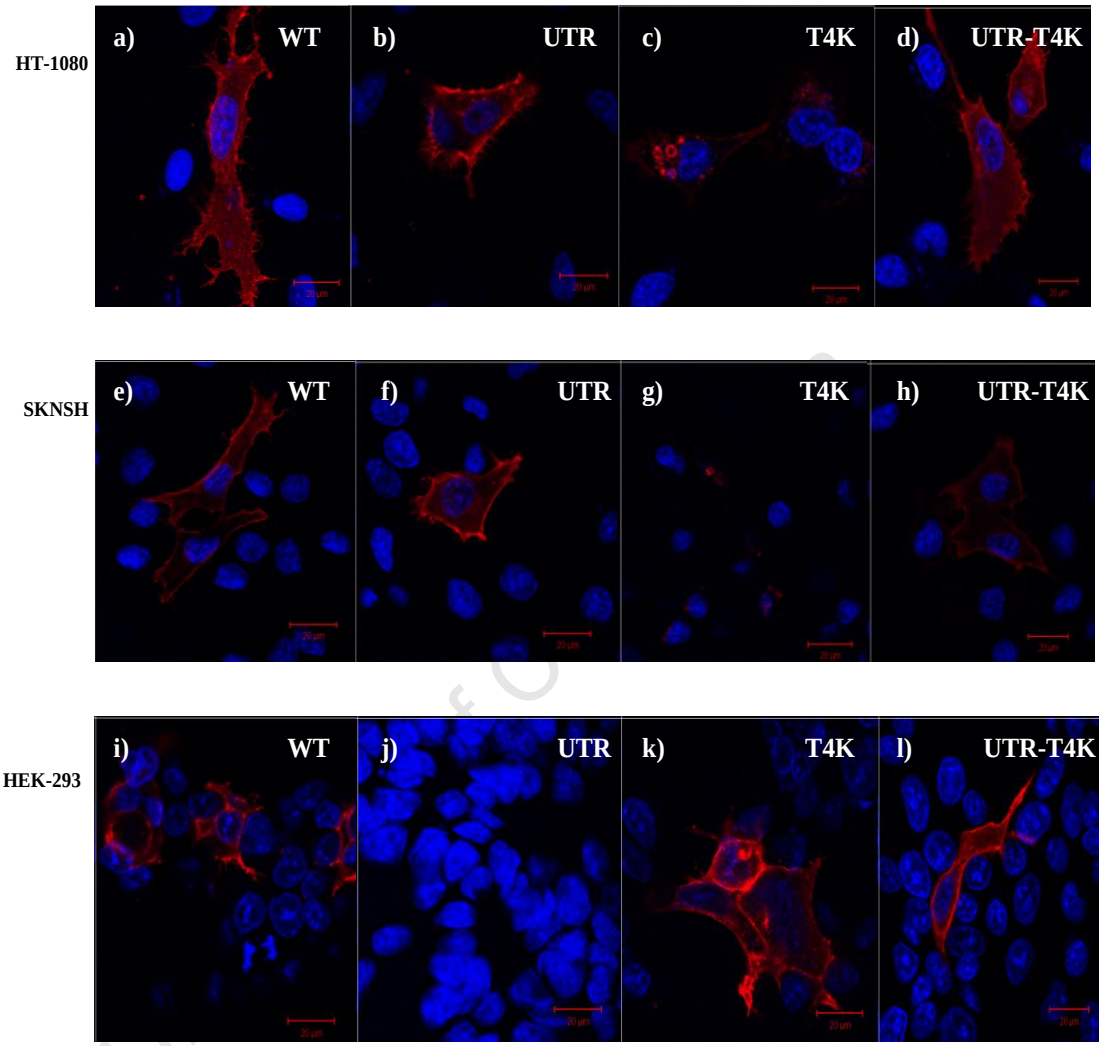

Figure 3. : Fluorescent images of cells expressing WT RHO and the T4K mutant constructs. All images were taken using the same settings on the Carl Zeiss confocal microscope. The scale bar in each of the images is 20µm. The red stain is indicative of RHO protein localisation as labelled by Cy3 fluorescent secondary antibody whereas the blue stains (DAPI) indicate nucleus staining and positioning in relation to the cell. Each panel is representative of expression in the three different cell lines. These images are representative of two or more independent ICC experiments performed for this construct.

3.2.2.2. Threonine 17 Methionine (T17M)

Similar to T4K, T17M is a known misfolding mutant that has been reported to exhibit aggregate formation in the juxtanuclear regions of the cell i.e. the endoplasmic reticulum (ER) and golgi of cells (Sung et al. 1991; Kaushal and Khorana, 1994; Mendes et al. 2005). In comparison to WT RHO, the T17M mutation appeared to form aggregates in juxtanuclear regions, in all three cell lines (Figure 3.15 c, g, k) with a more pronounced accumulation in the HT-1080 cell line (Figure 3.15 c) and little protein translocation to the plasma membrane. Interestingly, the fluorescent intensity exhibited by the T17M variants appeared to be generally low compared to expression of WT RHO protein and protein containing the 5′UTR variant. Expression of the T17M mutant protein *in cis* with 5′UTR variant in three cell lines appeared to increase fluorescence intensity suggesting increased protein presence, however, these levels were still lower compared to the WT (Figure 3.15 d, h, l). Expression of T17M mutant protein with the 5′UTR variant in both the HT-1080 and SKNSH cell lines was similar to that reported for the T4K panel, where fluorescent intensities were comparable to WT.

In the HEK-293 cell line, expression of the 5′UTR RHO protein labelled with Cy3 fluorescent antibody was very faint and almost undetectable (Figure 3.15 j). Interestingly, there appeared to be a small aggregation of protein when the T17M protein was expressed alone (Figure 3.15 k) which was in contrast to what was observed for the T4K panel (Figure 3.14 k).

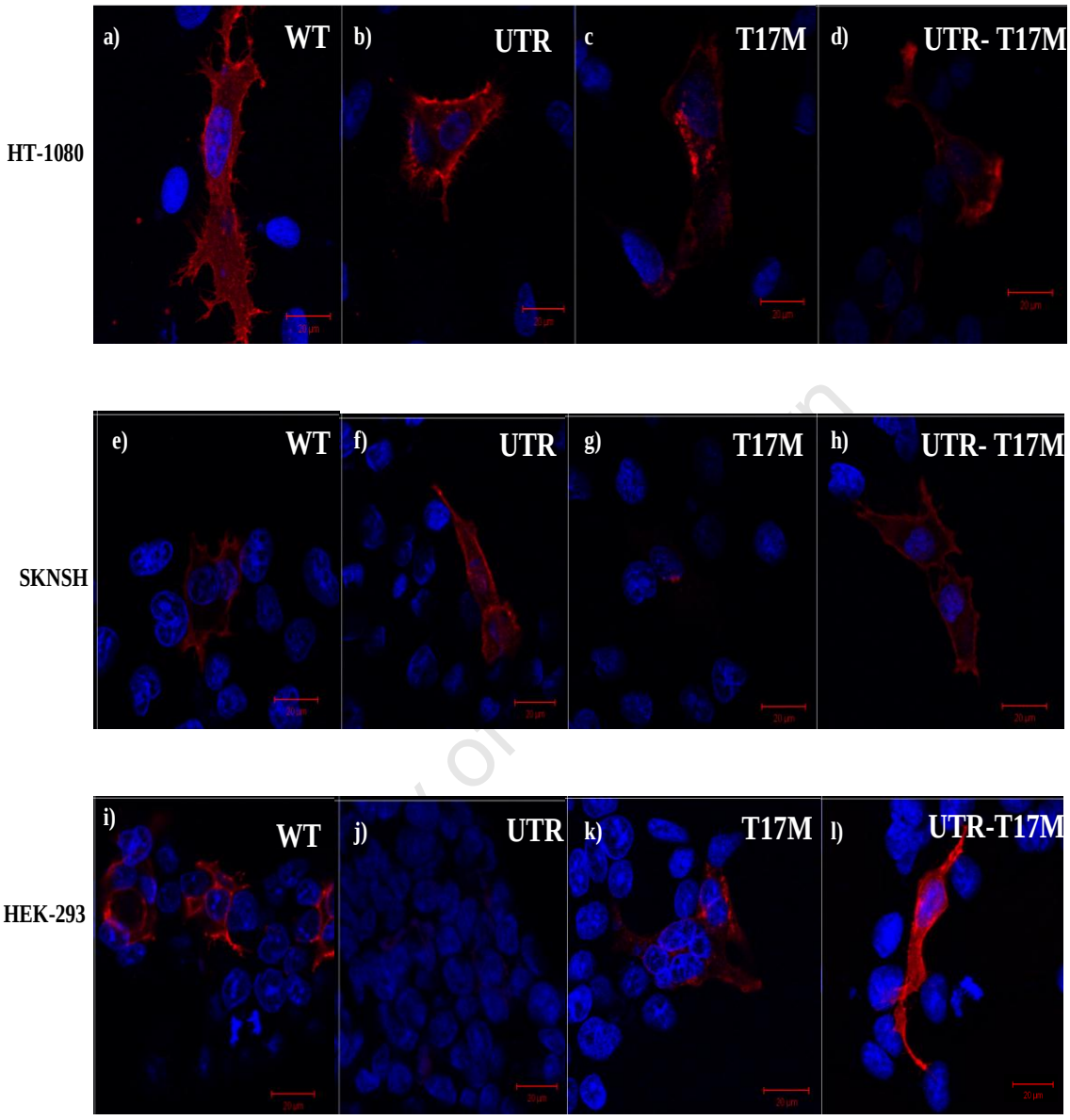

Figure 3. : Fluorescent images of cell lines expressing WT RHO and T17M mutant constructs. All images were taken using the same settings on the Carl Zeiss confocal microscope. The scale bar in each of the images is 20 µm and the red stain is indicative of RHO protein localisation as labelled by Cy3 fluorescent secondary antibody whereas the blue stain (DAPI) indicates nucleus staining and positioning in relation to the cell. Each panel is representative of expression in the three different cell lines. These images are representative of two or more independent ICC experiments performed for this construct.

3.2.2.3. Proline 347 Leucine (P347L)

In addition to protein misfolding as a mechanism for rod degeneration leading to RP, some mutations in the *RHO* gene such as P347L, may confer protein instability to RHO. This may be a consequence of the disruption of the Golgi-trafficking signal within the last four amino acids of the RHO C-terminal. In order to determine the effect of the 5′UTR variant on the P347L mutant, constructs with the P347L mutation alone, and *in cis* with the 5′ UTR variant, were expressed in all three cell lines, and protein localisation was determined.

According to Mendes et al. (2005), P347L, a Class I mutation, binds to 11-*cis* retinal and has a RHO WT protein localisation (appearance), but is not transported effectively from the inner segment to the outer segment. This defective trafficking targets the mutated form of RHO for immediate degradation in the cell, hence the instability of the protein. In cultured cells, however, the mutant P347L protein has been reported to traffic to the plasma membrane (Sung et al. 1991). This is thought to be artifactual i.e. a feature of cells grown *in vitro*.

The expression of the *RHO* P347L construct revealed that the protein trafficked to the plasma membrane in two cell lines (Figure 3.16 g, k) albeit in diminished quantities (as determined by fluorescent intensities), compared to cells transfected with RHO WT construct. (Figure 3.16 a, e, i). In HT-1080 cells however, there was a more pronounced decrease (Figure 3.16 c) and increase (Figure 3.16 d) in fluorescence of cells expressing RHO P347L only and the UTR-P347L constructs, respectively. The decreased fluorescence in both HEK-293 and SKNSH cell lines expressing the *RHO* P347L constructs may be indicative of steady state levels of RHO present in the cell at a given time.

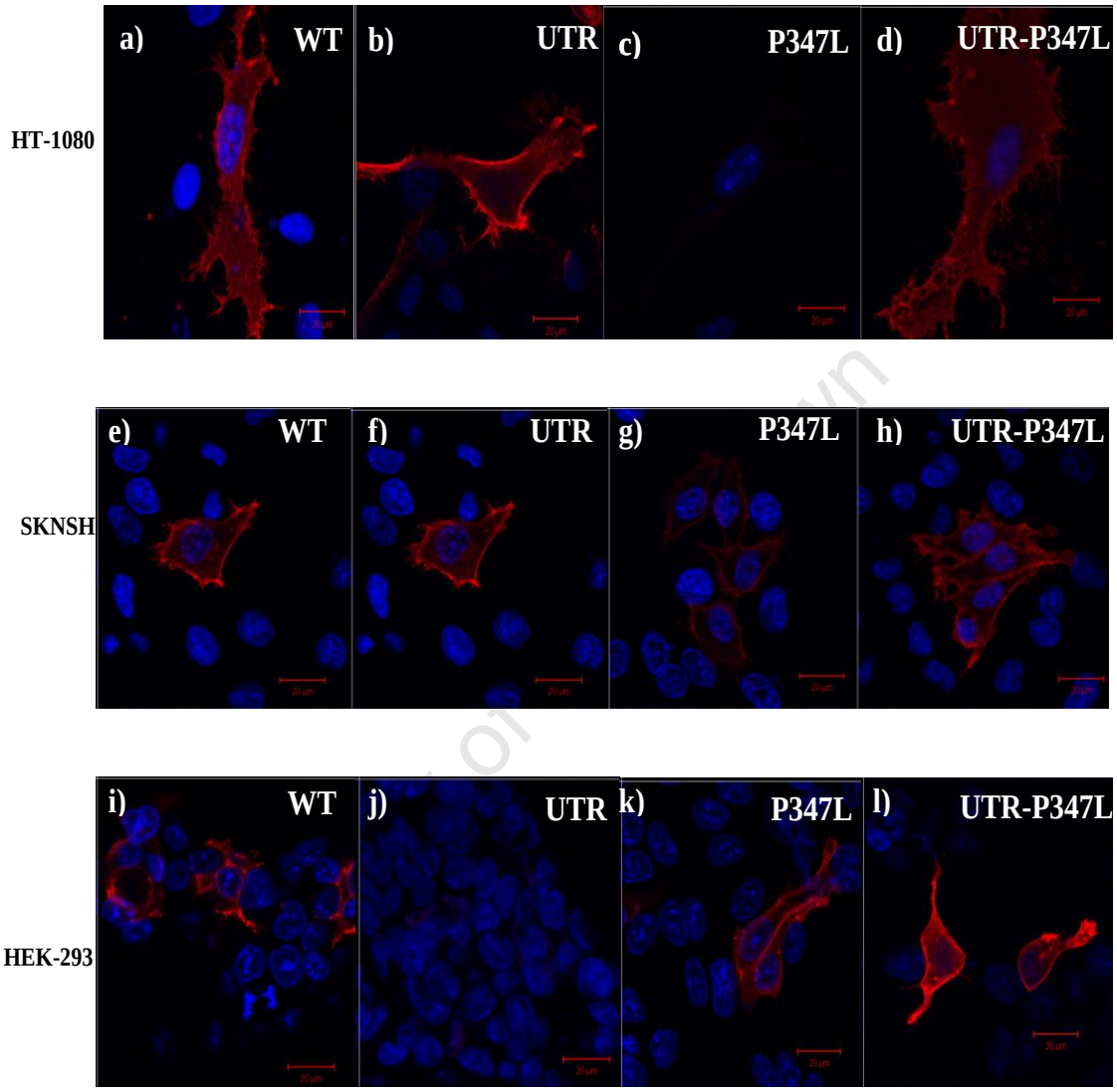

Figure 3. : Fluorescent images of cells expressing WT RHO and P347L mutant constructs. All images were taken using the same as settings on the Zeiss Confocal microscope. The scale bar in each of the images is 20 µm and the red stain is indicative of RHO protein localisation as labelled by Cy3 fluorescent secondary antibody whereas the blue stains (DAPI) indicate nucleus staining and positioning in relation to the cell. Each panel is representative of expression in the three different cell lines. These images are representative of two or more independent ICC experiments performed for this construct**.**

3.2.3. Protein expression differences between WT and mutation variants of RHO

Protein expression differences were analysed using SDS-PAGE mobility shift assays. Protein was harvested from cells 24 hr after transfection, electrophoresed on 10% SDS_PAGE, blotted onto nitrocellulose membrane and visualised by exposure on X-ray film (New Film, AGFA) for various lengths of time. It should be noted here, that optimisation for the detection of the RHO protein by means of western blot analysis proved to be difficult and could not be completed due to time constraints. The images provided here, were selected as the most representative of the blotting results obtained. As such, western blot analyses were only performed for the HT-1080 and SKNSH cell lines.

3.2.3.1. HT-1080

In cell lysates from HT-1080 WT RHO was visible at high intensity between the 35 kDa and 70 kDa size markers. The expected band size of WT mature RHO is 42 kDa. The deglycosylated form of RHO is detectable at 35-36 kDa (Ernst et al. 2007). It has also been previously reported that the RHO protein forms dimers which range from 60-100 kDa (Ernst et al. 2007), which may be an explanation for the bands observed at higher sizes in the western blot analysis (Figure 3.17).

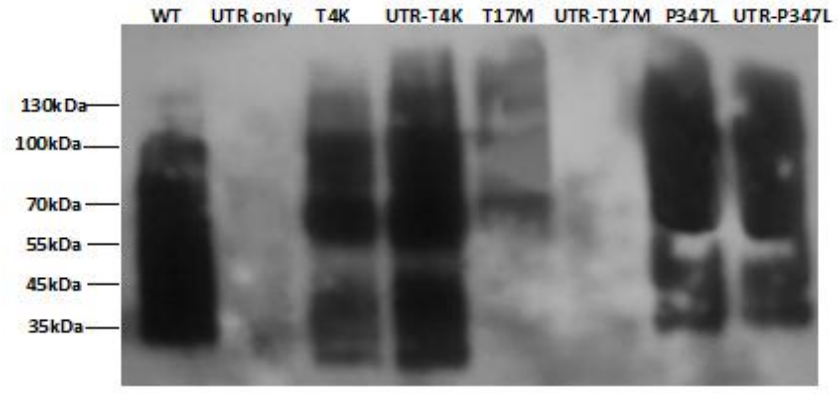

Figure 3. : Western blot analysis of WT and mutant opsins in cell lysates from HT-1080 cells. Total protein (15 µg) was separated on a 10% SDS-PAGE gel and lanes labelled as follows; WT, UTR only (5′UTR c.-26A>G), T4K, T17M and P347L. Mutant variants containing the 5′UTR variant were run adjacent to their specific mutation expressed alone for ease of comparison. RHO was detected by the ID4 antibody. The protein ladder is indicated on the left. This image is representative of numerous repeat experiments conducted on HT-1080 cells. A negative control cell lysate containing no transfected RHO was included in each run (not shown).

Apart from forming dimers, RHO also exhibits variable glycosylation patterns (Sung et al. 1991) in different cells lines, which appear as smearing on the western blot images. There is evidence of smearing in Figure 3.17, including the higher band sizes discussed previously. Interestingly, in all western analyses conducted on the HT-1080 cell line, there was no detectable protein in the 5′UTR only lane, even after numerous repeated blotting experiments. When protein was analysed from cells expressing the T4K mutant protein, bands were visible in ranges below 35 kDa (deglycosylated RHO) and above 70 kDa, with the highest intensities between 55 kDa and 70 kDa. In comparison to the WT, there was decreased intensity in the range of the 35-45 kDa, which is representative of mature RHO protein. Furthermore, when the T4K mutation was expressed *in cis* with the 5′UTR variant (UTR-T4K), there appeared to be an increase in band intensities at the same sizes, indicative of increased protein presence in cell lysates (Figure 3.17). The T17M mutant protein however, exhibited low band intensities, which appeared to decrease to non-detectable levels when the mutation was expressed *in cis* with the 5′UTR variant (UTR-T17M) (Figure 3.17). In comparison to the WT protein, there was almost no detectable protein between 35 kDa and 45 kDa (Figure 3.17).

Lastly, for the P347L mutant, there were no detectable differences in levels of protein expression when protein was analysed from cells in which the mutant construct was expressed alone and when expressed *in cis* with the UTR variant. Possible explanations for this observation may be that the 5′UTR variant did not influence protein expression of the P347L mutant or that the change was too subtle to be detected by western blot analyses. The p38 loading control for the HT-1080 cell line could not be detected accurately and thus the Ponceau S stain (Appendix B) was used as a measure of protein levels loaded onto the gel.

3.2.3.2. SKNSH

In the SKNSH cell lines, there appeared to be less smearing compared to the HT-1080 blots which as mentioned previously, may be an indication of the different glycosylation patterns exhibited by the different cells (Sung et al. 1991; Tam and Moritz, 2010).

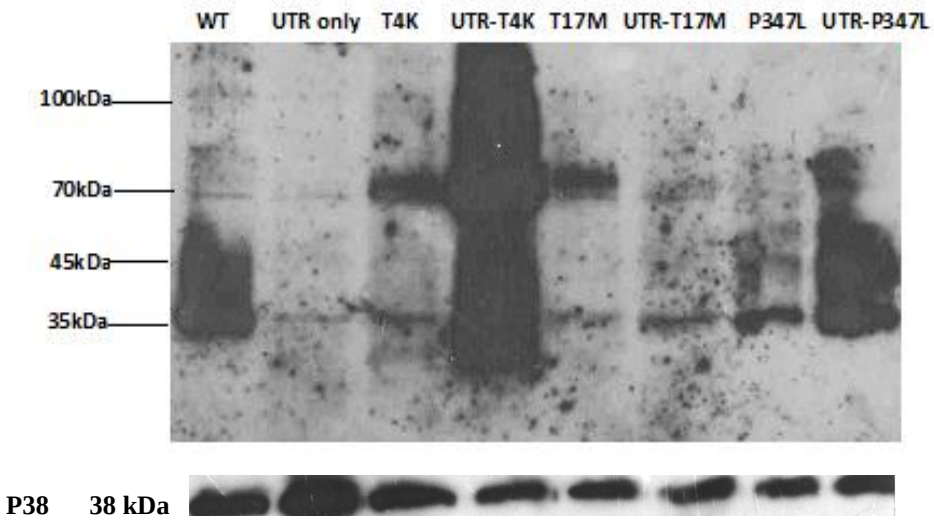

Figure 3. : Western blot analysis of WT and mutant opsins in cell lysates from SKNSH cells. Total protein (15 µg) was separated on a 10% SDS-PAGE gel and lanes labelled as follows; WT (wild-type), UTR only (5′UTR c.-26A>G), T4K, T17M and P347L. Mutant variants containing the 5′UTR variant were run on lanes adjacent to their specific mutation expressed alone for ease of comparison. RHO was detected by the ID4 antibody. The lower panel represents p389 (detected using anti-p38 antibody), which was included as a loading control to ensure even amounts of protein were loaded onto the gel. The protein ladder is indicated on the left. This image is representative of numerous repeat experiments conducted on SKNSH cells. A negative control cell lysate containing no transfected RHO was included in each run (not shown).

The WT protein band was observed to have highest intensity between 35 kDa and 45 kDa, as observed in the HT-1080 cell line (Figure 3.18). In the lane containing the UTR cell lysate, there was little detectable protein, although a few faint bands were visible. For the T4K mutation, higher band intensities were visible at 35 kDa and 70 kDa. A similar trend (as observed in the HT-1080 cell line), in which the band intensities increased significantly with smearing, when the mutation was expressed *in cis* with the 5′UTR variant, was observed. It can also be deduced from Figure 3.18 that the T4K cell lysate contained some form of mature WT RHO, as a band of 35 kDa similar to that found in the WT lane was visible. The increase in band intensities may be indicative of increased protein expression as a result of the 5′UTR variant. Protein from cells in which the T17M mutant construct was expressed alone showed bands at 35 kDa and 70 kDa, with higher band intensity at the 70 kDa which may be indicative of increased presence of dimers (Sung et al. 1991) or immature protein. The band intensities appeared to decrease significantly when the T17M mutation was expressed *in cis* with the 5′UTR variant. Although the same trend (of decreased protein for the UTR-T17M) was observed in the HT-1080 cells, this was in contrast

to what would be expected if the 5′UTR variant was responsible for increased expression of the protein (as observed for the other glycosylation mutation, T4K).

In the SKNSH cell line, the P347L mutant protein appeared to have decreased band intensity compared to the P347L mutant protein expressed *in cis* with the 5′UTR variant. Furthermore, for the UTR-P347L, protein bands were also detected at similar sizes to WT (between 35 kDa and 45 kDa) with slightly increased smearing, which is indicative of heterogeneously glycosylated protein (Sung et al. 1991). This was in contrast to the observed band intensities in the HT-1080 cell line.

The fact that the p38 loading control was readily detectable in this cell line, implies that the difficulty in RHO detection may have been due to the properties of the protein or the conditions in which the protein was electrophoresed. Dot blot analyses performed independently, established that there was sufficient anti-body and protein interaction (Appendix C).

3.2.4. Altered transcript expression in *RHO* mutants carrying the 5′UTR variant

Quantification of transcripts was performed to determine whether the differences observed at the protein level were relative to mRNA transcript expression. Quantification was performed in all three cell lines. Data retrieved from the experiments was analysed using the ‘standard curve method’ (Nolan et al. 2006; Pabinger et al. 2009). Figure 3.19 depicts the results observed for each of the cell lines, for all RHO variants.

Compared to the WT, the 5′UTR variant transcript expression was much lower in all three cell lines (Figure 3.19). Similarly, in cells transfected with the T4K mutation construct, transcript expression was much lower and comparable to the 5′UTR variant transcript levels, except for the SKNSH cell line, in which transcript expression levels were higher. Conversely, when the T4K mutant construct was expressed *in cis* with the 5′UTR variant in all three cell lines, expression increased significantly, although transcript levels were still low when compared to WT. Interestingly, UTR-T4K transcript expression in the SKNSH cell line was much higher and even exceeded WT levels (Figure 3.19). This observation was in contrast to the ICC results since it is expected that an increase in expression of mutant

transcript, would result in an increase in aggregate formation, however this was not observed.

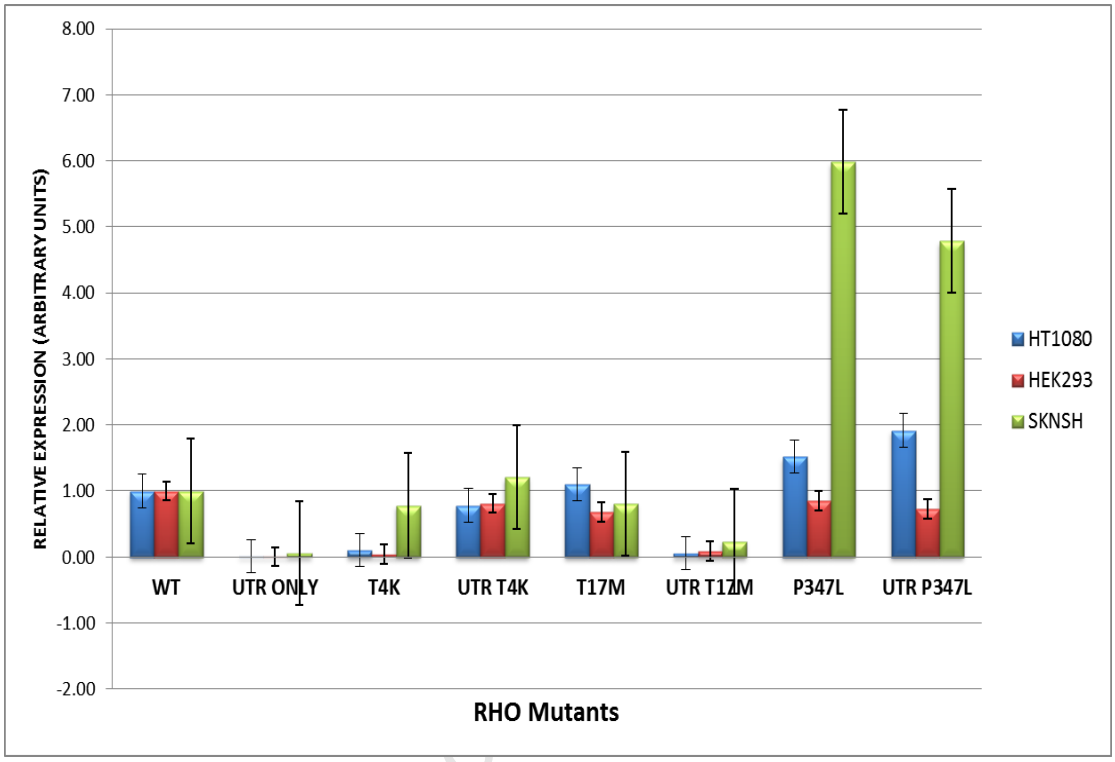

Figure 3. : Graph showing expression differences between WT RHO and mutant constructs. All differences in transcript expression were calculated in relation to the WT transcript. Differences in expression are expressed in units representing fold increase or decrease in expression of the transcripts.

In contrast to the expression levels of the T4K mutant construct, T17M transcript expression decreased significantly in all three cell lines when the mutation was expressed *in cis* with the 5′UTR variant. This observation is in agreement with the ICC results, where fewer aggregates were visible in UTR-T17M expressing cells as decreased transcript expression should, in theory, result in a decrease in protein expression and thus decreased aggregate formation.

Transcript expression levels of the P347L mutant varied significantly within all three cell lines. In HT-1080 cells, the P347L transcript increased almost two-fold compared to transcript expressed from constructs carrying the P347L mutation *in cis* with the 5′UTR variant. Conversely, in the HEK-293 cell line, P347L transcript

expression decreased slightly when the mutant was expressed with the 5′UTR variant. A similar trend was also observed in the SKNSH cell line, in which transcript levels decreased one-fold when P347L was expressed *in cis* with the 5′UTR variant. Transcript levels for both P347L and UTR-P347L were higher compared to the other variants and the WT. The differences in expression exhibited in the different cell lines signifies the different features of the three cell lines which may contribute to the observed varied response to the same mutation.

A summary of the functional results is provided in the Table 3.1 below.

Table 3. : Summary of results from functional analyses of each of the different mutations and RHO 5′UTR variant. Reported clinical and biochemical features are also provided.

Mutation/Variant	Biochemical Features	Clinical/Phenotypic Data	Cell Line used for Expression Work	Functional Analyses		
				ICC	WB	qPCR
g.269A>G (-26A>G)	Unknown; Proposed to increase risk of RP (Wang et al. 2005)	N/A	HT-1080	Localisation to plasma membrane, RHO WT appearance	Not detected in western blot	Very low transcript expression levels compared to WT *RHO*
			SKNSH	Localisation to plasma membrane, with a WT RHO appearance	Not detected in western blot	Very low transcript expression levels compared to WT *RHO*
			HEK-293	Hardly detectable with no visible localisation in plasma membrane	N/A	Very low transcript expression levels compared to WT *RHO*
T4K	Mutation disrupts RHO Glycosylation at N2, Protein instability (Hargrave, 1977; Murray et al. 2007; Tam and Moritz, 2009)	Sectoral RP; Light sensitive degeneration (Tam and Moritz, 2009)	HT-1080	**T4K only**-aggregate formation; **UTR-T4K**-No visible aggregates	**T4K only**-mature RHO protein detected with low band intensities and smearing of high molecular weight bands indicative of dimers; **UTR-T4K**-Similar features as above with increased intensity suggesting increase in protein expression	**T4K only**-low levels of transcript compared to WT *RHO;* **UTR-T4K**-Increased transcript expression compared to the **T4K** mutant

			SKNSH	**T4K only**-visible aggregate formation; **UTR-T4K-** No visible aggregates	**T4K only**-mature RHO protein detected at low band intensities and another band at 70 kDa (dimer); **UTR-T4K**-Similar features as above with increased intensity suggesting increase in protein expression	**T4K only**-low levels of transcript compared to WT *RHO;* **UTR-T4K-** Increased transcript expression compared to the **T4K** mutant
			HEK-293	**T4K only**-No visible aggregate formation; **UTR-T4K**-No visible aggregates; protein localisation to plasma membrane	N/A	**T4K only**-low levels of transcript compared to WT *RHO;* **UTR-T4K-** Increased transcript expression compared to the **T4K** mutant
T17M	Mutation disrupts glycosylation at N15 –forms aggregates in cell culture, (Sung et al. 1993); misfolding mutation that has been shown to accumulate in the ER and golgi (Mendes et al. 2005)	light-sensitive photoreceptor degeneration in RP (Tam and Moritz, 2009)	HT-1080	**T17M only**-visible aggregate formation; **UTR-T17M-**Protein localisation to the plasma membrane with little to no visible aggregates	**T17M only**-mature RHO not detected, with smearing at higher molecular weights indicating presence of immature RHO; **UTR-T17M**-Hardly any protein detected	**T17M only-** relatively high transcript expression (comparable to WT *RHO*); **UTR-T17M-**Very low levels of transcript expression (comparable to ***UTR only*** transcript expression)
			SKNSH	**T17M only**-visible aggregate formation; **UTR-T17M**-Protein localisation to the plasma membrane with no visible aggregates	**T17M only**- mature RHO protein detected at low band intensities and another band at 70 kDa (dimer); **UTR-T17M**- little protein detected with the	**T17M only-** relatively high transcript expression (comparable to WT *RHO*); **UTR-T17M-**Very

					same banding patterns as T17M, except for increased presence of mature protein than dimers (70 kDa)	low levels of transcript expression (comparable to **UTR only**) transcript expression
			HEK-293	**T17M only**-visible protein localisation to plasma membrane and little aggregate formation; **UTR-T17M**-Protein localisation to the plasma membrane with a few visible aggregates	N/A	**T17M only**- relatively high transcript expression (comparable to WT *RHO*); **UTR-T17M**-Very low levels of transcript expression (comparable to ***UTR only*** transcript expression)
P347L	Mutation disrupts the highly conserved golgi trafficking signal consensus sequence (VAPA) (Deretic et al. 1998; Kaushal and Khorana, 1994; Kennan et al. 2005; Sung et al. 1991; Sung et al. 1993)	Early onset night blindness (Cideciyan et al. 1998; Chan et al. 2001)	HT-1080	**P347L only**-Protein hardly detectable; **UTR-P347L**- Protein localisation to plasma membrane, appearance similar to WT RHO, increased fluorescence compared to above	**P347L only**-Protein smearing of uniform intensity through the length of the lane. No definitive bands; **UTR-P347L**- Protein smearing of uniform intensity through the length of the lane. No definitive bands, No discernable difference between the P347L and UTR-P347L protein lane	**P347L only**- Transcript expression slightly higher than WT *RHO*; **UTR-P347L**- Increased transcript expression compared to the above
			SKNSH	**P347L only**-Protein hardly detectable;	**P347L only**- very little protein detected with a distinct band at 35 kDa (mature RHO)	**P347L only**- Transcript expression much higher than WT *RHO*;

				UTR-P347L- Protein localisation to plasma membrane, appearance similar to WT RHO, slightly increased fluorescence compared to above	**UTR-P347L-**Smearing pattern, with the 35 kDa (mature RHO) band being visible with increased intensity.	**UTR-P347L-** Slightly decreased transcript expression compared to the above
			HEK-293	**P347L only-**Protein localisation to plasma membrane, appearance similar to WT RHO with decreased fluorescence; **UTR-P347L-** Protein localisation to plasma membrane, appearance similar to WT RHO, increased fluorescence compared to above	N/A	**P347L only-** Transcript expression comparable to WT *RHO*; **UTR-P347L-** Decreased transcript expression compared to the above

Chapter 4: Discussion

Inherited forms of RDDs predominantly exhibit monogenic Mendelian inheritance, and are reported to be the main cause of blindness in individuals between the ages of 20-64 years (Wright et al. 2010). The most common form of these RDDs is RP, which is reported to affect 1 in 3,500-4,000 individuals worldwide (Bowne et al. 1999; Hartong et al. 2006; Tan et al. 2009; Wright et al. 2010). Mutations in *RHO* are arguably the most common cause of RP (Cideciyan et al. 1998; Rajan & Kopito 2005; Saliba et al. 2002; Wright et al. 2010). To date, over 150 mutations in the *RHO* gene have been identified (www.sph.uth.tmc.edu/Retnet/disease.htm). The incidence of RP in South Africa is still unknown, however *RHO* mutations that are common in other parts of the world such as Europe, have been reported to be uncommon in South Africa (Roberts et al. 2000).

The highly heterogeneous nature of RP (Rattner et al. 1999; Phelan & Bok 2000; Daiger et al. 2006; Daiger et al. 2007; Wright et al. 2010) has brought to light the effect of factors other than primary disease-causing mutations, which may contribute to the penetrance and expressivity of the disease. One example of such factors is that of genetic modifiers, which have been associated with exacerbating, ameliorating or altogether preventing manifestation of disease. Genetic modifiers may present in various forms including *trans*-acting genes, or genetic variations such as SNPs in non-coding regions of DNA, whose effects are determined by their location (Knight 2003).

In this study, a 5′UTR variant (c.-26A>G) in *RHO*, proposed by Wang et al. (2005a) to be associated with an 'increased risk' of RP, was analysed for functional significance in regard to the RHO protein using three mammalian cell lines. Interestingly, this SNP had previously been found to occur at a high frequency in indigenous African individuals (Roberts L, MSc Thesis, UCT, 2006). To our knowledge, this is the only study that has examined the functional significance of the 5′UTR *RHO* variant. The results obtained from this investigation on the effect of the c.-26A>G variant will be discussed according to ICC protein localisation, which is

more relevant to the RP phenotype, and subsequently, in relation to western blots and mRNA quantification.

4.1. The Predicted effects of the c.-26A>G variant and frequencies in AdRP families

Bioinformatic analyses of the *RHO* c.-26A>G variant were employed in order to determine the potential effects of this variant on the RHO protein. Analyses using BioGrid and STRING revealed that the RHO protein interacts with a total of ten proteins (section 3.1.1.1), most of which are involved in the visual transduction pathway. Interestingly, one of the major proteins that interact with RHO, Transducin, has not been included, which could highlight a limitation of these databases. Nonetheless, it is not difficult to imagine that a change in gene and protein expression such as that observed in this study (as a result of the c.-26A>G change), may alter overall proteome homeostasis (Wiseman et al. 2007), which, when coupled to a disease-causing mutation may alter binding affinities for any of the proteins that interact with RHO. Furthermore, examination of the conservation status of the 5′UTR region surrounding the c.-26 nucleotide position reveals that it is not conserved, with variable frequencies of the 'A' 'G' and 'C' nucleotides. Although the 'G' allele is reported to be ancestral (NCBI, SNP Cluster report), it occurs at a much lower frequency (3/12), compared to the 'A' allele (5/12) in all twelve vertebrate species (Figure 3.2), which may imply that evolutionary mechanisms do not favour this allele. SNP frequency analysis from the 1 000 Genomes project (http://browser.1000genomes.org) for the c.-26A>G variant in other populations, namely, Chinese, European, Japan and African (Yoruba) revealed that the 'G' allele occurred at highest frequencies in Africans and the lowest in Europeans, which correlated to previous genotyping data reported in South Africa. The Asian populations had both the 'A' and 'G' alleles equally represented.

The fact that the SNP position is not highly conserved could imply that the c.-26A>G SNP may not have a significant functional effect on expression or regulation of RHO. Nonetheless, the c.-26A>G variant may alter a consensus sequence for a transcriptional factor, regulatory binding factor or microRNA binding sequence, that may exert the cellular effects observed in this study. Certainly, microRNAs have

been reported to alter gene expression through post-transcriptional mechanisms (Loscher et al. 2007).

Analysis of the mRNA sequence carrying either the 'A' or 'G' allele using TESS, revealed that the presence of the 'G' allele abolished a consensus sequence (binding site) for the ARP-1 (Apolipoprotein A1 regulatory protein) transcription factor. The ARP-1 protein is a member of the nuclear receptor superfamily and reportedly has a retinoic acid binding site (Widom et al. 1992). This may have important implications for RHO which is covalently bound to retinoic acids such as 11-*cis* retinal.

In addition, the effect of the c.-26A>G change may be linked to mRNA secondary structure folding. Analysis of the *RHO* 5′UTR mRNA using mFOLD revealed that the introduction of the 'G' allele resulted in only two possible secondary structures as opposed to the three structures obtained using the 'A' allele. Such a change in the 5′UTR of *RHO* may alter the overall stability of the full mRNA sequence. The stability of RNA is reported to be dependent on numerous factors, including free energies, GC content and formation of stem-loop structures (Schultes et al. 1997). Furthermore, the more negative the free energy of a particular RNA structure, the more likely that the structure will be formed. This has important implications for subsequent tertiary mRNA structures, as this final configuration is believed to be important for molecular function i.e. enabling the binding of *trans*-acting factors including translation initiating proteins (Jiang, 2010).

In AdRP family members in this study, the 'G' allele of the c.-26A>G variant was found to occur at low frequencies (21/70 compared to the 'A' allele (49/70). The 'GG' genotype was identified to occur in only four individuals in the entire cohort, two of whom were of indigenous African ethnicity. In the patient population, the 'G' allele was also found to be under-represented and was identified in nine patients as opposed to the 'A' allele (identified in eleven patients). In addition, the 'GG' genotype was found in four patients, two of which were of indigenous African ancestry and carried the P347L mutation. It is important to note, however, that the study cohort in this investigation represents a bias, as most samples were from individuals of Caucasian ancestry. A number of factors may contribute to this bias, including socio-economic factors, disease awareness and initial modes of

recruitment. It was not possible to infer the relative location (*cis* or *trans*) of the c.-26A>G variant in patients with disease-causing mutations due to a lack of biological material from all family members. It was also not possible to determine the clinical effect of the c.-26A>G variant on phenotype as the cohort of patients with different combinations of the variant and disease-causing mutations, was too small for evaluation.

4.2. The differential effect of the 5'UTR variant on glycosylation mutants: T4K and T17M

4.2.1. T4K and UTR-T4K

The N-terminal region of RHO is glycosylated at two points, N2 and N15 (Hargrave, 1977; Murray et al. 2009; Tam and Moritz, 2009). Mutations at these residues or within the glycosylation consensus sequence, such as the T4K mutation, have been shown to disrupt N-linked glycosylation and result in sectoral RP which primarily affects the inferior retina (Krebs et al. 2009; Tam & Moritz, 2009). A mutation similar to T4K in humans, the Thr-4-Arg (T4R) was found in a naturally occurring dog model of RP, and was reported to exhibit light sensitive retinal degeneration (Kijas et al. 2002). It is thought that the human T4K mutation causes retinal degeneration through a similar mechanism.

According to Mendes et al. (2005) the T4K mutation is classified as a Class IV *RHO* mutation, which is described as affecting the stability and post-translational modification of the protein. It should be noted that there are several reports on the classification of *RHO* mutations, including the T4K mutation which has been classified as Class II (Sung et al., 1991; Sung et al., 1993), Class III (Kaushal & Khorana 1994; Krebs et al. 2009) and Class IV(Mendes et al. 2005). For instance, Sung et al. (1993) classified *RHO* mutations into two main classes (Class I and II) based on their genetic location and *in vitro* cell culture studies; the T4K mutation was grouped into Class II (N-terminal cytoplasmic and intradiscal domain mutations). Yet another group classified the T4K mutation as a Class III mutation, based on clinical and biochemical data (Murray et al. 2009). In addition to the differing classifications, the highly heterogeneous nature of the RHO-related RP phenotype has been a confounding factor, as not all classification schemes correlate

with clinical expression and severity of disease (Iannaccone et al. 2006). In addition, the lack of conclusive phenotypic and molecular pathological data for certain mutations has hindered the classification process. Indeed, for the T4K mutation, there is little data on the molecular pathology of the mutation, and most of the information available has been deduced from animal models.

The incidence of the T4K mutations is reportedly low in various countries including China (<2%) (Chan et al., 2001; Zhang et al. 2006; Li et al., 2010). This mutation has however, not been reported in South Africa, to date. Nonetheless, it does make an interesting case for study.

In this study, the T4K *RHO* mutation construct was expressed exclusively and *in cis* with the 5′UTR variant in three different cell lines. Analyses for protein localisation were carried out using ICC, and protein expression differences were determined using western blot analyses. When expressed exclusively, the T4K RHO mutant protein formed aggregates in the perinuclear regions of two of the cell lines, i.e. HT-1080 and SKNSH, but not in the HEK-293 cell line. No other studies have reported this aggregate-forming feature of the T4K mutation, however, as stated previously, Sung et al. (1993), classified T4K as a Class II mutation, a group of mutations that are reported to alter stability and folding of the protein. Since the T4K mutation forms part of the RHO glycosylation consensus sequence, it is conceivable that a mutation of this nature would have some kind of effect on folding of the protein. Indeed, the T17M mutation, which is also located in the RHO glycosylation consensus sequence, has been reported to form intracellular inclusions with little to no protein trafficking to the plasma membrane (Sung et al. 1991).

In the HEK-293 cell lines, the T4K mutant protein appeared to traffic to the plasma membrane akin to the WT RHO protein. A possible explanation for this observation may be similar to that reported by Pandor et al. (2010) in which mutant CAIV protein expressed in HEK-293 cell lines appeared to fold and traffic normally to the plasma membrane. It is possible that these HEK-293 cell lines may have increased expression of specific posttranslational processing proteins that enable folding of certain mutant proteins.

A previous study reported that different cells have different concentrations and components of chaperones (Wiseman et al. 2007). Furthermore, in the case of misfolding mutants, not only is the unfolded protein response (UPR) (which involves activities of the Endoplasmic Reticulum-associated degradation (ERAD) pathway) activated; misfolded proteins also activate the Endoplasmic Reticulum-associated folding (ERAF) pathway (Matus et al. 2011). According to Wiseman et al. (2007), the ERAF pathway can compete with ERAD machinery to recover misfolded proteins and export them efficiently to the plasma membrane. Furthermore, different cell types have different distributions and concentrations of ERAD, ERAF and export components, which determine the cell's ability and efficacy in folding misfolded proteins (Wiseman et al. 2007; Matus et al. 2011).

Interestingly, when the T4K mutant construct was expressed *in cis* with the 5′UTR variant, the RHO protein appeared to fold and traffic to the plasma membrane, in the same way as the WT. This feature, whereby no protein accumulation or aggregate formation was visible, was observed in both the HT-1080 and SKNSH cell lines. A possible explanation may be that since the c.-26A>G variant is located in the untranslated (UTR) region of RHO, which is part of the promoter, the variant may have altered expression of the protein by reducing the amount of protein being expressed. This reduced protein expression may meet the export threshold of the cell and allow cellular machinery to process the RHO protein (Wiseman et al. 2007). However, analysis of protein expression differences between T4K and UTR-T4K mutant proteins by means of western blotting, revealed that there was an increase in protein expression when the T4K mutant construct was expressed *in cis* with the 5′UTR variant. Although the western blot results proved to be inconclusive and not reproducible, the same trend was observed in all attempted western blots for the T4K and UTR-T4K mutants. If, in fact, an increase in protein expression occurs due to the c.-26A>G variant, this suggests that there may be an increase in protein translation efficiency.

There are two possible explanations for an increase in protein translation efficiency potentially caused by the c.-26A>G 5′UTR variant. Firstly, the variant may have altered the overall folding efficiencies and stable energies of the protein, making it more stable and thus less susceptible to degradation (Wiseman et al. 2007).

Secondly, the 5′UTR variant may have positively altered the translational efficiency of the mRNA transcript, either by stabilising the mRNA or changing the conformation of the secondary structure such that the translational machinery has increased access to mRNA (Jiang, 2010; Lammich et al. 2010).

Interestingly, mRNA quantification analyses of the T4K and UTR-T4K mutants, revealed an increase in transcript expression for the UTR-T4K variant, in all three cell lines. This increase in expression varied between the different cell lines, which is attributable to the diverse features of each of the cell lines. As previously suggested, this increase in transcript expression (Figure 3.19) may be a function of the increased stability of mRNA due to the 5′UTR variant (Lammich et al. 2010). This increased stability may either be due to altered free energy (delta G) or the decrease in binding of mRNA decay enzymes (such as *Dcp* 2) as a result of altered RNA structure, thus interfering with their ability to initiate degradation (Lammich et al. 2010).

The combined analyses of the T4K mutant construct expression on its own and *in cis* with the 5′UTR variant, suggests that there may be a delicate interplay between cellular proteome homeostasis (ERAD, ERAF and export machinery), including translational machinery and structural integrity i.e. stability of RNA and protein. All of the above factors may interact to result in the observed phenotype (increased mRNA and protein expression with no aggregate formation); the extent of which is determined by each specific cell line.

4.2.2. T17M and UTR-T17M

As mentioned previously, the T17M RHO mutation also forms part of a glycosylation consensus sequence for the RHO protein (Murray et al. 2009; Tam & Moritz 2009). The T17M mutation is a known misfolding mutation (Mendes et al. 2005) that has been shown to accumulate in the ER and golgi body, as well as reconstitute poorly or only partially with 11- *cis* retinal (Sung et al. 1991; Kaushal & Khorana 1994; Mendes et al. 2005). The T17M mutation has also been linked to light-sensitive photoreceptor degeneration in RP with a sectoral or regional RP phenotype (Tam & Moritz 2009). Although the T17M mutation has been classified variably (Class II and Class III), the main features of the two classes have essentially remained the same i.e. the proteins remain in the ER and reconstitute with 11-*cis*

retinal only partially (Sung et al. 1991; Kaushal & Khorana 1994; Mendes et al. 2005).

Similar to the T4K mutation, the frequency of the T17M mutations reported in other countries, such as the USA, is low (<3%) (Dryja et al. 1991; Cideciyan et al. 1998). In South Africa, the T17M mutation has been identified in three related individuals, who were affected with RP (Unpublished data).

In this study, the T17M mutation was expressed exclusively as well as *in cis* with the 5′UTR variant, and analysed to determine protein localisation and changes in transcript expression. In all three cell lines, the T17M RHO mutant protein, exhibited protein aggregation similar to that seen with the T4K mutant protein, in perinuclear regions. This is consistent with previous reports in which the T17M mutant protein, expressed in various cells including COS-1 and HEK-293, exhibited protein accumulation in the ER and surrounding regions (Sung et al. 1991; Kaushal & Khorana 1994). The degree of protein accumulation observed varied amongst the different cell lines, with the HEK-293 cells translocating some protein to the plasma membrane (Figure 3.15 k). This observation may be attributed to varying inherent features of the different cell lines, as described above.

When the T17M mutation was expressed *in cis* with the 5′UTR variant, little to no protein aggregation was visible in all three cell lines. This change in cellular phenotype could be attributed to a decrease in protein expression that enables the cell to cope with the decreased amount of misfolded protein i.e. is below the folding threshold (Wiseman et al. 2007). Indeed, this hypothesis is in part supported by the western blot analyses (Figures 3.17 and 3.18) which revealed a decrease in protein levels when the T17M mutation construct was expressed *in cis* with the 5′UTR variant. This decrease in protein expression may be due to a number of reasons. Firstly, the incorporation of the 5′UTR variant may have negatively altered the folding efficiency and thus stability of the protein, thereby targeting the protein for faster degradation (Wiseman et al. 2007). This hypothesis supports previous classification schemes of *RHO* mutants, where the T17M mutant protein was reported to result in misfolding and or instability of the protein (Sung et al. 1991;

Sung et al. 1993; Mendes et al. 2005) since, if the mutation is already unstable, then the c.-26A>G change may exacerbate this feature.

Secondly, the proximity of the 5′UTR variant to the T17M mutation may result in an altered secondary RNA structure that does not allow for sufficient translation initiation or continuation of translation of the protein (Pickering & Willis, 2005; Lammich et al. 2010). Such cases of translational repression have been reported to be due to the blocking of translational machinery i.e. blocking of eIF4A/B binding sites or through the formation of stem loop structures that are proximal to 5′ translation initiation sites (Pickering & Willis 2005).

In this investigation, mRNA transcript quantification data revealed that there was a decrease in transcript levels observed in all three cell lines, when the T17M mutation construct was expressed *in cis* with the 5′ UTR variant (Figure 3.19). Apart from altering the RNA secondary structure, the proximity of the 5′UTR variant to the T17M mutation could render the RNA structure unstable by altering free energies (delta G) or by increasing its affinity for degrading enzymes, making it susceptible to degradation (Lammich et al. 2010). Suppression of gene expression leading to decreased transcript expression may also be attributed to the formation of stable G-quadruplex structures (since the c.-26A>G incorporates another 'G' nucleotide), which have been reported to be mostly present in promoters and untranslated regions (Halder et al. 2009).

The collective data obtained from this investigation of the RHO T17M mutant protein implies that there is a decrease in protein expression when the c.-26A>G variant is present. This decreased protein may be due to translational repression, RNA instability or protein instability, and could result in the observed cellular phenotype.

4.3. The effect of the 5'UTR variant may be determined by the distance between the c.-26A>G variant and the mutation; the case of P347L

The P347L mutation, located at the carboxyl terminal of RHO, forms part of a consensus sequence for a golgi trafficking signal that is responsible for the transportation of the RHO protein from the rod inner segment (IS) to the rod outer segment (OS) where it is embedded in the membrane discs (Deretic et al. 1998; Oh 2003; Kennan et al. 2005; Rakoczy et al. 2011). The P347L mutation has been reported in various populations including China, Germany, Italy, Japan, the UK and the USA (Dryja et al. 1991; Cideciyan et al. 1998; Chan et al. 2001; Ziviello et al. 2005; Ando et al. 2007). The codon, 347 by itself, is a mutation 'hot spot' with up to six possible mutations. In South Africa, the P347L mutation has been reported in only one individual (Greenberg et al. 1999; Roberts et al. 2000). Patients who have the P347L mutation have been reported to have an early onset of night blindness (Cideciyan et al. 1998; Chan et al. 2001).

The P347L mutation has been classified as a class I mutant and reportedly exhibits typical WT features *in vitro*, trafficking to the plasma membrane and reconstituting with 11-*cis* retinal (Sung et al. 1991; Sung et al. 1993; Mendes et al. 2005). The fact that expression of the P347L mutant *in vitro* did not exhibit any evidence of mis-localisation prompted the idea that the carboxyl terminus of RHO may be involved in a specific process in the photoreceptor cell, which is not apparent in mammalian cell models (Sung et al. 1993). Animal models carrying the P347L mutation have since provided *in vivo* evidence of mis-localisation (Li et al. 1998; Kennan et al. 2005). In this study, protein localisation analysis of the RHO P347L mutant protein using ICC revealed localisation similar to that observed for the WT RHO protein i.e. protein trafficking to the plasma membrane in HT-1080, SKNSH and HEK-293 cells, albeit with reduced fluorescence (Figure 3.16).

Interestingly, when the P347L mutation construct was expressed *in cis* with the 5′ UTR variant, there were no major differences, except for a slight increase in fluorescent intensity in all cell lines studied. Western blot analysis revealed that there

was no marked difference between the P347L and the UTR-P347L mutant proteins, especially in the HT-1080 cell line (Figure 3.17). In the SKNSH cell line (Figure 3.18), there appeared to be an increase in protein expression, which substantiated the increased fluorescence observed in the ICC results for this cell line. Quantification of transcripts from the same constructs (P347L and UTR-P347L mutants) revealed no real trend in terms of a decrease or increase in transcript levels, which appeared to be dependent on the cell line.

There are several explanations for the observed features of the P347L mutation. This mutation may confer instability to the RHO protein, which would make the protein more susceptible to faster degradation. This instability could occur despite the presence of the 5′UTR variant, which would account for the variable protein fluorescence intensity and expression in the HT-1080 and SKNSH cell lines. Furthermore, the variable transcript levels between each of the cell lines implies that the expression and stability of the mutant UTR-P347L transcript is a function of cell-specific features (Wiseman et al. 2007) or due to the temporal stability of the mutant transcript.

In contrast to what was observed with the other two *RHO* mutations (T4K and T17M), the presence of the 5′UTR variant appears not to greatly influence expression and or localisation of the P347L mutant protein. This highlights the fact that of the three mutations, P347L is situated the furthest from the 5′UTR. This physical distance in the mRNA could determine the extent of the influence of the 5′UTR variant on each of the mutations. This observation may also be a plausible explanation for the differences observed between proteins expressed from UTR-T4K and UTR-T17M mutant constructs. A potential hypothesis is that the variable RNA instability observed here is a function of the proximity of the 5′UTR variant to the mutations, which supposedly alter the RNA secondary structure conformation and thus the free energies (delta G) (Ross, 1995; Pickering & Willis 2005; Halder et al. 2009; Jiang 2010; Lammich et al. 2010).

4.4. Does the 5'UTR variant elicit transcriptional regulation or translational repression?

Functional analyses (by means of ICC) of the 5′UTR variant revealed that when the c.-26A>G mutant construct was expressed exclusively, RHO protein had a similar WT appearance in all three cell lines with variable fluorescent intensities. For instance, in both the SKNSH and HT-1080 cell lines, protein localisation along the membrane was readily observed, whereas in the HEK-293 cells the red fluorescent label of RHO protein was hardly detectable. A possible explanation could be that the 5′UTR variant elicits varying responses in each of the cell lines (Wiseman et al. 2007).

Furthermore, during western blot analysis, protein from cells transfected with the 5′UTR expression construct was hardly detectable in two of the cell lines (Figures 3.17 and 3.18). This data combined with the low transcript levels observed from the mRNA quantification data, suggests that the 5′UTR variant (expressed exclusively) prompts some kind of transcriptional regulation, which results in diminished protein expression. If indeed the 5′UTR variant regulates transcription to such low levels (as observed when the 5′UTR variant is expressed alone), then transcript levels for all three mutations expressed *in* cis with this variant would be expected to be just as low. However, for each of the three mutations expressed *in cis* with the variant expression of UTR-T17M is considerably lower than WT in all three cell lines; and expression of UTR-P347L is variable compared to WT in HEK-293s and SKNSH respectively. Transcriptional regulation by c.-26G>A may therefore not be plausible.

This analysis suggests that the mode of action of the 5′UTR variant may be through translational repression. If the hypothesis of translational repression is considered to be true, the question of the mechanism of repression remains. A number of these mechanisms have been discussed previously, including RNA instability, altered secondary structures, stem-loop formation in close proximity to translation initiation sites and altered affinities for *trans*-acting translational proteins (Davuluri et al. 2000; Pickering & Willis 2005; Halder et al. 2009; Lammich et al. 2010). Other mechanisms such as 5′ terminal oligopyrimidine tracts (TOP) and microRNAs

binding sites have also been proposed as mechanisms by which translational repression may occur (Baker & Coller 2006; Loscher et al. 2007).

The regulatory effects of polymorphisms in non-coding regions of DNA have slowly been gathering interest (Knight, 2004b; Cooper et al. 2010). These apparently 'silent' variations may be accountable for the heterogeneity in disease progression and severity observed in many disorders including RP. In the case of the *RHO* 5′UTR variant, the regulation of gene expression observed in this study could have clinical implications for RP.

Nonetheless, it is important to note that the use of mammalian cell lines as experimental models may mean that the results obtained may not represent what actually occurs in photoreceptor cells in humans. Mammalian cell culture provides an accessible means of studying physiological and biochemical processes in cells due to disease. However, apart from being poor substitutes for specialised tissue, immortalised human cells have cancerous properties, which include differential protein expression, and may not mimic even their own native human cell environment. Photoreceptor cells are highly specialised and other human cells may not mimic their underlying biochemical processes.

If the results obtained here reflect a genuine functional role for the 5′UTR variant, a few questions arise. If there is indeed some kind of regulation, what is the precise mechanism? Furthermore, if the same kind of regulation is taking place in human photoreceptors, what would the phenotype be for individuals who are heterozygous or homozygous for this variant? A potential answer to the latter could be determined through allelic expression imbalance (AEI) studies (Knight, 2004a; Wang & Sadee 2006) or genotype-phenotype correlations in patients. This type of clinical correlation was an initial objective of this study however, due to insufficient clinical data and low numbers of patients with the same mutation (with or without the variant), inference into the effect of the 5′UTR variant on clinical phenotype was not possible. If, as observed in all the cell lines, the 5′UTR depresses RHO expression, it is possible that the amount of protein expressed by individuals who are homozygous for this variant, may still reach the required threshold levels for physiological function (Kennan et al. 2005). This is worth noting, especially since the variant is

found at high frequencies (95%) in the indigenous African population and there are individuals without the disease who are homozygous for the c.-26A>G variant. It would be interesting to determine, through evaluation by ophthalmologists, whether these individuals exhibit a subclinical phenotype.

In essence, the effect of the 5′UTR variant may be a combined consequence of both transcriptional and translational regulation, resulting in differential protein expression and the observed cellular functional phenotypes.

Chapter 5: Conclusions

In an attempt to understand factors that may contribute to the heterogeneous nature of RP in family members with the same mutation, the functional effects of the c.-26A>G variant in the 5′UTR of *RHO*, which was previously found to occur at a high frequency in the indigenous South African population, were investigated.

Functional analyses performed to determine the effect of this 5′UTR variant in *RHO* revealed a number of interesting trends. To begin with, the 5′UTR c.-26A>G variant appears to elicit transcriptional and or translational regulation of the *RHO* mRNA transcript. Although ICC revealed that cells (HT-1080 and SKNSH) expressing the *RHO* 5′UTR (c.-26A>G) construct had similar protein localisation to that of WT RHO expressing cells, protein products from this construct, could not be detected in these same cell lines (HT-1080 and SKNSH cells), when analysed by western blots. In HEK-293 cells, RHO protein expressed from the c.-26A>G construct was not detectable by ICC analyses, which also indicates cell specific effects.

In addition, the c.-26A>G variant appeared to have differential effects when expressed *in cis* with three known disease-causing mutations; T4K, T17M and P347L. This differential effect observed in cells expressing T4K and T17M RHO mutants, is proposed to be a function of structural change (secondary or tertiary) as a result of the 'G' nucleotide substitution, which alter access to translational or transcriptional machinery (Jiang, 2010; Lammich et al. 2010). Furthermore, the 5′UTR variant may alter the stability of mRNA in transcripts expressing the T4K and T17M mutations and this could account for the variable transcript levels observed. In the instance of the T4K mutation, a known glycosylation mutant which appeared to form aggregates in this study, expression of this mutant *in cis* with the c.-26A>G variant, resulted in increased mRNA transcript expression. The increase in transcript expression compared to T4K only transcripts, correlated with the increased protein expression observed in the western blots. Interestingly, the increase in protein expression did not result in an increase in the number of aggregates as would be expected. Expression of the construct containing the T17M mutation (a glycosylation mutation that forms intracellular aggregates), *in cis* with the c.-26A>G variant,

resulted in a decrease in mRNA transcript expression and no intracellular aggregate formation as revealed by ICC. Western blot analysis of cells expressing the mutant RHO T17M protein also revealed a decrease in RHO protein levels when the mutation was expressed *in cis* with the c.-26A>G variant.

The effect elicited by the 5′UTR c.-26A>G variant appeared to be a function of physical distance between the 5′UTR variant and the disease-causing mutation. This hypothesis was inferred from the results obtained for the P347L *RHO* mutation. In this instance, there was no detectable difference in protein expression in cells expressing P347L mutation only, and in cells that expressed the mutation construct *in cis* with the 5′UTR variant. However, there appeared to be variable levels of mRNA transcript expression (as determined by qPCR) in each of the three cell lines expressing the P347L mutation only and the P347L mutation *in cis* with the 5′UTR g.269A.G variant. These varying levels of transcript, may point towards the temporal stability of P347L transcripts, coupled with cell specific effects.

In conclusion, the results obtained in this study suggest the 5′UTR (c.-26A>G) variant has an effect on the transcription and translational regulation of RHO. This is evident in the differential effects observed when this variant was expressed *in cis* with various disease-causing mutations. These data also imply that the extent of the effect of the c.-26A>G variant is influenced by the nature and proximity of downstream mutations. The presence of the c.-26A>G SNP could thus potentially impact on the severity or course of RHO-related RP, thereby acting as a disease modifier.

5.1. Future prospects

Since the results of this study have culminated in more questions than answers, future investigations should aim to examine in detail, features related to RHO transcription and translation as well protein expression.

This study was in part limited by the difficult optimisation of the western blot analyses. Further optimisation of this functional analysis, should be performed to determine the most optimal conditions for the detection of the RHO protein. Isolation of RHO using immuno-precipitation may enhance the detection process. A review of literature containing published images of RHO blotting experiments, reveals that most studies have included Endoglycosidase H and Peptide: N-glycosidase F (deglycosylating agents) treatments. Such treatments may have enabled better detection of the RHO protein and should be considered in future western blotting experiments. This may serve to either support or disprove the hypotheses proposed in this study.

In terms of the effect of the SNP on translational regulation, the main mode of RHO translation should be established i.e. whether translation is initiated through the 5′cap start site or an internal ribosome entry site (IRES), which if proximal to the c.-26A>G may result in a structural change that alters translation efficiency. Transcription-translation coupled assays such as those described in Lammich et al. (2010) may also improve understanding of the mechanisms underlying the elicited effect of the SNP.

In addition, analyses of cellular protein expression profile, i.e. up-regulation or down-regulation of proteins expressed when the 5′UTR c.-26A>G variant is present *in cis* with known mutations such as those analysed in this study, may provide an indication of some of the mechanisms that allow for protein translocation to the plasma membrane and even clearance of aggregates. Such an analysis could be performed using PCR expression arrays. In conjunction with the protein profile analysis, investigations into whether the 5′UTR variant results in a change in interaction between RHO and any of the proteins mentioned previously, would be essential.

Since the effect of the 5′UTR variant appears to be influenced in some manner by the distance between the variant and mutation, it would be essential to establish what specific section or length of region in the 5′UTR is responsible for the observed effects. This could be determined by analyses of deletion constructs in Luciferase reporter assays. In addition, functional analyses with other classes of mutations spread along the length of the *RHO* gene could create insight as to whether the effect of the 5′UTR is a function of physical distance.

Expression work in closely-related cell lines, including the p661w and y-79 cell lines, may also provide a better understanding as to the effect of the c.-26A>G variant. The use of photoreceptor cell lines or retinal cells expressing RHO may provide better insight into the functional significance of the c.-26A>G variant with or without disease-causing mutations. Indeed studies such as those of Jin et al. (2011), in which induced pluripotent stem cells from patients carrying RP mutations, could be replicated with the c.-26A>G variant and this may provide a better modelling system for functional studies. Such a study would be able to determine whether the c.-26A>G variant, expressed *in cis* with different disease-causing mutations, differentially influences cell viability and function.

Of possible and immediate practical significance, is the issue of detailed phenotypic analysis and follow-up of a larger cohort of patients with a range of combinations of the 5′UTR c.-26A>G variant and various disease-causing mutations, as described in Appendix A. Detailed clinical information on an expanded cohort, including affected and unaffected individuals, would serve to provide insight into the proposed effects of the c.-26A>G variant.

References:

Ando Y, Ohmori M, Ohtake H, Ohtoko K, Toyama S, Usami R, O'hira A, Hata H, Yanashima K, Kato S. 2007. Mutation screening and haplotype analysis of the rhodopsin gene locus in Japanese patients with retinitis pigmentosa. *Molecular Vision*. (13) pp. 1038-1044.

Baehr W & Frederick JM. 2009. Naturally occurring animal models with outer retina phenotypes. *Vision Research*. 49 (22) pp. 2636-52.

Baker KE & Coller J. 2006. The many routes to regulating mRNA translation. *Genome Biology*. (7) pp. 332.

Biedler JL, Helson L & Spengler BA. 1973. Morphology and growth, tumorigenicity, and cytogenetics of human neuroblastoma cells in continuous culture. *Cancer Research*. (33) pp. 2643-2652.

Bowne SJ, Daiger SP, Hims MM, Sohocki MM, Malone KA, McKie AB, Heckenlively JR, Birch DG, Inglehearn CF, Bhattacharya SS, Bird A, Sullivan LS. 1999. Mutations in the RP1 gene causing autosomal dominant retinitis pigmentosa. (8) 11 pp. 2121-2128.

Breikers G, VandeLuytgaarden JM, Bovee-geurts PHM & Degrip WJ. 2002. Retinitis pigmentosa-associated rhodopsin mutations in three membrane-located cysteine residues present three different biochemical phenotypes. *Biochemical and Biophysical Research Communications*. (297) pp. 847-853.

Cenik C, Derti A, Mellor JC, Berriz GF & Roth FP. 2010. Genome-wide functional analysis of human 5'untranslated region introns. *Genome Biology*. (11) R29.

Chan WM, Yeung KY, Pang CP, Baum L, Lau TC, Kwok AKH, Lam DSC. 2001. Rhodopsin mutations in Chinese patients with retinitis pigmentosa. *British Journal of Opthalmology*. (85) pp. 1046-1048.

Chuang J-zen, Vega C, Jun W & Sung, C-hwa. 2004. Structural and functional impairment of endocytic pathways by retinitis pigmentosa mutant rhodopsin-arrestin complexes. *Journal of Clinical Investigation*. (114) pp. 131-140.

Chung BYW, Simons C, Firth AE, Brown CM & Hellens, RP. 2006. Effect of 5'UTR introns on gene expression in Arabidopsis thaliana. *BMC Genomics*. (13) pp. 1-13.

Cideciyan AV, Hood D, Huang Y, Banin E, Li Z-yi, Stone EM, Milam AH, Jacobson SG. 1998. Disease sequence from mutant rhodopsin allele to rod and cone photoreceptor degeneration in man. *Proceedings of the National Academy of Sciences*. (95) pp. 7103-7108.

Clarke G, Heon E & McInnes R. 2000. Recent advances in the molecular basis of inherited photoreceptor degeneration. *Clinical Genetics*. (57) pp. 313-329.

Cooper DN, Chen ÃJ-min, Ball EV, Howells K, Mort M, Phillips AD, Chuzhanova N, Krawczak M, Kehrer-Sawatzki H, Stenson PD. 2010. Genes, mutations, and human inherited disease at the dawn of the age of personalized genomics. *Human Mutation*. (31) pp. 631-655.

Cvekl A & Mitton KP. 2010. Epigenetic regulatory mechanisms in vertebrate eye development and disease. *Heredity*. 105 (1) pp. 135-51.

Daiger S.P, Bowne S & Sullivan L. 2007. Perspective on genes and mutations causing retinitis pigmentosa. *Archives of Opthalmology*. (125) pp. 151-158.

Daiger SP. 2004. Identifying retinal disease genes: how far have we come, how far do we have to go? *Norvatis Found Symposium*. (255) pp.17-178.

Daiger SP, Shankar SP, Schindler AB, Sullivan LS, Bowne SJ, King TM, Daw EW, Stone EM, Heckenlively JR. 2006.Genetic factors modifying clinical expression of autosomal dominant RP. *Advances in Experimental Medical Biology*. (572) pp. 3-8.

Daiger Stephen P, Sullivan LA & Rodriguez JA. 1995. Correlation of phenotype with genotype in inherited retinal degeneration. *Cambridge Journals* (18) pp. 452-467.

Davuluri RV, Suzuki Y, Sugano S & Zhang MQ. 2000. CART Classification of human 5' UTR sequences. *Genome Research*. (11) 10 pp. 1807-1816.

Deretic D, Schmerl S, Hargrave P, Arendt A & McDowell, JH. 1998. Regulation of sorting and post-Golgi trafficking of rhodopsin by its C-terminal sequence QVS(A)PA. *Proceedings of the National Academy of Sciences*. (95) 18 pp. 10620-5.

Dowling, JE. 1987. The retina: an approachable part of the brain. *Harvard University Press*. pp 251-271.

Dryja TP, McGee TL, Reichel E, Hahn LB, Cowley GJ, Yandell DW, Sandberg MA, Berson EL. 1990. A point mutation of the rhodopsin gene in one form of retinitis pigmentosa. *Nature*. (343) 6256 pp. 364-6.

Dryja TP, Hahn LB, Cowley GS, Mcgee TL & Berson EL. 1991. Mutation spectrum of the rhodopsin gene among patients with autosomal dominant retinitis pigmentosa. *October* (88) pp. 9370-9374.

Ernst, OP, Gramse V, Kolbe M, Hofmann KP, & Heck M. 2007. Monomeric G protein-coupled receptor rhodopsin in solution activates its G protein transducin at the diffusion limit. *Proceedings of the National Academy of Sciences*. (104) 26 pp. 10859-64.

Farrar GJ, Kenna P, Redmond R, Mcwilliam P, Bradley DG, Humphries MM, Sharp EM, Inglehearn CF, Bashir R, Jay M, Watty A, Ludwig M, Schinzel A, Samanns C, Gal A, Bhattacharya S, Humphries P. 1990. Autosomal dominant

retinitis pigmentosa: Absence of the Rhodopsin proline- histidine substitution (codon 23) in pedigrees from Europe. *American Journal of Human Genetics. (*47) pp. 941-945.

Farrar GJ, Kenna PF & Humphries P. 2002. On the genetics of retinitis pigmentosa and on mutation-independent approaches to therapeutic intervention. *EMBO Journal*. (21) 5 pp. 857-864.

Fishman GA, Alexander KR & Anderson RJ. 1985. Autosomal dominant retinitis pigmentosa: A method of classification. *Archives of Opthalmology.* (103) pp. 366-374.

Gal A, Apfelstedt-sylla E, Janecke AR, Zrennert E. 1997. Rhodopsin mutations in inherited retinal dystrophies and dysfunctions. *Science* (16) 1 pp. 51-79.

Garriga P & Manyosa J. 2002. The eye photoreceptor protein rhodopsin. Structural implications for retinal disease . *FEBS Letters* (528) pp. 17-22.

Goliath R, Bardien S, September A, Martin R, Ramesar R, Greenberg J. 1998. Rhodopsin mutation G109R in a family with autosomal dominant retinitis pigmentosa. *Human mutation*. Suppl 1 pp. S40-1.

Graham FL, Smiley J, Russell WC & Nairn R. 1977. Characteristics of a human cell line transformed by DNA from human adenovirus type 5. *Journal of General Virology*. (36) 1 pp. 59-74.

Greenberg J, Ramesar R & Beighton P. 1994. Genetic mapping of retinitis pigmentosa- implications for South African patients. *South African Medical Journal*. (84) pp. 410-412.

Greenberg J, Franz T, Goliath R & Ramesar R. 1999. A photoreceptor gene mutation in an indigenous black african family with retinitis pigmentosa. *South African Medical Journal*. (89) pp.877-878.

Griciuc A, Aron L, Piccoli G & Ueffing M. 2010. Clearance of Rhodopsin P23H aggregates requires the ERAD effector VCP. *Biochimica et Biophysica Acta*. (1803) 3 pp. 424-434.

Haider N, Ikeda A, Naggert, JK & Nishina, PM. 2002. Genetic modifiers of vision and hearing. *Human molecular Genetics*. (11) 10 pp. 1195-1206.

Hall, T. 1999. BioEdit: a user-friendly biological sequence alignment editor and analysis program for Windows 95/98/NT. *Nucleic Acids, Symposium series*. (41) pp. 95-98.

Halder, K, Wieland, M & Hartig J. 2009. Predictable suppression of gene expression by. *Nucleic Acids Research* (1) 34 pp. 1-7.

Hargrave, P. 1977. The amino-terminal tryptic peptide of bovine rhodopsin A glycopeptide containing two sites of oligosaccharide attachment. *Biochimica et Biophysica Acta*. *Protein Structure*, (492) 1 pp. 83-94.

Hartong DT, Berson Eliot L & Dryja TP. 2006. Retinitis pigmentosa. *Lancet*. (368) pp. 1795-1809.

Hartong DT, Mcgee TL, Sandberg MA, Berson EL, Asselbergs FW, van der Harst P, De vivo P, Dryja TP. 2009. Search for a correlation between telomere length and severity of retinitis pigmentosa due to the dominant rhodopsin Pro23His mutation. *Molecular Vision*. (15) 2008 pp. 592-597.

Hims MM, Daiger SP & Inglehearn CF. 2003. Retinitis Pigmentosa: Genes, proteins and prospects. *Developmental Opthalmology* (37) pp. 109-125.

Iannaccone A, Man D, Waseem N, Jennings BJ, Ganapathiraju M, Gallaher K, Reese E, Bhattacharya SS, Klein-Seettharaman J. 2006. Retinitis pigmentosa associated with rhodopsin mutations: Correlation between phenotypic variability and molecular effects. *Vision Research* . (46) pp. 4556-4567.

Jacobson SG, Kemp CM, Cideciyan AV, Macke JP, Sung C-hwa, Nathans J. 1994. Phenotypes of stop codon and splice site rhodopsin mutations causing retinitis pigmentosa. *Investgative Ophthalmology Vision Science*. (35) 5 pp. 2521-2534.

Jensen LJ, Kuhn M, Stark M, Chaffron S, Creevey C, Muller J, Doerks T, Julien P, Roth A, Simonovic M, Bork P, von Mering C. 2009. STRING 8 — A global view on proteins and their functional interactions in 630 organisms. *Nucleic Acids Research*. (37) pp. 412-416.

Jin, Z.-B., Okamoto, S., Osakada, F., Homma, K., Assawachananont, J., Hirami, Iwata T, Takahashi M. 2011. Modelling retinal degeneration using patient-specific induced pluripotent stem cells M. Mattson, ed. *PLoS ONE*, (2), 6 pp. e17084.

Jiang, M. 2010. Approximation algorithms for predicting RNA secondary structures with arbitrary pseudoknots. (7) 2 pp. 323-332.

Kaushal S & Khorana G. 1994. Structure and function in Rhodopsin. 7. point mutations associated with autosomal dominant retinitis pigmentosa. *Biochemistry*. (33) pp. 6121-28.

Kennan A, Aherne A & Humphries P. 2005. Light in retinitis pigmentosa. *Trends in genetics* (21) 2 pp. 103-10.

Kijas JW, Cideciyan AV, Aleman TS, Pianta MJ, Pearce-Kelling SE, Miller BJ, Jacobson SG, Gustavo DA, Gregory MA. 2002. Naturally occurring rhodopsin mutation in the dog causes retinal dysfunction and degeneration mimicking human dominant retinitis pigmentosa. *Proceedings of the National Academy of Sciences.* (99) 9 pp. 6328-33.

Knight JC. 2004a. Allele-specific gene expression uncovered. *Trends in genetics* (20) 3 pp. 113-16.

Knight JC. 2003. Functional implications of genetic variation in non-coding DNA for disease susceptibility and gene regulation. *Clinical Science*. (501) pp. 493-501.

Knight JC. 2004b. Regulatory polymorphisms underlying complex disease traits. *Journal of Molecular Medicine*. (83) pp. 97-109.

Kosmaoglou M, Schwarz N, Bett JS & Cheetham M. 2008. Progress in retinal and eye research molecular chaperones and photoreceptor function. *Progress in Retinal and Eye Research* (27) pp. 434-49.

Krebs MP, Holden DC, Joshi P, Clark (III) CL, Lee AH, Kaushal S. 2009. Molecular mechanisms of rhodopsin retinitis pigmentosa and the efficacy of pharmacological rescue. *Journal of Molecular Biology*. (395) 5 pp. 1063-1078.

Lammich S, Buell D, Zilow S, Ludwig A-K, Nescher B, Lichtenthaler SF, Prinzen C, Fahrenholz F, Haass C. 2010. Expression of the anti-amyloidogenic secretase ADAM10 is suppressed by its 5'untranslated region. *Journal of Biological Chemistry*. (285) 21 pp. 15733-60.

Larionov A, Krause A & Miller W 2005.A standard curve based method for relative real time PCR data processing. *BMC Bioinformatics*. (16) pp. 1-16.

Lavail MM, Yasumura D, Matthes MT, Lau-villacorta C, Unoki K, Sung C-hwa, Steinberg RH. 1998. Protection of mouse photoreceptors by survival factors in retinal degenerations. *Investigative Ophthalmology & Visual Science*. (39) pp. 592-602.

Li S, Xiao X, Wang P, Guo X & Zhang Q. 2010. Mutation spectrum and frequency of the rho gene in 248 chinese families with retinitis pigmentosa. *Biochemical and Biophysical Research Communications*. (401) 1 pp. 42-47.

Li ZY, Wong F, Chang JH, Possin DE, Hao Y, Petters RM, Milam AH. 1998. Rhodopsin transgenic pigs as a model for human retinitis pigmentosa. *Investigative ophthalmology & visual science*, (39) 5 pp. 808-19.

Liu Q, Zuo J & Pierce EA. 2004. The retinitis pigmentosa 1 protein is a photoreceptor microtubule-associated protein. *Journal of Neuroscience*. (24) 29 pp. 6427- 6436.

Livak K & Schimttgen T. 2001. Analysis of relative gene expression data using real-time quantitative pcr and the delta delta Ct method. *Methods*. (25) pp. 402-408.

Loscher CJ, Hokamp K, Kenna PF, Ivens AC, Humphries P, Palfi A, Farrar GJ. 2007. Altered retinal microRNA expression profile in a mouse model of retinitis pigmentosa. *Genome Biology*. (8) R248.

Macke JP, Davenport CM, Jacobson SG, Hennessey JC, Gonzalez-Fernandez F, Conway BP, Heckenlively J, Palmer R, Maumenee IH, Seiving P, Gouras P, Good W & Nathans J. 1993. Identification of novel rhodopsin mutations responsible for retinitis pigmentosa: implications for the structure and function of rhodopsin. *American Journal of Human genetics*. (53) 1 pp. 80-9.

Mansergh F, Millington-ward S, Kennan A, Kiang S, Humphries M, Farrar GJ, Humphries P & Kenna P. 1999. Retinitis pigmentosa and progressive sensorineural hearing loss caused by a c12258a mutation in the mitochondrial mtts2 gene. *The American Journal of Human Genetics*. (64) 4 pp. 971-985.

Matus S, Glimcher LH & Hetz C. 2011. Protein folding stress in neurodegenerative diseases: a glimpse into the ER. *Current Opinion in Cell Biology*. (23) pp. 1-14.

Mendes HF & Cheetham ME. 2008. Pharmacological manipulation of gain-of-function and dominant-negative mechanisms in rhodopsin retinitis pigmentosa. *Human molecular Genetics*. (17) 19 pp. 3043-54.

Mendes HF, Spuy JVD, Chapple JP & Cheetham ME. 2005. Mechanisms of cell death in rhodopsin retinitis pigmentosa: implications for therapy. *Trends in Molecular Medicine* (11) 4 pp. 176-185.

Molday RS. 1998. Photoreceptor membrane proteins, phototransduction, and retinal degenerative diseases. *Investigative Ophthalmology*. (39) 13 pp. 2493-2513.

Morris MB, Dastmalchi S & Church WB. 2009. Rhodopsin: Structure, signal transduction and oligomerisation. *International Journal of Biochemistry*. (41) pp. 721-724.

Murray AR, Fliesler SJ & Al-ubaidi MR. 2009. Rhodopsin: The functional significance of asn-linked glycosylation and other post-translational modifications. *Sciences-New York* (6810) pp. 109-120.

Nadeau JH. 2003. Modifier genes and protective alleles in humans and mice. *Current Opinion in Genetics & Development*. (13) pp. 290-5.

Niemeyer G, Peter T, Schinzel A & Gal A. 1992. Clinical and ERG data in a family with autosomal dominant RP and Pro-347-Arg mutation in the rhodopsin gene. *Neurophysiology*. (79) pp. 303-311.

Nolan T, Hands RE & Bustin SA. 2006. Quantification of mRNA using real-time RT-PCR. *Online*. (1) 3 pp. 1559-82.

Oh K, Longmuir R, Oh DM, Stone EM, Kopp K, Gehrs K & Weleber R. 2003. Comparison of the clinical expression of retinitis pigmentosa associated with rhodopsin mutations at codon 347 and codon 23. *American Journal of Ophthalmology*. (136) 2 pp. 306-313.

Oswald A.H, Goldblatt J, Sampson G, Clokie R & Beighton P. 1985. Retinitis pigmentosa in South Africa. *South African Medical Journal* (68) 12 p. 863-866.

Ozawa Y, Kurihara T, Tsubota K & Okano H. 2010. Regulation of posttranscriptional modification as a possible therapeutic approach for retinal neuroprotection. *Journal of Ophthalmology*. (2011) doi:10.1155/2011/506137.

Pabinger S, Thallinger GG, Snajder R, Eichhorn H Rader R & Trajanoski S. 2009. QPCR : application for real-timePCR data management and analysis. *BMC Bioinformatics*. (10) pp. 1-10.

Pacione LR, Szego MJ, Ikeda S, Nishina PM & Mcinnes, RR. 2003. Genetic and biochemical mechanisms of inherited photoreceptor degenerations. 26 pp. 657-700.

Pandor A, Ramesar R. & Prince S. 2010. Cell-specific differences in the processing of the R14W CAIV mutant associated with retinitis pigmentosa 17. *Journal of Cellular Biochemistry*, 111(3), pp. 735-41.

Phelan JK & Bok D 2000. A brief review of retinitis pigmentosa and the identified retinitis pigmentosa genes. *Molecular Vision*. (6) pp no. 116-124.

Pickering BM & Willis AE. 2005. The implications of structured 5'untranslated regions on translation and disease. *Seminars in Cell & Developmental Biology*. (16) pp. 39-47.

Rajan R & Kopito RR. 2005. Suppression of wild-type rhodopsin maturation by mutants linked to autosomal dominant retinitis pigmentosa. *Journal of Biological Chemistry*. (280) 2 pp. 1284-1291.

Rakoczy EP, Kiel C, Mckeone R, Stricher F & Serrano, L. 2011. Analysis of disease-linked rhodopsin mutations based on structure function and protein stability calculations. *Journal of Molecular Biology*. (405) 2 pp.584-606.

Rasheed S, Nelson-Rees W, Toth E, Arnstein P & Gardner MB. 1974. Characterization of a newly derived human sarcoma cell line (HT-1080). *Cancer*. (33) pp. 1027-33.

Rattner A, Sun H & Nathans J. 1999. Molecular genetics of human retinal disease. *Annual Review of Genetics*. (33) 89-131 pp 89-131.

Rebbeck TR, Ambrosone CB, Bell DA, Chanock SJ, Hayes RB, Kadlubar FF & Thomas DC. 2004. SNPs, haplotypes, and cancer: applications in molecular epidemiology. *Biomarkers*. (13) pp. 681-687.

Rebello G, Greenberg J & Ramesar R. 2002. A computer-based register for inherited retinal dystrophies in Southern Africa. *Opthalmic Genetics*. (23) 1 pp. 61-65.

Roberts L, Ramesar R & Greenberg J. 2000. Letter to the editor low frequency of rhodopsin mutations in South African patients with autosomal dominant retinitis pigmentosa. *Clinical Genetics*. (58) 5 pp. 77-78.

Roberts, LJ. 2006. Mutation analysis of important retinal candidate genes: Progressing from research to diagnostic service, MSc (Med) Human Genetics, Thesis UCT.

Ross, J. 1995. mRNA stability in mammalian cells. *Microbiological Reviews*. (59) 3 pp. 423-450.

Saliba RS, Munro PMG, Luthert PJ & Cheetham ME. 2002. The cellular fate of mutant rhodopsin: quality control degradation and aggresome formation. *Journal of Cell Science*. (159) pp. 2907-2918.

Sambrook J, Fritsch E.F, and Maniatis T. 1989. In molecular cloning: A Laboratory Manual. *Cold Spring Harbor Laboratory Press*, NY, Vol. 1- 3.

Schug J & Overton GC. 1998. Transcription Element Search Software on the WWW 1. pp. 1-10.

Schultes E, Hraber P & Labean T. 1997. Evidence for adaptive evolutionary convergence in the base composition of single-stranded RNA. T *TECHREPORT Network*. 96-12-091.

Smith AJ, Bainbridge JW & Ali Robin R. 2009. Prospects for retinal gene replacement therapy. *Trends in genetics*. (25) 4 pp. 156-165.

Soest S van, Westerveld A, De Jong P, Bleeker-wagemakers E & Bergen A. 1999. Retinitis Pigmentosa defined from a molecular point of view. *Survey of Ophthalmology*. (43) 4 pp. 321-334.

Sung C-hwa, Davenport Carol M & Nathans J. 1993. Rhodopsin Mutations Responsible for Autosomal Dominant Retinitis Pigmentosa. *Journal of Biological Chemistry*. (268) 35 pp. 26646-49.

Sung C-hwa, Schneider BG, Agarwal N, Papermaster DS & Nathans J. 1991. Functional heterogeneity of mutant rhodopsins responsible for autosomal dominant retinitis pigmentosa. *Proceedings of the National Academy of Sciences*. (88) pp. 8840-44.

Tam BM & Moritz OL. 2006. Characterization of rhodopsin P23H-induced retinal degeneration in a Xenopus laevis model of retinitis pigmentosa. *Investigative Ophthalmology*. (47) 8 pp. 3234-41.

Tam BM & Moritz OL. 2009. The role of rhodopsin glycosylation in protein folding trafficking , and light-sensitive retinal degeneration. *Journal of Neuroscience*. (29) 48 pp. 15145-54.

Tan MH, Smith AJ, Pawlyk B, Xu X, Bainbridge JB, Basche M, McIntosh J, Tran HV, Nathwani A, Li T & Ali RR. 2009. Gene therapy for retinitis pigmentosa and Leber congenital amaurosis caused by defects in AIPL1 : effective rescue of mouse models of partial and complete Aipl1 deficiency using AAV2 / 2 and AAV2 / 8 vectors. *Human Molecular Genetics*. (18) 12 pp. 2099-114.

Tartellin E, Al-Marghtheh M, Keen J, Battacharya S & Inglehearn CF. 1996. Simple tests for rhodopsin involvement in retinitis pigmentosa. *Journal of Medical Genetics*. (33) pp. 262-263.

Wang DY, Chan WM, Tam POS, Baum L, Lam DS, Chong KK, Fan BJ, Pang CP. 2005 Gene mutations in retinitis pigmentosa and their clinical implications. *Clinica Chimica Acta*. (351) pp. 5-16.

Wang D-yi, Fan B-jian, Chan W-man, Tam O-sin, Chiang WY, Lam SC, Pang CP. 2005a. Digenic association of RHO and RP1 genes with retinitis pigmentosa among Chinese population in Hong Kong. *Zhonghua yi xue za zhi*. (85) 23 pp. 1613-7.

Wang D & Sadee W. 2006. Searching for polymorphisms that affect gene expression and mRNA processing: Example ABCB1 (MDR1). *AAPS Journal*. (8) 3 pp. 515-520.

Weleber RG. 2003. Comparison of the clinical expression of retinitis pigmentosa associated with rhodopsin mutations at codon 347 and codon 23. (136) pp. 303-13.

Widom RL, Rhee M & Karathanasis SK. 1992. Repression by ARP-1 sensitizes Apolipoprotein Al gene responsiveness to RXROX and retinoic acid. *Microbiology*. (12) 8 pp. 3380-89.

Wilkie GS, Dickson KS & Gray NK. 2003. Regulation of mRNA translation by 5'and 3' UTR-binding factors. *Trends in biochemical sciences*. (28) 4 pp. 182-188.

Wiseman RL, Powers ET, Buxbaum JN, Kelly JW & Balch. 2007. An adaptable standard for protein export from the endoplasmic reticulum. *Cell*. (103) pp. 809-821.

Wright AF, Chakarova CF, El-aziz MMA & Bhattacharya SS. 2010. Photoreceptor degeneration: genetic and mechanistic dissection of a complex trait. *Nature Review*. (11) 4 pp. 273-284.

Zhang XL, Liu M, Meng XH, Fu WL & Yin ZQ. 2006. Mutational analysis of the rhodopsin gene in Chinese ADRP families by conformation sensitive gel electrophoresis. *Life Sciences*. (78) pp. 1494-98.

Ziviello C, Simonelli F, Testa F, Anastasi M, Marzoli SB, Falsini B, Ghiglione D, Macaluso C, Manitto MP, Garrè C, Ciccodicola A, Rinaldi E, & Banfi S. Molecular genetics of autosomal dominant retinitis pigmentosa (ADRP): a comprehensive study of 43 Italian families.*Journal of Medical Genetics*. 42 pp. e47.

Zuker, M 2003. Mfold web server for nucleic acid folding and hybridization prediction. *Bioinformatics*. (31) 13 pp. 3406-3415.

Appendix A: Consent forms and cohort pedigrees

SPECIMEN TUBES REQUIRED: 2 X 4 ml Plastic purple top tubes (containing EDTA)
NAME AND DATE OF BIRTH TO BE ON EACH TUBE

BLOODS ARE TO BE KEPT REFRIGERATED. SPECIMENS ARE TO BE CAREFULLY PACKAGED AND TRANSPORTED IN A POLYSTYRENE COOLBOX WITH AN ICE BRICK. DO NOT FREEZE.

COURIER SERVICES CAN BE ARRANGED BY THE DIVISION OF HUMAN GENETICS UPON REQUEST

BLOODS ARE CODED ON ARRIVAL IN LABORATORY ACCORDING TO FAMILY NAME

RESULTS ARE GIVEN TO PARTICIPANTS ACCORDING TO ESTABLISHED PROTOCOL WHEN AVAILABLE

CONSENT FORM REQUIRED FOR DNA ANALYSIS AND STORAGE

PLEASE DELETE DETAILS THAT ARE NOT APPLICABLE:

1. I, _____, request that an attempt be made using genetic material to assess the probability that, I / my child / my unborn child, might have inherited a disease-causing mutation in the gene for:

(Name of Disorder):

2. I understand that the genetic material for analysis is to be obtained from: blood cells / skin sample / other (specify)

3. I request that no portion of the sample be stored for later use. ☐ *(MARK IF APPLICABLE)*
OR I request that a portion of the sample be stored indefinitely for: *(DELETE WHERE NOT APPLICABLE)*

(a) Possible re-analysis
(b) Analysis for the benefit of members of my immediate family
(c) Research purposes, subject to the approval of the University of Cape Town Research Ethics Committee, provided that any information from such research will remain confidential

4. The results of the analysis carried out on this sample of stored biological material will be made known to me, via my doctor, in accordance with the relevant protocol, if and when available.
In addition, I authorise that these results may be made known to: *(DELETE WHERE NOT APPLICABLE)*

Doctor's name or other doctors involved in my care: _____

Names of family members: _____

Other persons: _____

5. I authorise / do not authorise my doctor(s) to provide relevant clinical details to the Division of Human Genetics, UCT.

6. I have been informed that:

- There are risks and benefits associated with genetic analysis and storage of biological material and these have been explained to me.
- The analysis procedure is specific to the genetic condition related to the visual impairment mentioned above and cannot determine the complete genetic makeup of an individual.
- The genetics laboratory is under an obligation to respect medical confidentiality.
- Genetic analysis may not be informative for some families or family members.
- Even under the best conditions, current technology of this type is not perfect and could lead to incorrect results.

Where biological material is used for research purposes, there may be no direct benefit to me.

7. I understand that I may withdraw my consent for any aspect of the above at any time without this affecting my future medical care.

ALL OF THE ABOVE HAS BEEN EXPLAINED TO ME IN A LANGUAGE THAT I UNDERSTAND, AS WELL AS THE QUESTIONS THAT WERE ANSWERED BY: _____

DATE _____ /_____ /____ **PLACE:** _____

PATIENT'S SIGNATURE: _____ **WITNESS CONSENT:** _____

REQUEST FOR MOLECULAR STUDIES (DNA) BLOOD FORM

DIVISION OF HUMAN GENETICS, WERNHER & BEIT NORTH
FACULTY OF HEALTH SCIENCES, UNIVERSITY OF CAPE TOWN, OBSERVATORY, 7925
TEL: 021 406-6299 FAX: 021 406-6826 EMAIL: Gameda.Benefeld@uct.ac.za

SURNAME: _____ **NAME:** _____

Mother:

DATE OF BIRTH: ____/ ____/_____ **DETAILED ETHNIC ORIGIN: Father:**_____

NEW FAMILY: YES - ☐ NO - ☐ (If NO please fill in family name) FAMILY NAME: _____

SEX: FEMALE - ☐ MALE - ☐ Number of Children ___ Number of affected family members: ___

CONTACT ADDRESS: _____

_____**CODE** _____

TEL: ……... FAX: …… E-mail …….

NAME OF REFERRING DOCTOR: _____ **HOSPITAL:** _____

FAX: _____ **TEL**_____**E-mail:** _____

ADDRESS: _____

REASON FOR REFERRAL (CLINICAL DIAGNOSIS):

AFFECTED ☐ AT RISK ☐ CARRIER ☐ SPOUSE ☐ QUERY ☐ UNAFFECTED ☐

RETINITIS PIGMENTOSA ☐	**USHER SYNDROME ☐**	**DOMINANT INHERITANCE ☐**
STARGARDT DISEASE ☐	**MACULAR DYSTROPHY ☐**	**DOMINANT INHERITANCE ☐**
ARMD – WET ☐	**ARMD – DRY ☐**	**RECESSIVE INHERITANCE ☐**
OTHER DISORDER:	**AGE OF ONSET:** **DIAGNOSIS AGE:**	**X-LINKED INHERITANCE ☐** **ISOLATED CASE ☐**

ADDITIONAL FAMILY HISTORY _____ Pedigree on separate page please

ADDITIONAL DISORDERS (APPARENT OR PREVIOUSLY TREATED): _____

RELEVANT CLINICAL DETAILS: _____

PHYSICAL DISABILITY ☐ MENTAL RETARDATION ☐ DEAFNESS ☐ IMPAIRED VISION ☐
NIGHT BLINDNESS ☐ AGE OF ONSET: _____ OTHER: _____

Have samples from this patient been sent to a DNA lab before? Yes / No / Don't Know. If "Yes", Where: _____

Medical Aid _____ **Medical Aid No.**_____

For Laboratory use only: DNA number: _____ *Vol.Blood:* _____ *(ml)*

Other: _____ *Date Received: Year:* _____ *Month:*____ *Day:*____ *Computer Index No:* _____

Study Cohort Pedigrees

In the following pedigrees, standard symbols are used to represent the family members. Circles represent females whereas squares represent males. Symbols with diagonal lines crossing through them represent deceased individuals and shaded symbols indicate individuals affected with RP. The genotypes of the c.-26A>G variant are indicated below the symbol and in the subsequent tables. Individuals with identifier numbers in the pedigrees are representative of individuals for whom biological material (blood) was available.

Visual acuities are described according to the metric system. A 6/6 acuity means that the individual has acuity comparable to an individual with normal sight. Descriptions of lower visual acuities such as 6/12 means that the individual could see at 6 metres detail that an individual with normal sight could see at 12 metres. The lowest visual acuity recorded in these pedigrees is 6/60.

Family 2: Caucasian family with the Asp-190-Asn mutation

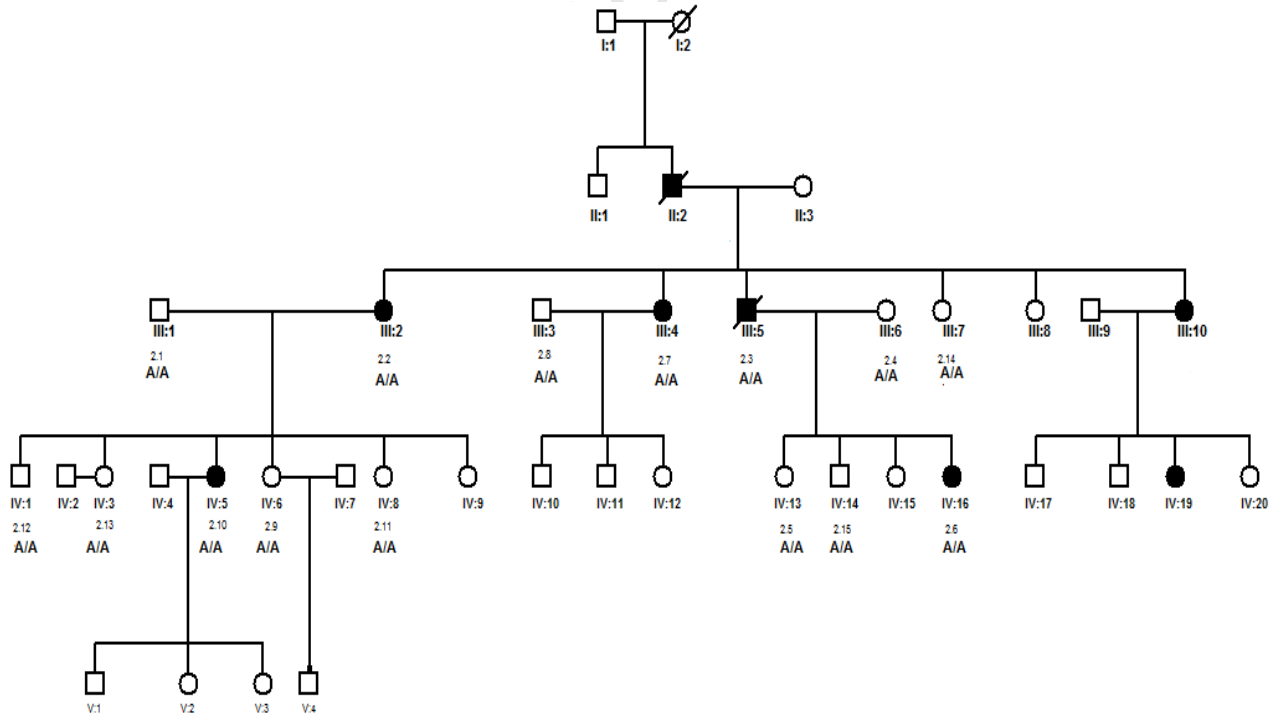

Individual	5'UTR c.-26A>G genotype	Age of Onset	Visual Acuity	Clinical Information	Status	Mutation
2.1	A/A			Night Blindness	Not Known	
2.2	A/A	25 yrs		Sectoral RP, Night Blindness at age 25	Affected	Asp-190-Asn
2.3	A/A					
2.4	A/A				Unaffected/Spouse	
2.5	A/A				At Risk	
2.6	A/A	16 yrs			Affected	Asp-190-Asn
2.7	A/A	20 yrs	L:6/9, R:6/12	Night Blindness	Affected	Asp-190-Asn
2.8	A/A				Unaffected	
2.9	A/A				Unaffected	
2.10	A/A				Affected	Asp-190-Asn
2.11	A/A				Unaffected	
2.12	A/A				Unaffected	
2.13	A/A				Unaffected	
2.14	A/A				Affected	Asp-190-Asn
2.15	A/A				Unaffected	

In this family, the c.-26A allele is the only allele present in this family. The lack of sufficient clinical information hinders the genotype-phenotype correlation and inference into the supposed effect of the c.-26A>G variant.

<u>Family 6</u>: Caucasian family with the Gly-109-Arg mutation

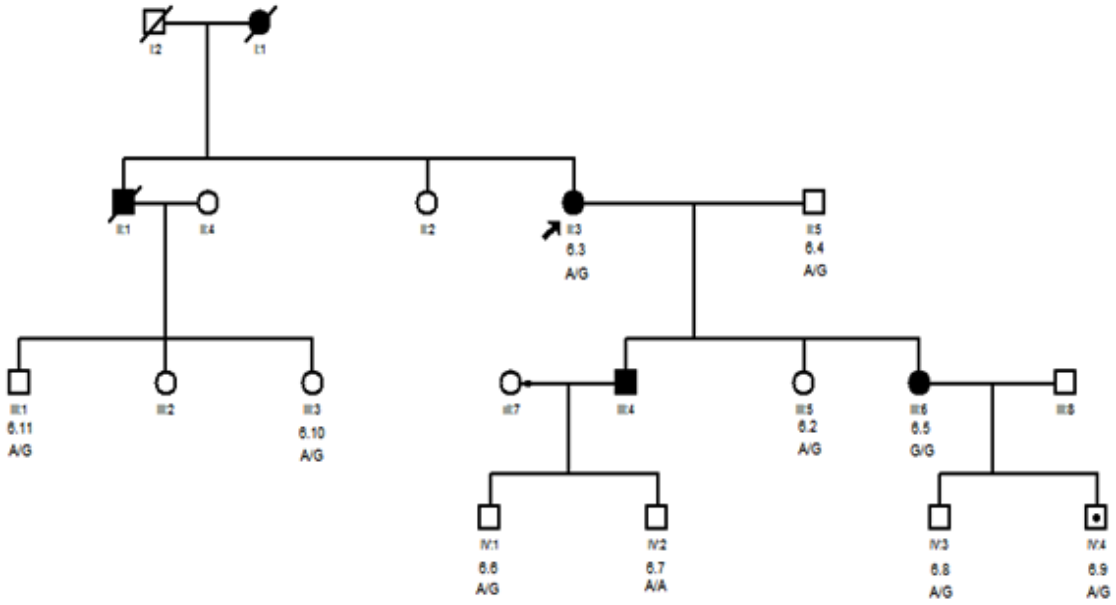

Individual	5'UTR c.-26A>G genotype	Age of Onset	Visual Acuity	Clinical Information	Status	Mutation
6.1	A/G	n/a	n/a		n/a	n/a
6.2	A/G				At risk	
6.3	A/G	22 yrs	L:20/70, R:21/50, by 1993, vision had deteriorated- L:6/24, R:6/36,	Sectoral RP, asteroid hyalitis, Night blindness, Internal quadrant RP and limited filed vision	Affected	Gly-109-Arg
6.4	A/G				Unaffected	
6.5	G/G	teen yrs	L:6/24, R:6/9	Limited Field Vision, Night Blindness	Affected	Gly-109-Arg
6.6	A/G				Unaffected	
6.7	A/A				Unaffected, Night blindness	
6.8	A/G				Unaffected	
6.9	A/G					
6.10	A/G				At risk, Night blindness	
6.11	A/G				Unaffected	

In this family, the c.-26A>G variant was present in all family members except for individual 6.7. Interestingly for the individual who is homozygous (GG) for the variant, clinical information recorded an earlier age of onset of RP than the affected individual who was heterozygous (AG). Similarly, here the lack of sufficient clinical data hinders inference into the genotype-phenotype correlation.

Family 45: Indigenous African Family with the Pro-347-Leu mutation

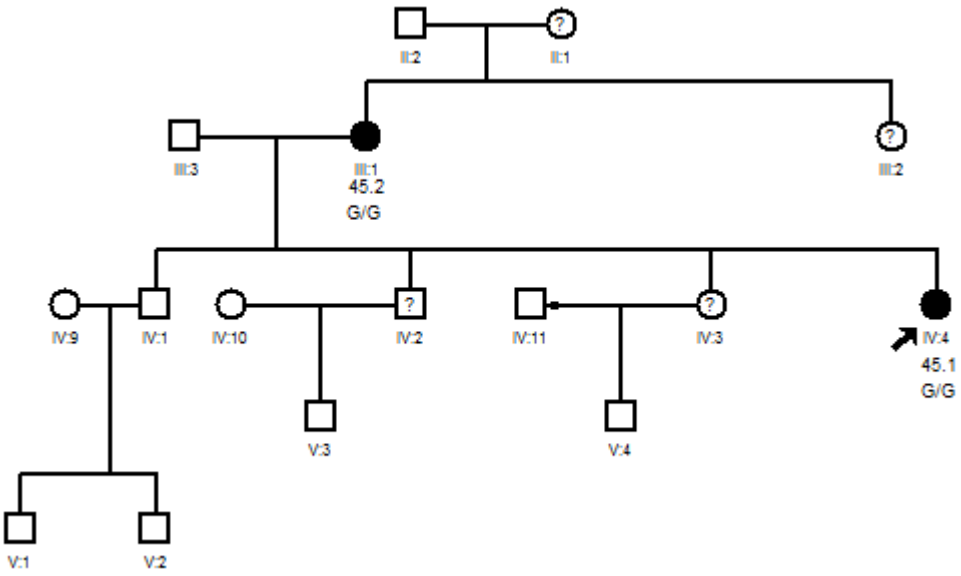

Individual	5'UTR c.-26A>G genotype	Age of Onset	Visual Acuity	Clinical Information	Status	Mutation
45.1	G/G				Affected	Pro-347-Leu
45.2	G/G				Affected	Pro-347-Leu

The two members of this family were homozygous (GG) for the c.-26A>G variant, however, no clinical information was available for either of them. A follow up of clinical data for these patients may be able to provide a genotype-phenotype correlation and is worth pursuing. Interestingly, the P347L mutation has previously been reported to cause an early age of onset phenotype.

Family 63: Caucasian family with the Thr-17-Met mutation

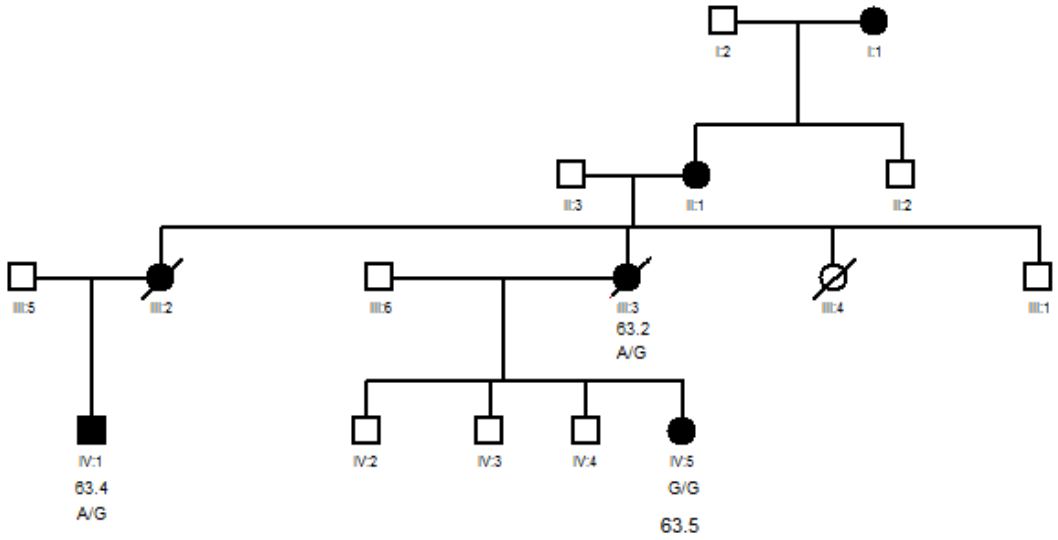

Individual	5'UTR c.-26A>G genotype	Age of Onset	Visual Acuity	Clinical Information	Status	Mutation
63.2	A/G	N/A		Limited Field Vision, Night Blindness	Affected/Deceased	Thr-17-Met
63.4	A/G	20	L:6/15, R6/6.5	Diffuse RP, Night blindness, restricted visual field, myopia, loss of central vision in left eye at 64, Vitamin A therapy 1999-2006,stable vision during this time	Affected	Thr-17-Met
RPD63.5	G/G	N/A		At risk, Myopia, Night Blindness	Affected	Thr-17-Met

All individuals in this family that were tested were affected. The 'G' allele of the c.-26A>G is also present in all family members for whom we had DNA samples. The 'G' allele appears to be transmitted *in cis* in this family although useful clinical data including age of onset is absent for individual 63.5 and 63.2 and as such a genotype-phenotype correlation cannot be inferred.

Family 199: Caucasian Family with the Thr-58-Arg mutation

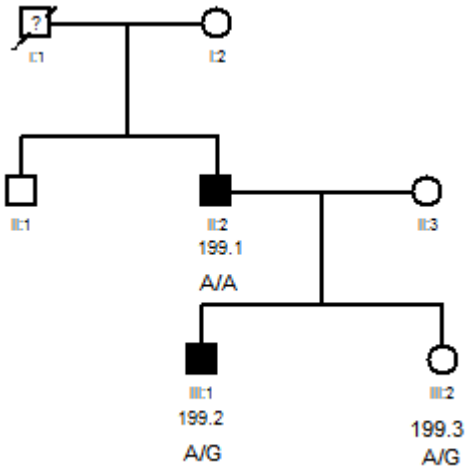

Individual	5'UTR c.-26A>G genotype	Age of Onset	Visual Acuity	Clinical Information	Status	Mutation
199.1	A/A	12	L:6/20, R:6/24	Night Blindness	Affected	Thr-58-Arg
199.2	A/G	3		Night Blindness from a young age, Central vision poor at night	Affected	Thr-58-Arg
199.3	A/G				Unaffected	

In this family, there are incidences of early age of onset of RP, which may provide insight into the effect of the c.-26A>G variant. It is difficult however, to infer whether the c.-26A>G variant is transmitted *in cis* or *trans* as DNA sample of the mother in the second generation is not available. Although, the one heterozygous (AG-199.2) individual has the earliest age of onset, no other clinical information is available for the other heterozygous individual (199.3) and thus a genotype-phenotype correlation cannot be inferred.

Appendix B: Reagents and protocols

B.1: Agarose gels

1% gel: 0.5 g Seakem® LE Agarose in 50 ml 1X TBE buffer, with 3.5 µl ethidium bromide

2% gel: 1 g Seakem® LE Agarose in 50 ml 1X TBE buffer, with 5 µl ethidium bromide

10X TBE Buffer: 0.89 M (216 g) Tris (B&M Scientific, SA)
0.89 M (110 g) Boric Acid (ICN, Biomedicals Inc, USA)
0.04 M (14.8 g) EDTA (BDH Electron® Laboratory Supplies, UK)
Made up to 2 L with distilled H_2O

1XTBE buffer (Working Solution): 10X stock diluted to 1X

Ethidium bromide stock: 10 mg/ml

Loading dye: 0.125 g (0.25%) Bromophenol blue and 40 g (40% w/v) Sucrose (Merck Pty Ltd, SA) pH8.0, made up to 50 ml with distilled H_2O

Molecular weight markers

GeneRuler™ 1 kb DNA Ladder (Fermentas Life Sciences, Hanover, USA)

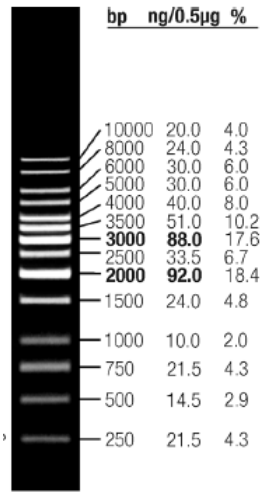

Image reproduced from www.fermentas.com

0.5 µg/lane 2% Agarose gel containing ethidium bromide

GeneRuler™ 100 bp DNA Ladder Plus (Fermentas Life Sciences, Hanover, USA)

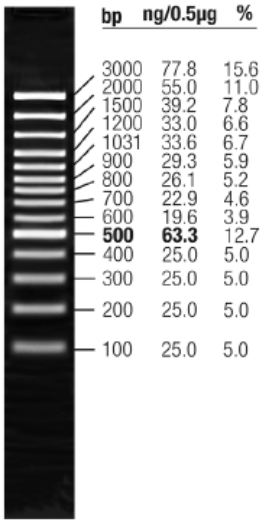

Image reproduced from www.fermentas.com

0.5 µg/lane 1% Agarose gel containing ethidium bromide

B.2: <u>QIAquick® gel extraction kit protocol (using a microcentrifuge)</u>

*All centrifugation steps are carried out 13, 000 rpm in a conventional bench-top microcentrifuge.

1. Excise the region containing the DNA fragment from the agarose gel with a scalpel ensuring that the slice of the gel is minimal.
2. Weight the gel slice in a 1.5 microcentrifuge and add 3 volumes of Buffer QG to 1 volume of the gel (e.g 300 µl= 100 mg gel).
3. Incubate at 50°C for 10 min (or until gel slice is completely dissolved). The dissolving process may be enhanced by 'vortexing' every 2-3 min during incubation.
4. After the gel slice is dissolved, ensure that the colour of the mixture is yellow (this is similar to the original buffer colour before gel is dissolved). If the colour of the mixture deviates from yellow i.e. orange or violet, then add 10 µl of 3 M sodium acetate, pH 5.0 and mix. The adsorption of DNA to the QIAquick membrane is most efficient at pH 7.5.Buffer QG contains and indicator which is yellow at pH 7.5.

5. Add a volume of isopropanol equivalent to the weight of the gel slice, to the sample mix (e.g 100 mg gel=100 µl isopropanol). This step increases the DNA yield of fragments that are less than 500 bp but not more than 4 kb.
6. Assemble QIAquick spin column and collection tube as directed, then apply the sample to the column and centrifuge for 1 min on a standard bench top centrifuge.
7. Discard flow-through and place column back onto the same collection tube. It is recommended that 0.5 ml of Buffer QG be added to the QIAquick spin column to remove all residual agarose. Centrifuge for 1 min.
8. To wash, add 0.75 ml of Buffer PE to QIAquick spin column and centrifuge for 1 min. Discard subsequent flow-through and centrifuge further for 1min at 13, 000 rpm.
9. Place QIAquick spin column in a clean 1.5 microcentrifuge tube and elute DNA by adding 50 µl of distilled H_2O-pH 7.0-8.5 to the centre of the membrane and centrifuge the column for 1 min.

B.3: <u>Ethanol precipitation protocol</u>

Following the sequencing reaction, sequence products were purified using ethanol precipitation as follows:

1. Add 2.5 µl of Sodium Acetate (NaAc-3 mM, pH 5.5) and 50 µl of absolute ethanol to each PCR tube containing sequencing products.
2. Mix thoroughly by vortexing and incubate at -20°C for a minimum of 1 hr.
3. Centrifuge the mixture at 10, 000 rpm for 10 min and discard supernatant.
4. Add 30 µl of 70% ethanol to each tube, vortex and centrifuge for 10 min at 10,000 rpm.
5. Air-dry samples for approximately 60 min.
6. Resuspend in 10 µl dH_2O, mix gently.

B.4: <u>Cloning materials and protocols</u>

pCDNA 3.1+ Vector

The *RHO* insert was cloned into the vector using the *Hind* III an *EcoR* I restriction sites.

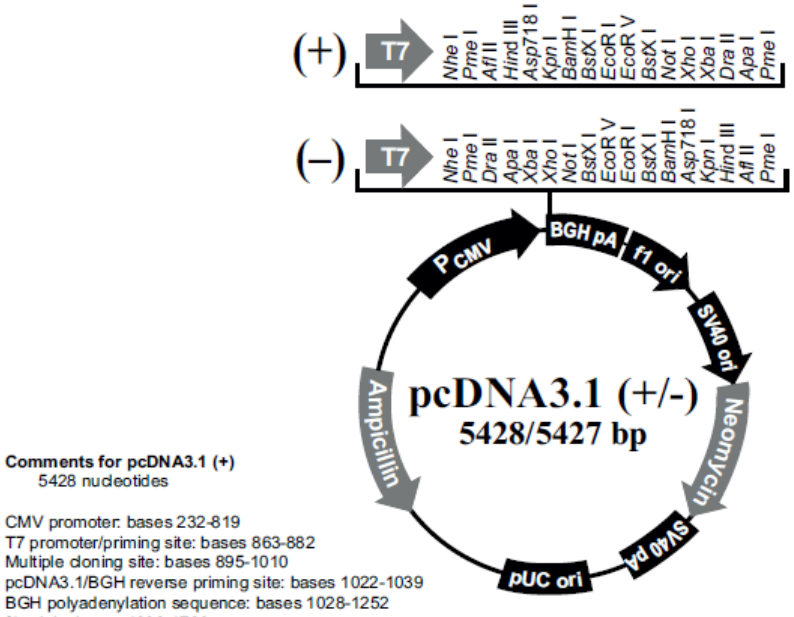

Comments for pcDNA3.1 (+)
5428 nucleotides

CMV promoter: bases 232-819
T7 promoter/priming site: bases 863-882
Multiple cloning site: bases 895-1010
pcDNA3.1/BGH reverse priming site: bases 1022-1039
BGH polyadenylation sequence: bases 1028-1252
f1 origin: bases 1298-1726
SV40 early promoter and origin: bases 1731-2074
Neomycin resistance gene (ORF): bases 2136-2930
SV40 early polyadenylation signal: bases 3104-3234
pUC origin: bases 3617-4287 (complementary strand)
Ampicillin resistance gene (*bla*): bases 4432-5428 (complementary strand)
ORF: bases 4432-5292 (complementary strand)
Ribosome binding site: bases 5300-5304 (complementary strand)
bla promoter (P3): bases 5327-5333 (complementary strand)

Vector image reproduced from www.invitrogen.com

Luria-Bertani broth (100 ml): 1 g Bacto-Tryptone
0.5 g Bacto-yeast
1 g Sodium Chloride (NaCl)
Make up to100 ml with dH_2O, autoclave.

Agar (100 ml): 1 g Bacto-tryptone
0.5 g bacto-yeast extract
1 g NaCl
1.5 g Bacto-Agar

Make up to 100 ml with dH_2O, autoclave. Add antibiotic while still warm, pour approximately 20 ml onto 10cm petri dishes (plates) and stand at room temperature until it sets.

Antibiotic: Ampicillin (Roche Diagnostics, Germany)

Working stock (50 mg/ml)

B.5: Site-directed mutagenesis flow diagram

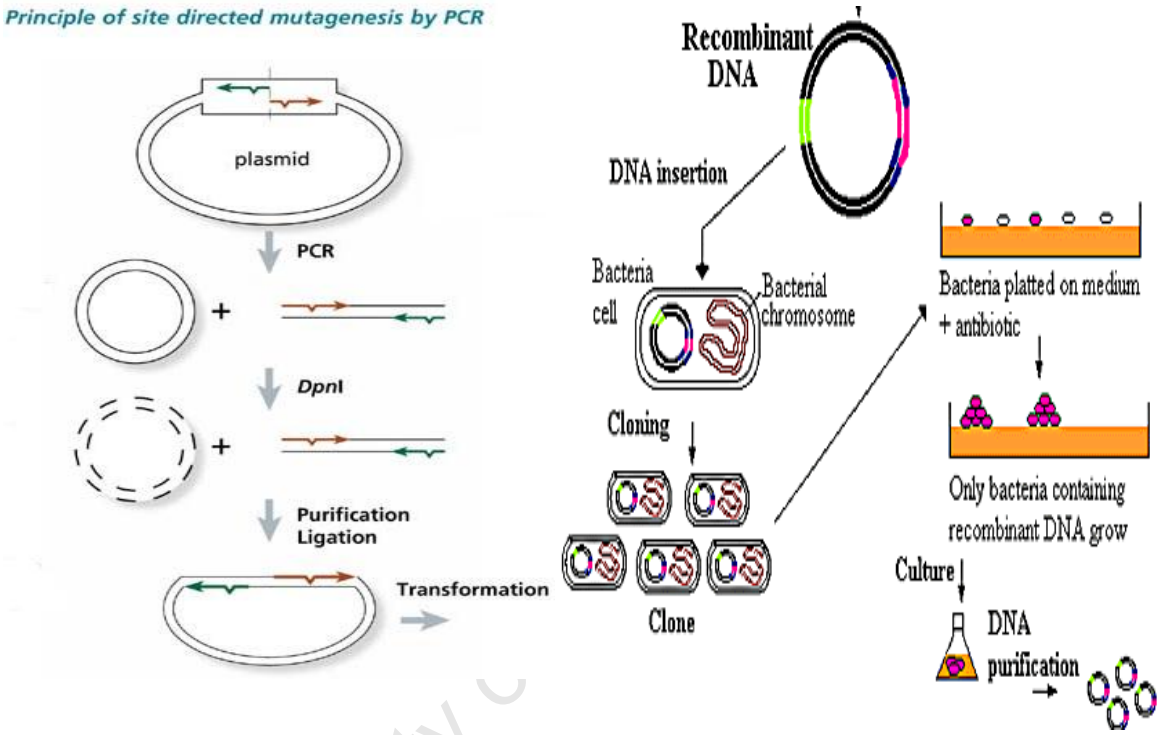

http://www.qbiogene.com/products/gene-expression/tfu-direct.shtml / and

http://www.bio.davidson.edu/Courses/Molbio/MolStudents/spring2003/Keogh/plasmids.html

STET (boiling) minilysate prep for plasmid DNA

Reagents:

STET buffer:

8 g sucrose

5 g triton X-100

10 ml 0.5M EDTA (pH 8.0)

5 ml 1M TRIS (pH 8.0)

Sterile dH_2O to 100 ml

Luria broth – 3 ml aliquots

Luria agar Plates

Isopropanol

10 X TE

1. Fill 20 ml McCartney bottles with 3.0 ml LB (containing antibiotic)
2. Pick colonies using sterile toothpicks and inoculate into LB medium. Remember to prepare a reference plate as well.
3. Shake tubes vigorously overnight at 37°C, and grow reference grid-plate overnight as well.
4. Transfer 1.0 – 1.5 ml of overnight culture into 1.5 ml microfuge tubes.
5. Spin tubes for 2 min at RT.
6. Remove supernatant carefully. (Not the bacterial pellet)
7. Add 250 µl of STET containing 1 mg/ml lysozyme. (Mix 4.9 ml STET with 100 µl 50 mg/ml lysozyme, frozen at -20°C). Resuspend pellet.
8. Vortex and boil for 1 min. Prep should turn from yellow to white.
9. Spin for 8 min immediately following the boil.
10. Remove sticky pellet with toothpick and discard.
11. Add 250 µl of isopropanol and mix by inversion.
12. Spin for 8 min at RT.
13. Carefully remove the supernatant. Dry in vacuum dryer.
14. Resuspend in 20 µl 1/10 TE and heat for 10 min at 68°C. Vortex again and spin 1-2 min.
15. Use 1-3 µl for restriction endonuclease digests reaction.

B.6: <u>Sequencing primers used for the confirmation of cloned constructs</u>

The first set of forward and reverse primers was used to sequence the pCDNA3.1+ vector (confirm the presence of the *RHO* insert). Subsequently, for confirmation of inserted mutations, the forward primer was used to sequence the c.-26A>G, T4K and T17M mutant constructs. The P347L containing construct was sequenced with a separate newly designed primer.

Primer	**Sequence**	**Tm**	**GC Content**
Forward (20 bp)	5′-GTGTACGGTGGGAGGTCTAT-3'	54°C	55%
Reverse (20 bp)	5′-AGATGGCTGGCAACTAGAAG-3'	52°C	50%
Forward P347L (22 bp)	5′-GCGTGGCATTCTACATCTTCAC-3′	55°C	50%

B.7: Cell Culture protocols and reagents

Phosphate Buffered Saline (10X)

80 g NaCl (1.37 M)

2 g Potassium Chloride (KCl) (0.03 M)

12.6 g Disodium Hydrogen Phosphate (Na_2HPO_4) anhydrous (0.09 M)

2 g Monopotassium Phosphate (KH_2PO_4) (0.01 M)

Dissolve in 1 L dH_2O and autoclave.

1X PBS: Dilute 100 ml of 10X PBS in 1L ddH_2O, pH 7.4

Trypsin/ Ethylene Diaminetetraacetic acid (EDTA)

0.05% Trypsin (Difco, USA) 0.02%EDTA (Sigma-Aldrich, Germany)

0.05 g Trypsin

0.02 g EDTA

Dissolve Trypsin in 100 ml 1X PBS then add EDTA and dissolve. Filter solution using a 0.22 micron filter and store at -20°C in 20 ml aliquots.

Penicillin/Streptomycin (Pen/Strep)

100 U/ml Penicillin (Sigma-Aldrich, Germany)

100 µg/ml Streptomycin (Sigma-Aldrich, Germany)

100X working solution: Dissolve 6 g Penicillin, 10 g Streptomycin in 1 L autoclaved dH_2O, filter sterilise and store in 50 ml aliquots at -20°C.

jetPEI™ Transfection protocol

Reagents: jetPEI, 150 mM NaCl (autoclaved and filtered with a 0.22 micro filter), 6-well or 6 cm culture plates and DMEM +10% FCS+ 1% Pen/Strep

1. Cells were counted on a haemocytometer and seeded in 6-well culture plates at a concentration of $1x10^5$ with added DMEM to a total volume of 2 ml (6-well plates).
2. Controls included in each transfection included cells without any transfection reagent and cells transfected with only the transfection reagent and no DNA.
3. Following seeding, culture plates containing the cells were incubated at 37°C in a humidified 5% CO_2 incubator for 24 hr.

4. The next day, cells were checked for confluency (50%-90%) and transfection mix prepared as follows; in a 0.2 µl tube, 0.5 µg of plasmid and 50 µl of NaCl were mixed, vortexed and spun down, in a separate tube, 2 µl of jetPEI was added to 50 µl of NaCl, which was subsequently, mixed, vortexed and spun down. This mixture was then added to the previous mixture containing DNA and incubated at room temperature for 15-30 min. The mixture was subsequently added to each one of the experimental wells containing cells.
5. Plates were subsequently incubated at 37°C for another 24 hr before being harvested for various analyses.

5% Non-fat Milk

2.5 g Non-fat Milk (Pick n' Pay, RSA)

50 ml PBS/Tween (50 ml PBS and 500 µl Tween 20)

DAPI Stock (50 mg/ml)

Working stock- Dilute 1:50

Hoechst No. 33258

Hoechst trihydrochloride ((2'-[4-hydroxyphenyl]-5-[4-methyl-1-piperazinyl]-2,5′-bi-1H-benzimidazole) (Sigma-Aldrich, Germany)

Stock Solution (100 ml): 5 mg Hoechst
Dissolve in 100 ml 1XPBS, Cover with aluminium foil and store at 4°C

Hoechst Working Solution: Dilute stock 1:100 in 1X PBS, cover with foil and store at 4°C.

Triton-X 100 (0.2%)

1 mg Triton-X 100 dissolved in 1X PBS

B.8: Western blotting reagents and protocols

Cell lysis buffer

Incomplete: 1% (w/v) n-Dodecyl-β-D-Maltoside (DM) (Merck, Germany) dissolved in 1X PBS

Complete: 1% (w/v) DM/PBS, 2% Mammalian protease Inhibitor cocktail: Protease Inhibitor, (PMSF), pepstatin, Aprotinin

Protein quantification using the Bicinchoninic Acid Kit (BCA) Kit

***Bovine Serum Albumin (BSA*)**

BSA fraction V (Roche, Germany):

2 mg BSA solution (10 ml): 2 mg BSA powder dissolved in 10 ml 0.9% NaCl (0.9 g NaCl and 99.1 ml ddH2O).

Bicinchoninic Acid (BCA) Kit

BSA was used as protein standard and had to be thawed from the -80°C freezer. Serial dilutions (ranging from 2 mg/ml-0.1 mg/ml) specified by the kit were prepared prior to quantification.

1. Aliquot 10 µl of BSA standards in duplicate in a 96-well plate, followed by 10 µl protein samples in duplicate alongside the standards.
2. Make up BCA reagent by mixing 50:1 Reagent A and B respectively. Add 200 µl per well containing BSA or protein and incubate the plate at 37°C for a minimum of 30 min.
3. Read protein absorbance values on a spectrophotometer at a wavelength of 595 nm.
4. Unknown protein concentrations are determined using the slope obtained from plotting the BSA standards concentrations against their optical density readings.

If not using the protein lysate immediately, aliquot the remaining protein and store at -80°C.

Loading buffer (5X)

1.5 mM Tris-HCl pH6.8,

30 ml Glycerol,

2 g SDS

1 ml Bromophenol blue

Resolving gel buffer (1.5 mM Tris)

38.2 g Tris

0.8 g SDS

pH 8.9 and make up to 200 ml dH_2O-can heat slightly to dissolve SDS, Store at 4°C

Stacking gel buffer (0.5 mM Tris)

5.9 g Tris

0.4 g SDS

pH 6.8 and make up to 100 ml with dH_2O, Store at 4°C

Stacking gel (1 mm)

750 µl Stacking Buffer:

500 µl Acrylamide

1.75 ml dH_20

30 µl APS

3 µl TEMED*

Resolving gel Solution (10%)

3 ml Resolving Buffer:

3 ml Acrylamide (30% Bisacrylamide:Acrylamide)

3 ml dH_2O

180 µl Ammonium per Sulphate (APS)

18 µl N,N,N',N'-Tetramethylethylenediamine (TEMED)*

* Add TEMED as the last reagent making sure to pour the solutions as quickly as possible into the gel cast to avoid setting.

-The resolving gel is poured first followed by the stacking gel, which contains the pouring combs. Leave to set for 45 min-1 hr.

-Thawed protein was prepared for loading after the desired concentration was determined i.e 15 µg by adding, lysis buffer to make up volume and loading buffer to a 1X concentration, then heating for 5 min at 95°C.

10X Running buffer

30.2 g Tris

144 g Glycine

10 g SDS

Make up to 1 L with dH_2O, Store at 4°C

1X Running buffer: 1:100 dilution of 10X Running buffer in 1 L dH_2O (100 ml 10X in 900 ml dH_2O) Store at 4°C

10X Transfer buffer

144 g Glycine

38 g Tris

Make up to 1L with dH_2O, Store at 4°C

1X Transfer Buffer: 100 ml (10X Transfer Buffer), 700 ml dH_2O, 200 ml Methanol (Chill at 4°C before doing transfer).

Ponceau S staining

Ponceau S stain: 1g Ponceau S, 50 ml acetic acid, Make up to 1L with ddH2O

Rinse off transfer buffer and gel debris by washing membrane in twice PBS/T. Add Ponceau S solution and allow shaking for 5 min on a shaker. Subsequently, rinse off excess Ponceau S using distilled dH_2O and then once with PBS/T until pink protein bands are visible. Capture image and rinse stain off completely using PBS/T.

Stripping

Stripping Buffer

1.4 ml β-Mercaptoethanol

40 ml 10% SDS- 4g SDS Powder

12.5 ml 1M Tris-HCl pH 6.7

Make up to 200 ml with dH_2O.

Place membrane in a holder and wash once with PBS/T while shaking for 5 min. Add stripping buffer leave to shake for 5-7 min at 50°C incubator. Once 5 min have passed pour off stripping buffer and add tris-HCl pH 7.5 and shake for another 5 min at room temperature. Pour off tris-HCl and wash twice with PBS/T on shaker for min each. The membrane is now ready for detection again.

Appendix C: Supplementary figures

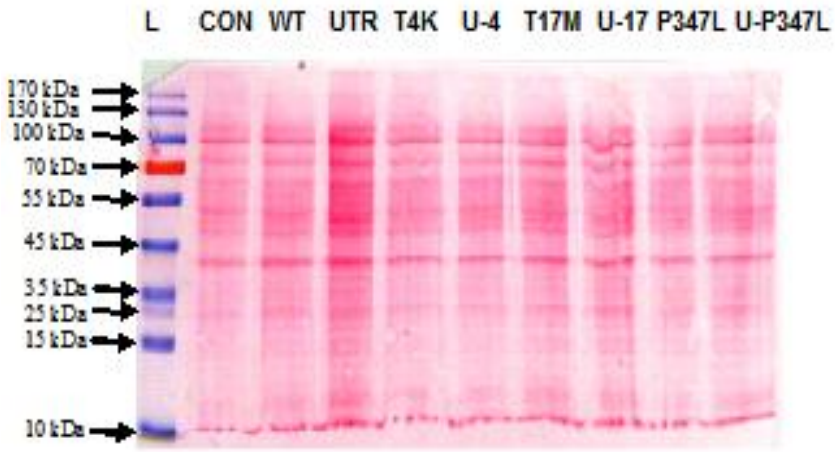

S1: Typical image of a Ponceau S - stained membrane. The horizontal lines in each lane are indicative of various proteins of different sizes. The ladder sizes are outlined on the left. Each of the labelled lanes is representative of protein extracted from cells transfected with the specific construct.

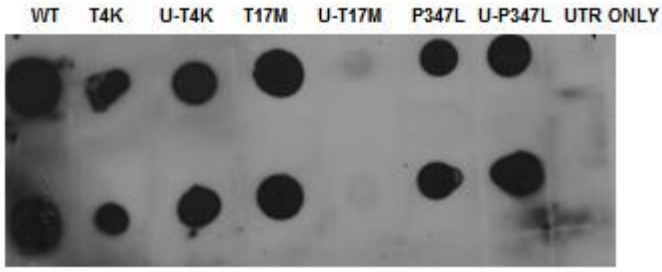

S2: Image of a dot blot performed for HT-1080 cell lysates. The dot blot was performed to test antibody-protein interaction as part of troubleshooting RHO western blot detection. Dot blots were performed by blotting protein onto the membrane, followed by subsequent detection as in western blots.